

Griffith School of Engineering
Griffith University

6002ENG – Industry Affiliates Program

Footfall Analysis of Residential Floor Beams Using CFS C-Shaped Built-Up Sections

Xueting Weng, s5216566

13th June, Trimester 1, 2022

Xstructe Consulting
Dr. Bin (Ben) Wang
Professor Hong Guan

A report submitted in partial fulfillment of the degree of Bachelor of Engineering (Honours)

The copyright on this report is held by the author and/or the IAP Industry Partner. Permission has been granted to Griffith University to keep a reference copy of this report.



EXECUTIVE SUMMARY

Among floor construction materials, cold-formed lightweight elements are becoming increasingly popular in practical construction. The various advantages of cold-formed steel (CFS) compared to conventional construction materials make it the preferred choice in residential construction today. However, light steel floors are prone to annoying vibrations due to their high strength-to-weight ratio. This affects not only the comfort of the occupants but also the structure's safety. Research into CFS has found that built-up CFS elements offer better performance in several areas. This project is concerned with solving floor vibration problems using built-up CFS beams with I-section and comparing the vibration of floor structures in three different composite cases. The method used for the thesis is a finite element model followed by finite element analysis (FEA).

The project was divided into three phases: the first phase was to investigate the CFS floor structure on-site and determine the structure and dimensions of the floor model. The second stage was to build a finite element model of the floor in Strand 7 for three scenarios and to verify the feasibility. The third stage was to quantify the floor vibrations using different parameters and to conduct an FEA of the model to compare and evaluate the vibrations in the three cases.

Based on the results of the analysis, it can be concluded that a floor with composite beams can control vibrations to meet construction requirements. Further comparison reveals that the vibration of the lightweight steel floor can be further controlled by bolted confinement or welded beams with better serviceability. In both cases, however, more time and cost are required. On balance, a partially composite beam with bolting is more suitable for modern construction.

ACKNOWLEDGEMENT

I would like to express my gratitude for all of the help I have gotten while working on this project.

- Professor Hong Guan: Thank you very much for your help as an academic supervisor in overcoming technical difficulties, for giving me useful advice during the project, and for taking time out of your busy schedule to help me. I am very grateful for the opportunity to work on this project under your guidance.
- Dr. Bin (Ben) Wang: Thank you so much for all the help you have given me in the industry, taking me on site to investigate and guide me through the project. I am grateful to have encountered an industry teacher like yourself in Australia.
- My classmates: I would like to thank my classmates for comforting me when I was confused and sharing their own experiences in doing projects. Thank you for your company and help!
- My parents and friends: thank you for always supporting me and giving me emotional help. Thank you so much for your concern.

Thank you so much for your support and the faith you have placed in me, to everyone else who is not expressly stated above. I would like to thank everyone around me, both for the academic help and the moral support that made the project come to fruition.

TABLE OF CONTENTS

EXECUTIVE SUMMARY	I
ACKNOWLEDGEMENT	II
TABLE OF CONTENTS	III
LIST OF FIGURES	V
LIST OF TABLES	VII
1 INTRODUCTION	8
1.1 Aims and Objectives.....	10
2 LITERATURE REVIEW	12
2.1 CFS in floor construction	12
2.2 CFS built-up sections	13
2.2.1 Types and properties of built-up sections	13
2.2.2 Composite action of CFS built-up sections.....	14
2.3 Vibration of CFS floors.....	16
2.3.1 Vibration generation and human perception	17
2.3.2 Loading methods for floor reactions caused by human walking	19
2.3.3 Laboratory testing of floor vibrations	21
2.3.4 In situ testing of floor vibrations	22
2.3.5 Parametric study of vibration	23
Natural Frequencies	23
Damping Ratio	23
RMS Acceleration	24
Static displacement	24
2.3.6 Methods for controlling vibration in CFS floors.....	24
3 METHODOLOGY.....	26
3.1 Theoretical methods	26
3.2 Site Survey	27
3.3 Validation of finite element models	28
3.3.1 Verification of fastening methods	28
3.3.2 Verification of support reaction forces.....	29
3.4 Finite element modelling of flooring structures	31
3.4.1 Geometrical modelling.....	31
3.4.2 Connection point modelling	35

3.4.3 Element types and meshing	35
3.4.4 Boundary conditions	36
3.4.5 Application of loading forces	36
4 FOOTFALL ANALYSIS RESULTS	38
4.1 Natural Frequency	38
4.2 Harmonic Response.....	42
4.3 Static Displacement	49
5 DISCUSSION	54
6 CONCLUSIONS.....	55
7 REFERENCE	56
8 APPENDICES	59
8.1 APPENDIX A—Natural frequency solving process	59
8.2 APPENDIX B—Harmonic response solving process.....	61
8.3 APPENDIX C—Static displacement solving process	67

LIST OF FIGURES

Figure 1. Different types of cold-formed sections.	9
Figure 2. Collapse site of steel frame of factory building under constructio.	10
Figure 3. Fully, partially and no composite action beams	11
Figure 4. composite CFS flooring system.....	13
Figure 5. Cross-section geometries of specimens.	14
Figure 6. Built-up beam with two and four fastener points.	15
Figure 7. Effect of height-to-width ratio (a) and flange width-to-thickness ratio (b) on the ultimate moment capacity.	16
Figure 8. Modified Reiher-Meister scale	18
Figure 9. ISO acceleration limits.....	18
Figure 10. Moving force loading.....	19
Figure 11. Single-footfall force loading system.....	20
Figure 12. Moving damped-oscillator loading.	20
Figure 13. Model of moving and stationary damped-oscillators.	21
Figure 14. Flooring test devices.	22
Figure 15. Top view and cross section of laboratory floor slab.....	22
Figure 16. Damper attached to the flange of beam	25
Figure 17. An irregular floor frame was subjected to a FEA.....	26
Figure 18. Construction site floor structure.	27
Figure 19. Verification of rigid links instead of bolted connections.....	28
Figure 20. Floor model of the Strand 7.	30
Figure 21. Top view of the floor (in mm).	31
Figure 22. Front view of the floor (Case 1: No Composite Action).	32
Figure 23. Front view of the floor (Case 2: Partial Composite Action).....	32
Figure 24. Front view of the floor (Case 3: Full Composite Action).....	32
Figure 25. Beam sections and dimensions.	33
Figure 26. Dimensions and properties of Chord.	33
Figure 27. Dimensions and properties of Web.....	33
Figure 28. Finite element model of the internal structure of the floor.	34
Figure 29. Finite element model of the floor.	34
Figure 30. Number of elements.....	35
Figure 31. Floor centre displacement for different element models.	36

Figure 32. Floor structure after adding load.....	37
Figure 33. Three cases of beams.	38
Figure 34. Natural frequency solver and setup details.	39
Figure 35. Floor model with natural frequencies at 7.63039 Hz and 8.926 Hz respectively (Case 1).	40
Figure 36. Floor model with natural frequencies at 9.11511 Hz and 12.7273 Hz respectively (Case 1).	40
Figure 37. Floor model with natural frequencies at 9.1495 Hz and 11.1261 Hz respectively (Case 2).	41
Figure 38. Floor model with natural frequencies at 9.15002 Hz and 11.1263 Hz respectively (Case 3).	41
Figure 39. Harmonic response solver.....	42
Figure 40. Peak Acceleration (Case 1).....	44
Figure 41. Response Factor (Case 1).	45
Figure 42. Peak Displacement (Case 1).	46
Figure 43. Peak Acceleration (Case 2).....	46
Figure 44. Response Factor (Case 2).	47
Figure 45. Peak Displacement (Case 2).	47
Figure 46. Peak Acceleration (Case 3).....	48
Figure 47. Response Factor (Case 3).	48
Figure 48. Peak Displacement (Case 3).	49
Figure 49. Linear Static Analysis Solver.	50
Figure 50. Colour chart for Beams Static displacement (Case 1).	50
Figure 51. Values of static displacement (Case 1).	51
Figure 52. Colour chart for beams static displacement (Case 2).	51
Figure 53. Values of static displacement (Case 2).	52
Figure 54. Colour chart for beams static displacement (Case 3).	52
Figure 55. Values of static displacement (Case 3).	53

LIST OF TABLES

Table 1. Value of the support reaction force in the Y-axis	29
Table 2. Node reaction results.....	31
Table 3. Coordinates of modelling points.	34
Table 4. Running times for different numbers of elements.....	36
Table 5. Parameters for four executions of the Harmonic Response solver.	43
Table 6. Three parameters in three cases.	49

1 INTRODUCTION

Cold-formed steel (CFS) is a steel structure product processed at ambient temperature through steel to form a more supportive shape. With the development of construction materials and the demand for higher-strength materials, CFS is being used more widely than traditional construction materials such as heavy hot-rolled steel elements (Hancock, 2003). At the same time, in Australia, light-gauge steel frames with cold-formed sections are the preferred choice for floor structures due to the shortage of timber and the time-consuming and expensive installation of Parallel Flange Channel (PFC) floor trusses.

The use of CFS as a structural material for flooring systems is due to its various advantages: according to Yu et al. (2019), CFS is light in weight, high in strength and stiffness, easy to install and transport, corrosion-resistant, termite resistant, low cost and recyclable. In contrast, Parallel Flange Channel (PFC), hot-rolled steel, is heavier, difficult to transport and install, and more expensive. Secondly, as shown in figure 1, they can be produced into an unusual cross-section with a favorable strength-to-weight ratio. It is worth mentioning that the residential floor beam studied here uses C-type opening built-up sections such as (2) in part (b) of Figure 1. The built-up section of CFS is a single-section splicing combination with a more substantial bending capacity and higher axial direction (Rasmussen et al., 2020).

Furthermore, the load-carrying panels and decks of CFS can provide a valuable surface for the floor and enclosed cell for electrical and other plumbing. However, using CFS for all floors is a new and unproven way of assembly. Its long span and lightweight have brought about a problem people tend to overlook: the vibration caused by normal walking (Xu, 2011). Although there are now studies and guidelines on CFS floor vibrations, they are almost always on single section members, as shown in Figure 1(a) (Rasmussen et al., 2020). It is, therefore, necessary to investigate the vibration of floor systems with CFS components.

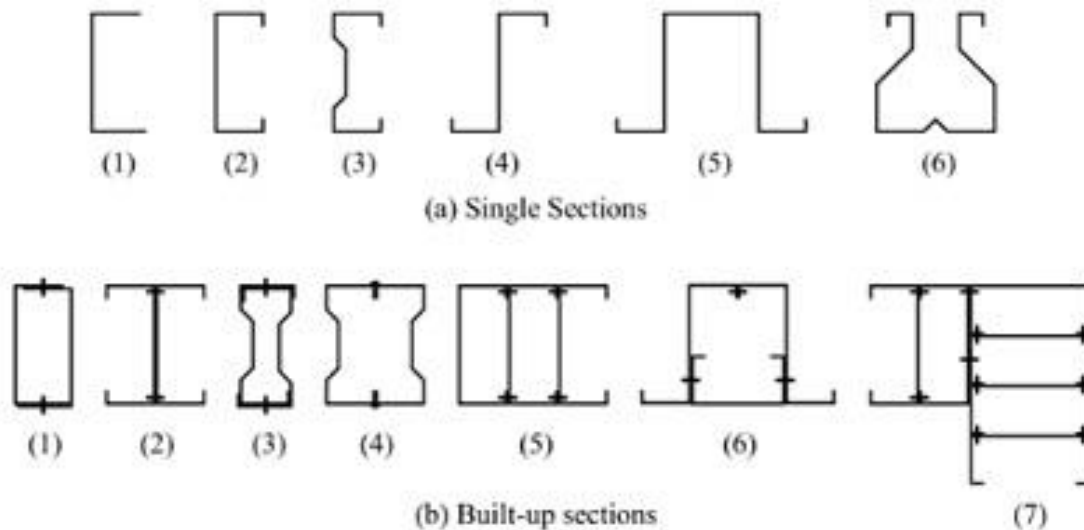


Figure 1. Different types of cold-formed sections (Rasmussen et al., 2020).

The vibration of the long-span lightweight floor caused by human activities has become a critical problem concerned technicians (Nguyen, 2013). As shown in Figure 2, a light-gauge steel plant under construction in Chongqing, China, collapsed in 2009. In the end, although only two people were injured, it is dangerous to build long-span light-gauge steel structures not strictly according to the requirements. There have also been cases of floor and stadium structures collapsing due to vibrations caused by crowds dancing or jumping (Debney & Willford, 2009). In addition, the floor is the main structure that carries human life. On the one hand, floor vibration reduces comfort, and on the other hand, its post-maintenance is also highly costly (Xu, 2011). This demonstrates the importance of vibration control during construction in compliance with design standards. To address the issue of floor slab vibration, constructors have utilized members with doubly symmetrical sections in the construction of mid-rise and high-rise buildings, increasing strength and torsional resistance and improving deformation buckling capacity (Phan & Rasmussen, 2019).



Figure 2. Collapse site of steel frame of factory building under construction (Wang, 2009).

While current analyses and studies have shown the factors influencing CFS floor systems and the assessment of the composite elements, there is still a lack of research on the overall structural vibration by placing the built-up members into the ground step system. Therefore, it is essential to study the vibration of floor structures using CFS built-up sections and give design guidelines to control vibration.

1.1 Aims and Objectives

The aim of using CFS built-up beams in residential flooring systems is to reduce vibrations and provide a more stable floor structure with higher comfort. Several studies have been carried out to obtain some usable data and formulas through different analytical methods to help build more comfortable CFS floors. This report will build on the existing theories and data to investigate the vibration of a floor structure consisting of three cold-formed cross-section beams (see Figure 3) with C-shaped CFS joists. In these three cases, the composite beams are connected in different ways: without welding, partially fastened, and fully welded. The finite element modelling method will be used to visualize the actual situation, and the analysis will be compared with existing engineering standards to give design guidelines.

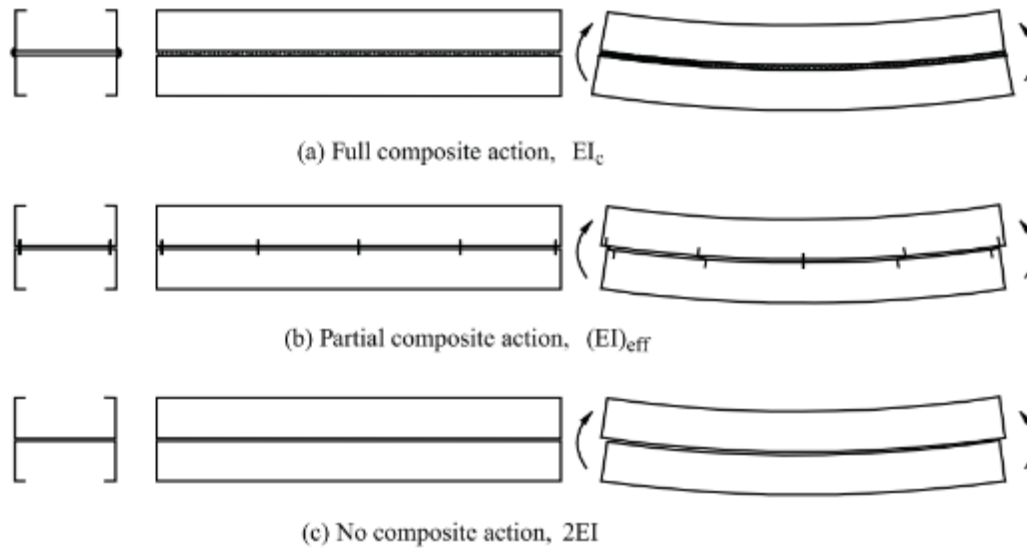


Figure 3. Fully, partially and no composite action beams
(Rasmussen et al., 2020).

The objectives of the report are as follows:

- Visit the construction site and specify the dimensions of the model. Draw the dimensions and details of the model in CAD.
- A realistic finite element model is built from the drawings using strand 7.
- The vibration of the model is obtained through footfall analysis: natural frequencies are obtained using the natural frequency solver. Moreover the harmonic response solver is used to calculate vertical acceleration.
- To acquire model static displacements and compare with actual engineering standards, use a linear static solver.
- Graph the parameters of the three models and compare them to give design guidelines.

2 LITERATURE REVIEW

This literature review focuses on the advantages and problems of using CFS in-floor slab construction, as well as research into developing its composite elements and controlling floor slab vibrations. Due to the diversity of practical projects and the importance of floor slab construction, approaches to solving floor slab vibrations vary. This section establishes the theoretical basis for this project by examining the literature. Furthermore, it is found that the research gap is that CFS built-up section elements have been used in building construction and that the dimensional requirements of built-up sections have been specifically studied. However, their specific effects in actual monolithic floor slab structures have not been fully described.

2.1 CFS in floor construction

Cold-formed light elements among floor construction materials are becoming increasingly popular in practical construction. Compared to conventional hot-rolled steel, CFS is more economical and more suitable for relatively light loads and short spans (Yu et al., 2019). In addition to its high strength, lightweight, high stiffness and ductility, termite resistance, corrosion resistance, and fast construction, it is a better choice for residential and commercial building materials (Xu, 2011). For example, Figure 4 shows a hybrid CFS flooring system that is now commonly used, which consists of CFS beams and a timber base plate (Kyvelou et al., 2017).

However, because the cold-formed part is thin and highly hardened, it is more susceptible to local and twisted buckling (Davies, 2000). On the one hand, this directly leads to a lack of stability and, on the other hand, indirectly to low serviceability of the light steel floor. To address these problems, CFS members have continued to develop more complex sections to obtain built-up sections with a higher load-carrying capacity (Roy et al., 2021).

From the literature discussed, it can be concluded that with the widespread use of CFS in building construction, ordinary thin-walled light steel poses a number of problems in practical construction. Moreover, using composite CFS to solve these problems is feasible, but this still needs theoretical and practical verification.

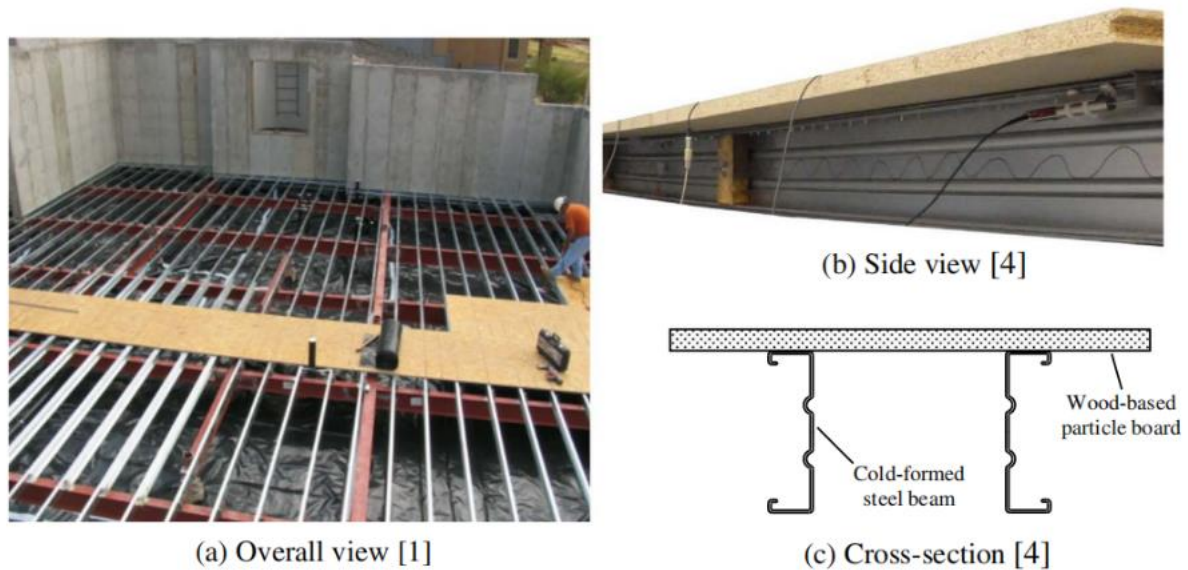


Figure 4. composite CFS flooring system
(Kyvelou et al., 2017).

2.2 CFS built-up sections

CFS built-up sections have been developed in response to the growing demand for CFS sections as a cost-effective design solution (Roy et al., 2021). Moreover, the structural behavior of CFS built-up section beams has been the subject of numerous studies (Yao et al., 2020).

2.2.1 Types and properties of built-up sections

According to Yao et al. (2020), as shown in Figure 5, the combined segment elements generally consist of two CFS openings forming a back-to-back open segment or interlocked to a closed box segment. In addition, from familiar built-up section members can be combined into more complex members such as (5), (6), (7) in (b) in Figure 1 or change the shape of the cross-section such as (3), (4) in (b) in Figure 1. This makes it possible to meet the needs of more types of construction.

Their nature is even more unique: the built-up sections have strong torsional rigidities and great lateral-torsional buckling capacity compared to CFS joists of single open sections such as lipped channels and Z-sections (Yao et al., 2020). As a result, a member with built-up parts may bear more weight and span greater distances. Struts in steel trusses and space frames, wall studs in wall frames, and columns in portal frames are all applications (Roy et al., 2018).

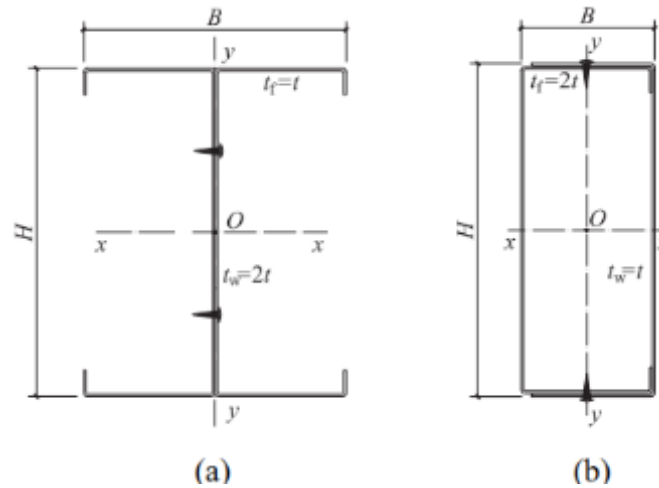


Figure 5. Cross-section geometries of specimens.

(a) Built-up I-section beam, (b) built-up box section beam (Yao et al., 2020).

2.2.2 Composite action of CFS built-up sections

The combined effect of CFS built-up elements is mainly manifested in their load-bearing capacity and bending resistance. Furthermore, many factors influence the composite action of assembled components. These two critical aspects of composite action influences studied in the literature will be described here.

The first is the impact of the way members are connected. According to Rasmussen et al. (2020), as shown in Figure 3, if two component pieces are welded along their whole length, the abutting surfaces of the webs will experience the same strain, resulting in full composite action. In contrast, if the pieces are not connected, they bend independently, with no combined effect. However, most fasteners experience relative longitudinal (shear) displacement of the part at the attachment site between these two limit instances, resulting in shear forces in the fastener. Moreover, the paper shows that the shear stiffness of the connections, comprising the shear stiffness of the fastener and the in-plane stiffness of the linked ply, as well as the axial stiffness of the component sections, determine the degree of composite action. The expressions for effective bending, buckling, and torsional stiffness are then deduced based on mechanical methods through linear and flexural analysis of the member in bending, thus studying the change in composite action as the fastener point changes. The study shows that the stiffness varies with the square of the enclosed area. In other words, the more fastener points there are, the greater the effective stiffness at the centre of the member, the less it is affected by external

influences, and the more stable it is, as shown in Figure 6. In addition, the distance between fasteners also affects the moment load capacity of CFS composite beams. Wanniarachchi (2005) investigated this by building a finite element model of a CFS beam and found that when the distance between fastening points was increased, it made the member more susceptible to deformation. It can be deduced that the smaller the distance between the forbidden fastening points, the stronger and more stable the CFS.

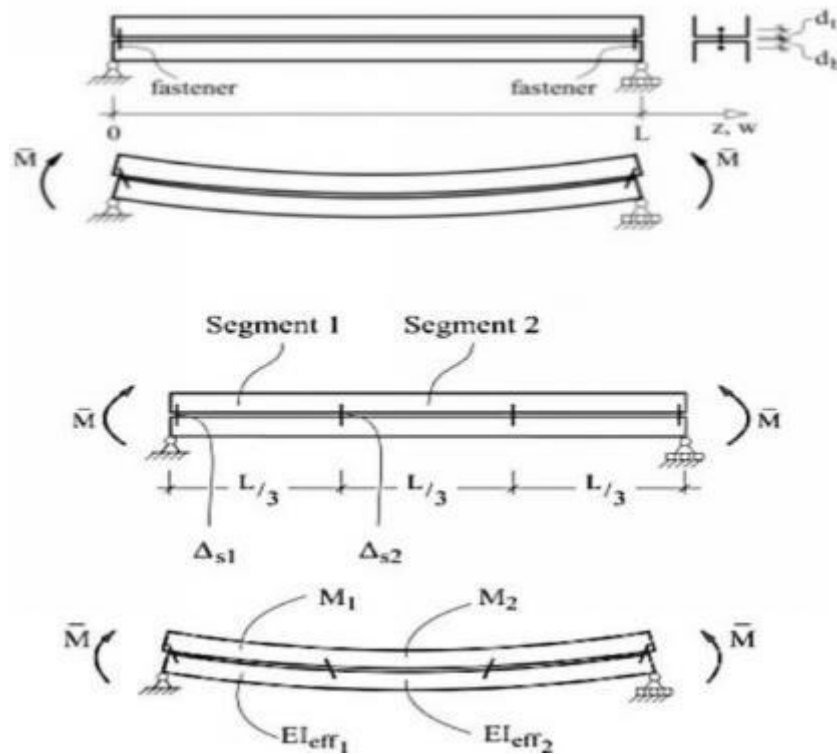


Figure 6. Built-up beam with two and four fastener points (Rasmussen et al., 2020).

Secondly, the size of the member, the height to width ratio, and the section's flange width to thickness ratio also significantly affect the composite action. Shi et al. (2015) and Zhou et al. (2016) have conducted experimental investigations and concluded that the flexural capacity of CFS double-limb built-up beams is primarily influenced by the flange width-to-thickness and the section height-to-width ratio. Recently, Yao et al. (2020) investigated the flexural performance of CFS built-up beams through experimental tests and numerical simulations to determine the effect of member size on the composite action. Firstly, the flexural load capacity of 30 supported beams of different configurations was tested experimentally, and a finite element model was built simultaneously for the same analysis. The structures were then compared, and the two results were in good agreement so that the finite element model could be used for parametric analysis. Finally, the model was used to analyse the effect of the

different section height to width ratios and flange width to thickness ratios on the load-carrying capacity. The conclusions drawn in Figure 7 show that the higher the section height to width ratio and the higher the flange width to thickness ratio of the composite member, the higher the moment carrying capacity of the CFS built-up beam.

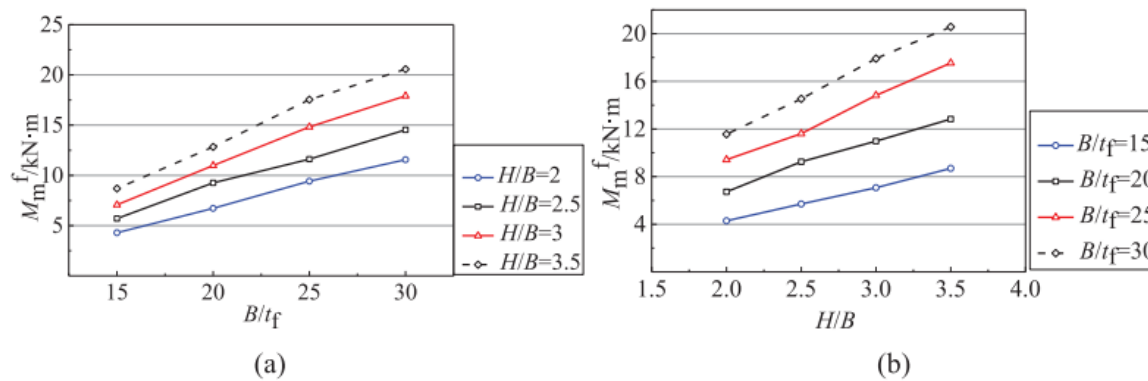


Figure 7. Effect of height-to-width ratio (a) and flange width-to-thickness ratio (b) on the ultimate moment capacity (Yao et al., 2020).

Although various studies have been devoted to the mechanics and influencing factors of CFS composite members, there has been no study of the performance of the whole floor system after controlling for these factors. Neither has it been studied in conjunction with actual construction to investigate their vibration in subfloor systems and give guidelines for the design of subfloor systems.

2.3 Vibration of CFS floors

The vibration of CFS floors has been discussed in several papers. Davis et al. (2008) show that CFS floor systems have a greater span than timber floor systems and are lighter than steel beam and concrete systems, but this high strength-to-weight ratio design makes them more prone to vibration. Debney and Willford (2009) also show in their article that many years ago, the only deflection was limited in the design of floor structures. However, with the advent of lighter, more efficient structures, floor structures have become more active. In addition, Xu (2011) indicates in his study that human activity is more likely to cause vibration in lightweight steel floors and that lightweight floor vibrations have not been well addressed regarding serviceability issues. A more detailed description of the existing literature on floor vibrations and the gaps in the research is presented below.

2.3.1 Vibration generation and human perception

CFS has been increasingly used in the modern building floor framing. However, due to its high strength-to-weight ratio, its inherent low damping makes it more susceptible to annoying vibrations caused by human activity (Zhang & Xu, 2022). Due to a lack of research, the only design criterion for lightweight steel structures was a span deflection limit of $L/480$ under uniform load in the early days. However, for medium to long-span lightweight steel floors, the performance was still not guaranteed using this criterion alone, and it was often costly to correct after construction (Xu, 2011). As a result, it is required to investigate floor vibrations; nevertheless, because floor vibrations primarily affect serviceability, it is necessary to begin with, human perceptions of vibrations.

Since the 1970s, a number of countries have conducted substantial research on floor vibration serviceability (Zhang & Xu, 2022). According to Lenzen (1966), floor vibrations from regular use are transient, and their rate of decay, frequency, and amplitude influence occupant comfort. Debney and Willford (2009) also indicate that human tolerance to vibration is complicated by changes in the direction, frequency, and duration. Tests were carried out using transient vibrations, as shown in Figure 8, reducing the original Reiher-Meister criterion by a factor of 10 to consider the human perception of transient excitation and referring to this updated criterion as the modified Reiher-Meister scale. According to a study by Xu (2011), it was found that the movement of the floor system, physical awareness, and psychological sensitivity to vibration all contribute to the human perception of vibration. Due to resonance within the body cavity, humans are most sensitive to vibration frequencies in the range of 4 Hz to 8 Hz (Grether, 1971). As shown in figure 8, the International Standards Organization (ISO) devised a floor vibration restriction criterion based on the maximum permissible root mean squared (RMS) acceleration for a given structure's fundamental frequency. The horizontal coordinates of the curve indicate the frequency of vibration, and the vertical coordinates indicate the practical value of acceleration. It can be seen that human beings have a low tolerable acceleration between 4 Hz and 8 Hz. Therefore, if the fundamental frequency is within this range, the floor system should take measures to ensure that the RMS acceleration is below the applicable limits.

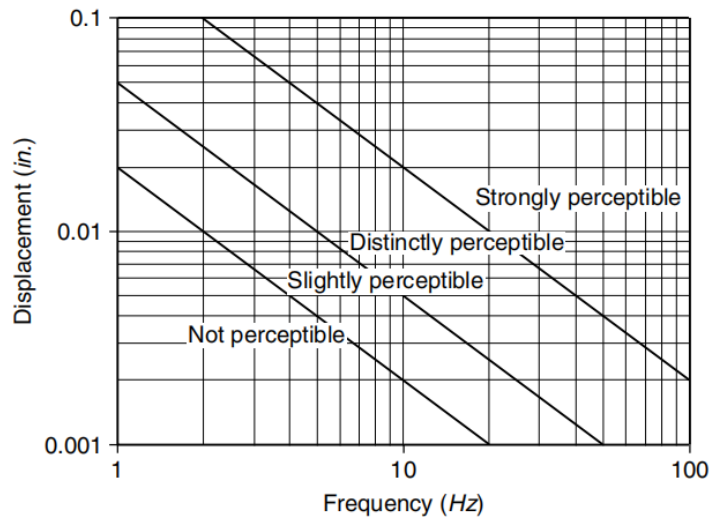


Figure 8. Modified Reiher-Meister scale (Lenzen 1966).

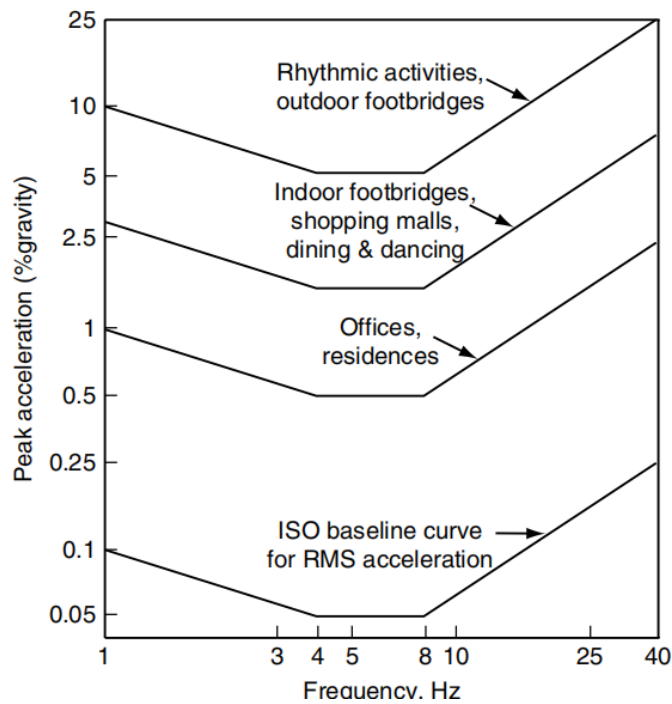


Figure 9. ISO acceleration limits (ISO 1989).

The human response to vibration depends not only on human physiology but is also influenced psychologically. Negreira et al. (2015) carried out a subjective psychological vibration test on a wooden floor after objective measurements on the floor in the laboratory. The participants sat in a chair to feel other people walking, then stood up, walked freely, and assessed the floor's performance. Finally, the answers provided by the subjects were compared with the measured

and calculated objective parameter values to determine the best design indicators for vibration acceptability and vibration disturbance, respectively. In summary, human perception of floor vibrations is primarily about the duration of floor vibrations, physiological and psychological. It is thus clear that floor vibrations appear to be challenging to measure and control compared to other structural criteria.

2.3.2 Loading methods for floor reactions caused by human walking

How the load is loaded is also a key factor affecting floor vibrations. Zhang et al. (2017) developed three different loading methods for a damped plate oscillator model that will be presented here.

The first is moving force (MF) loading, as shown in Figure 1, where the position of the feet models the human walking during walking. It is well known that both feet of an occupant contact the floor for a brief length of time, that is, one-foot initially contact the floor with 'heel strike,' while the other foot leaves with 'toe-off,' resulting in an overlapping of two feet throughout the walking process (Racic et al., 2009). Based on Racic et al. (2009), Zhang et al. (2017) determined the floor system's dynamic response to the footstep force by setting the number of oscillators or users $N_0=0$. Figure 11 depicts the loading technique while considering the overlap periods.

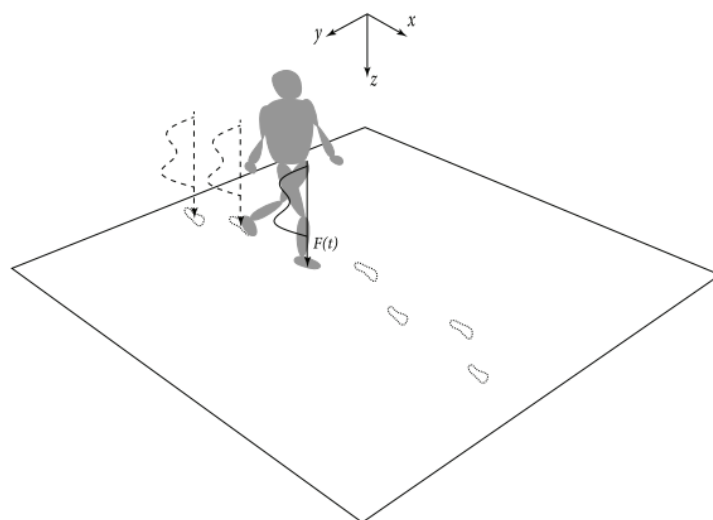


Figure 10. Moving force loading (Zhang & Xu, 2020).

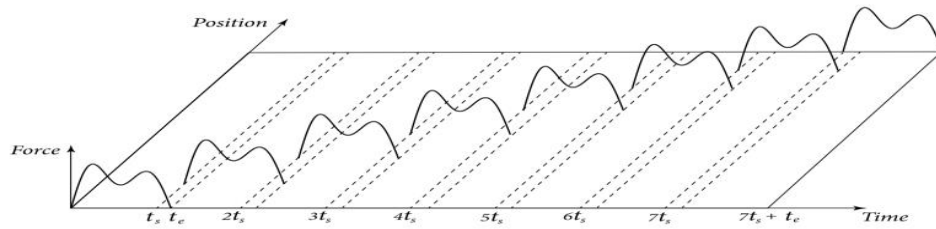


Figure 11. Single-footfall force loading system (Zhang & Xu, 2020).

The second way of loading the human body is modeled as a heavily damped oscillator moving over the structure, taking into account the HSI of human walking, as shown in Figure 12. Its floor response for each footprint is obtained by placing an oscillator with human dynamic characteristics on the footprint. Furthermore, the loading scheme is similar to that shown in Figure 11, where the principle of superposition is used to derive the complete response of the human body when walking on the floor. The moving damped-oscillator (MDO) is a method for forecasting the dynamic response of floor vibration that may be built using Zhang et al. (2017)'s damped-oscillator model with $N_0 = 1$.

The third loading method is to create a moving and stationary damper (MSDO) model to anticipate the dynamic response of moving and stationary floors, as shown in Figure 13. This is because humans not only activate the floor system to generate vibrations but also experience vibrations. As a result, the moving human is represented by a damped oscillator moving across the floor. In contrast, the stationary inhabitant is represented by an oscillator that remains in a fixed place (Zhang et al., 2017).

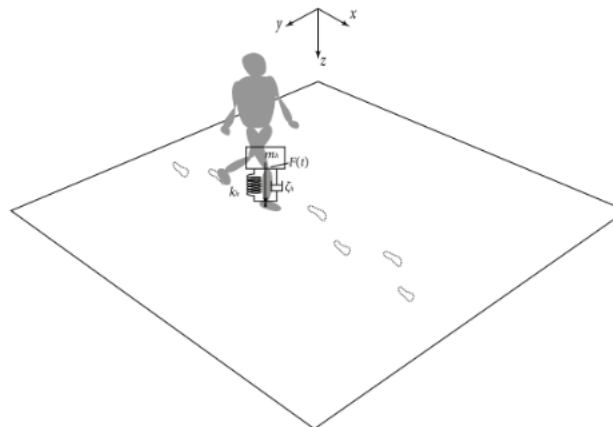


Figure 12. Moving damped-oscillator loading (Zhang & Xu, 2020).

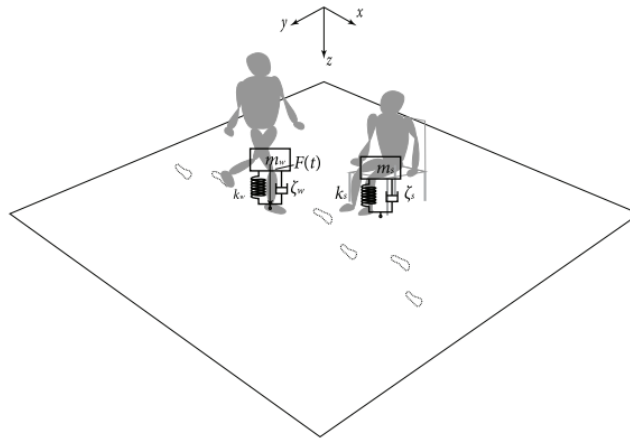


Figure 13. Model of moving and stationary damped-oscillators (Zhang & Xu, 2020).

2.3.3 Laboratory testing of floor vibrations

To better investigate the effect of construction details on the vibration performance of CFS floors and to verify the accuracy of the current design, the laboratory will test the response of the floor and compare it with the floor characteristics in the field. Moreover, testing is generally divided into static and dynamic testing. In particular, the static test quantifies the maximum deformation of the floor slab when subjected to a static load of 1 kN to determine the load sharing capacity, as shown in Figure 14 for the static test apparatus. Dynamic testing directly quantifies the vibration characteristics of the structure. The test is carried out by applying dynamic loads such as dropping sandbags from a height and monitoring the acceleration at different locations on the floor (Xu, 2011).

Such experimental methods have been used and tested in several papers. The University of Waterloo undertook a laboratory testing program that looked at 23 different full-scale floor systems. The floor system was mounted on the same sizeable CFS frame and freely supported to simulate the worst-case scenario (Davis et al., 2008). Figure 15 shows a top view and cross-section of the floor slab tested in the laboratory. A similar floor framing model to Davis et al. (2008) was used in the tests of Xu (2011), but the difference is that this test is more detailed. The experiments began by determining the floor spans and lengths of the bedroom and living room based on the deflection criteria of $L/480$ and then tested the vibration characteristics of 41 and 36 full-size floors with joist spans in the range of 4.270 to 6.755m at 1.4 kPa and 1.9 kPa respectively. The next phase tested 23 full-size floors with floor spans from 4.42 to 6.64m and a joist for back-to-back shaped C-shaped CFS with spans greater than 6.64m (Xu, 2011).



Figure 14. Flooring test devices (Xu, 2011).

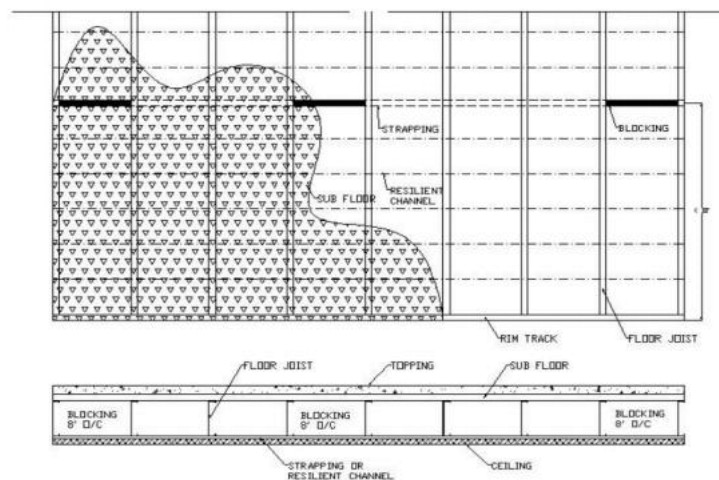


Figure 15. Top view and cross section of laboratory floor slab (Davis et al., 2008).

2.3.4 In situ testing of floor vibrations

Field tests are closer to reality than laboratory tests and are less conservative than laboratory tests. The primary purpose is to assess the vibration performance of lightweight steel floor structures and compare the results with those of laboratory tests (Xu, 2011). The field tests of Davis et al. (2008) were chosen in four mid-rise residences in the USA where the main structure of the site floor was CFS matched to a laboratory flooring system. The difference was that the site floors had been completed with underfloor ductwork and insulation. Xu (2011) selected over 25 residential floors in Canada for a site survey and conducted dynamic and static tests as in the laboratory. These selected dwellings ranged from partially finished to fully finished and furnished. Like the laboratory, the static test starts with a concentrated load of 1 kN applied to the centre of the floor and a mechanical dial gauge to measure the deflection of the floor beams. The dynamic test uses a 10kg sandbag to hit the floor from 0.305m in a free fall and an 80kg person dropping from the heel to impact the floor.

Field testing and laboratory testing complement each other, with laboratory testing predicting the worst case scenario and field testing validating the feasibility of laboratory results. However, both field and laboratory testing are time-consuming and costly and require financial support, and in some cases, cannot be considered the best testing method.

2.3.5 Parametric study of vibration

In order to quantify floor vibrations, many studies and experiments have chosen to apply several characteristic parameters. These characteristic parameters are presented below, mainly based on the literature of Davis et al. (2008).

According to Davis et al. (2008), the floor's vibration consists of dynamic and static responses. The natural frequency, damping ratio, and root mean square (RMS) acceleration are the critical components of the dynamic response of floor vibration, all of which are determined by acceleration response against time measurements.

Natural Frequencies

The floor system's natural frequencies (f_1 and f_2) were calculated in the frequency domain by picking the first two dominating peaks in the power spectrum. Due to the impulsive excitation, the contribution of higher-order multiples and torsional modes to the floor response is minimal (Johnson, 1994), and discussion in general studies have been limited to the fundamental frequency, which has the most excellent effect on the response of the floor system (Davis et al., 2008).

Damping Ratio

The greater the damping ratio, the faster the vibration decays and the shorter the duration; conversely, the smaller the damping ratio, the slower the decay of floor vibration, and the longer the duration, the longer the time humans feel uncomfortable. Based on structural dynamics, damping ratios are generally calculated in the frequency domain using the half-power bandwidth method and in the time domain using the logarithmic decay method. The half-power bandwidth approach cannot separate modal damping ratios for floor systems with closely spaced frequencies. Only the logarithmic decrement approach was applied (Davis et al., 2008).

RMS Acceleration

The values of the root mean square (RMS) of a floor's acceleration under vibration is generally obtained through software programs. In the study by Davis et al. (2008), the RMS values of acceleration were obtained by the procedure described in ISO 2631 (ISO, 1997) and without using weighted frequency components.

Static displacement

The static response of the floor is measured by the deflection of the central joist in the span, which is used to determine the floor system's static bending stiffness (Davis et al., 2008). The static deflection mainly reflects the displacement of the floor vibration and the static displacement of the floor in the field construction also directly reflects the vibration of the floor. The characteristic parameters of the static and dynamic response effectively quantify floor vibrations and contribute to studying solutions for CFS floor vibrations.

2.3.6 Methods for controlling vibration in CFS floors

Many studies have been conducted to offer possible ways of controlling the irritating vibrations of lightweight steel floors. Several lines of evidence suggest that The more extended the floor beam span, the lower the fundamental frequency and the lower the centre deflection (Davis et al., 2008). As low-frequency floors are prone to vibrations, in some modern buildings, the choice is made to reduce the span of light steel beams or to use more rigid beams to make the floor more stable. Another way to effectively increase the fundamental frequency and damping ratio and reduce deflection is to add a back plate to the frame with the end fixed to the wall studs (Xu, 2011). In the study by Nguyen (2013), the inherent frequency effect due to the structural elements' self-weight was eliminated by using a damper (as in Figure 16) to cancel the tuning. In addition, the frame conditions at the ends of the floor joists also affect vibration. The balloon frame provides a greater fundamental frequency and less deflection, giving better vibration performance than the platform frame. These methods of controlling floor vibrations are varied and have varying degrees of effectiveness.

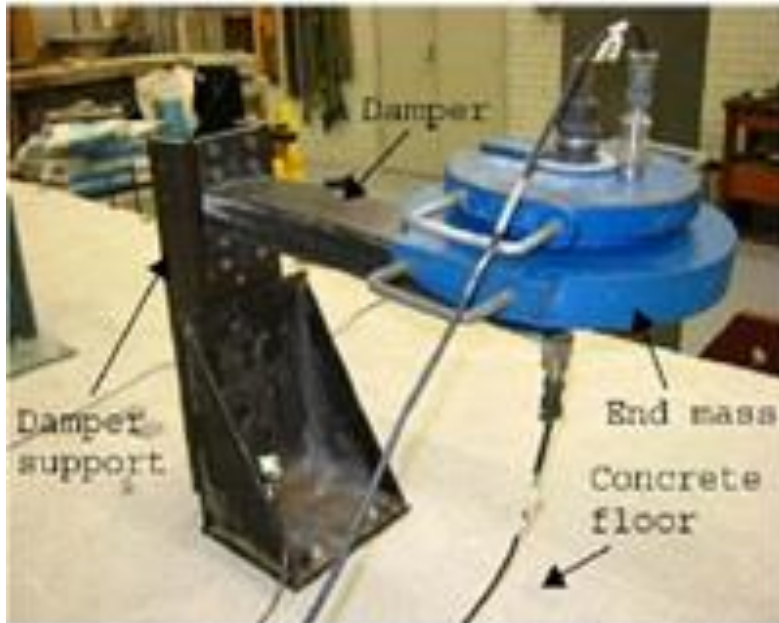


Figure 16. Damper attached to the flange of beam (Saidi et al., 2011).

In summary, current methods of controlling vibration in lightweight steel floors are mainly for single-section members. Nevertheless, little literature has been devoted to the details of floor vibration control for composite section members. Previous literature has shown that higher stiffness and lower centre deflection of built-up sections can reduce vibration. However, more research is still focused on the design and performance factors influencing the cross-sectional dimensions of composite section members. Very little has been done on the impact of their welding method on the floor system, particularly in terms of the intuitive impact on the whole floor system. Although Rasmussen et al. (2020) refer to the effect of welded joints on CFS beams, this is only for individual members. It is still unknown what results will occur when the members are placed into the floor system according to actual engineering requirements. Therefore, as composite CFS is increasingly used in residential applications, it is of interest that this report examining the effect of the welding method of built-up CFS beams on the vibration of floor systems can give helpful advice and guidance for modern construction.

3 METHODOLOGY

The primary method used in this project was the FEA method. Firstly, a structural sketch was made based on a site visit to the dwelling. A finite element model of the floor structure was built using Strand 7 based on the theoretical basis of structural mechanics. Finally, a footfall analysis was used to compare the results.

3.1 Theoretical methods

The study's theoretical basis is mainly the finite element analysis (FEA) method and the control variables method. FEA is a sophisticated structural engineering analysis method. Engineers and designers can get a better understanding of structural stress and strain distribution with FEA than they can with traditional analysis methods (Shaikh, 2012). In addition, Rinchen and Rasmussen (2019) have shown that this type of numerical modelling and analysis is now one of the most convenient ways to study CFS structures. Debney and Willford (2009) also indicated that finite element analysis (FEA) is a reliable and time-saving method for predicting the floor footprint response in both rectangular and non-rectangular frames (as in the example in Figure 17). The choice for this project was to use Strand 7 to build a finite element model and then use finite element analysis to obtain the vibration of the floor.

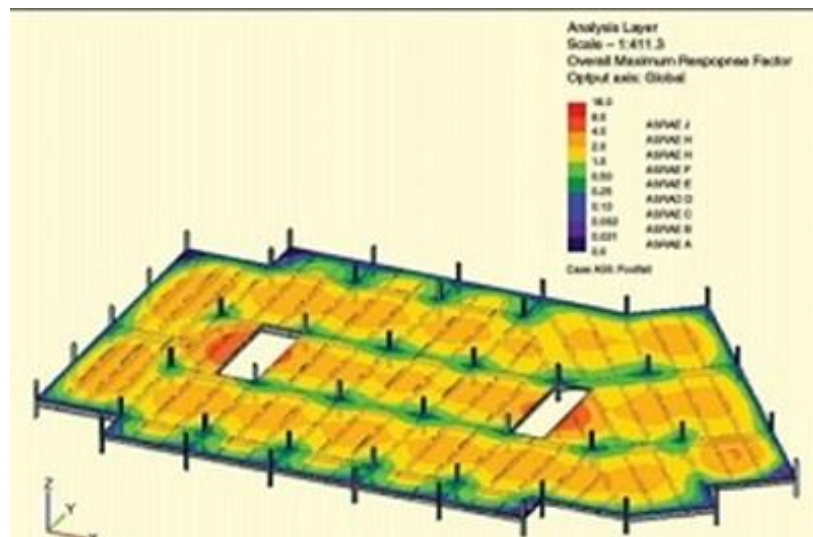


Figure 17. An irregular floor frame was subjected to a FEA (Debney & Willford, 2009).

For the different welding methods of CFS beams with back-to-back I-shaped sections, this project has chosen to use the controlled variable method to compare the vibration of different

welding situations more intuitively and scientifically. Firstly the welding situations are divided into three, as in Figure 3, the first with full composite action, the second with partial composite action, and the third with no composite action. The joists of the floor system are guaranteed to all be of the same C-open CFS. Then, separate finite element models are built to analyse the floor vibration using these three welding cases.

3.2 Site Survey

This project investigated a residential house under construction in Moorooka, Queensland, Australia, to get closer to reality. The internal structure of the floor is shown in Figure 18, which utilizes a hot rolled steel beam and a C-shaped CFS joist, which was investigated on-site and found to be a truss structure consisting of CFS bolted together. In addition, site construction staff said that to make the floor structure more stable and reduce vibration, the floor beams were chosen from hot-rolled steel, but this was more costly and labour intensive.



Figure 18. Construction site floor structure.

The structural model sketches for this project have been initially determined through site measurements and surveys. The floor beam span was set at 4500mm, the joist span at 4800mm, and the angle of the joist internal truss at 45°.

3.3 Validation of finite element models

This section will verify the feasibility of Strand 7 in this project from two aspects based on mechanical theory. The first part verifies the feasibility of idealizing the connection bolts with rigid links. The second part verifies whether the floor model built with Strand 7 is compatible with the structural mechanics.

3.3.1 Verification of fastening methods

To demonstrate the performance of a bolted connection idealized by a rigid link, a model of the connection with a rigid link was built and analysed in Strand 7. The following is the modelling and validation process.

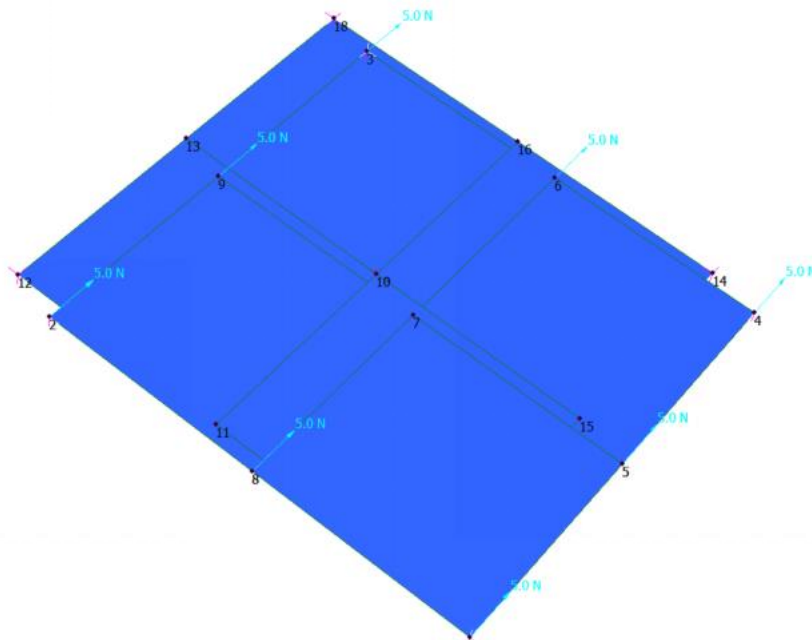


Figure 19. Verification of rigid links instead of bolted connections.

To demonstrate the performance of a bolted connection idealized by a rigid link, a model of the connection with a rigid link was built and analysed in Strand 7. As shown in Figure 19, the verification model consists of two rectangular plates with four corners connected by rigid links, i.e., points 1, 2, 3, and 4 are connected to points 17, 12, 18, and 14, respectively. A force of 5N in the y-axis direction is then applied at points 1, 2, 3, 4, 5, 6, 8, and 9, respectively. If the rigid link can be used instead of the bolted connection, the bearing reaction force at the other plate will also produce the same magnitude and force in the same direction. The resultant force at each point in the Y-axis is shown in Table 1, which shows that the combined force at the four

points of the connection is $10 \times 4 = 40\text{N}$, and the force applied to the other plate is $5 \times 8 = 40\text{N}$ of equal magnitude and opposite direction. From this, it can be seen that the verification is valid.

	FY (N)
Node 14	-1.000000×10^1
Node 12	-1.000000×10^1
Node 18	-1.000000×10^1
Node 17	-1.000000×10^1
Node 10	0.000000×10^0
Node 5	0.000000×10^0
Node 9	0.000000×10^0
Node 1	0.000000×10^0
Node 4	0.000000×10^0
Node 15	0.000000×10^0
Node 7	0.000000×10^0
Node 2	0.000000×10^0
Node 13	0.000000×10^0
Node 11	0.000000×10^0
Node 16	0.000000×10^0
Node 3	0.000000×10^0
Node 8	0.000000×10^0
Node 6	0.000000×10^0

Table 1. Value of the support reaction force in the Y-axis

3.3.2 Verification of support reaction forces

To verify that the modeling of the entire floor system is complex logical, and reasonable, one of the floors in this project was used for analysis. Figure 20 shows the floor model built-in Strand 7 with a surface force of 2 kPa applied in the Y-axis direction. The whole floor area is $4.8 \times 4.5 \times 2 + 0.002 \times 4.5 \times 3 + 0.096 \times 2 \times 4.5 = 44.091\text{m}^2$. It has a theoretical support reaction force of $44.091 \times 2 = 88.182\text{KN}$. The actual reaction force solved is shown in Table 2, and the combined force is 88.16KN using Excel. The floor model developed with Strand 7 is feasible because it is within the margin of error and in general agreement with the theoretical response force.

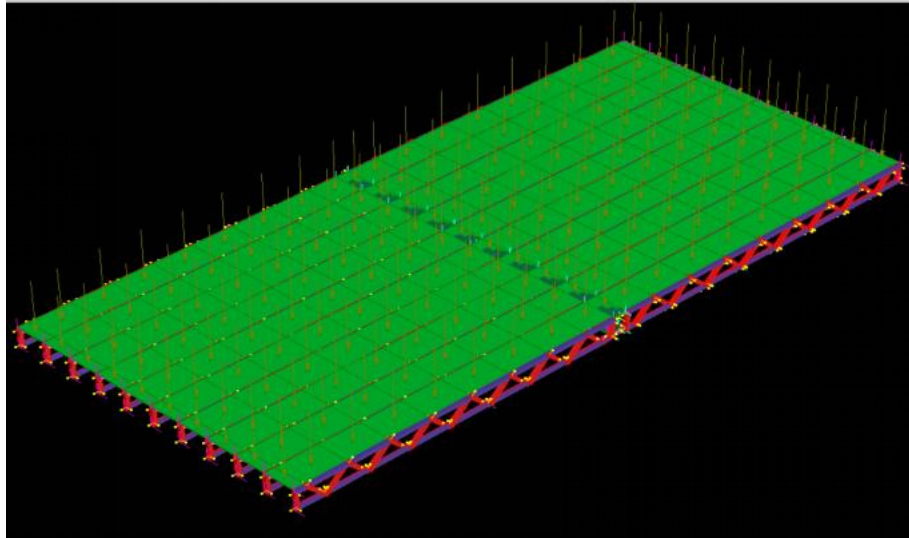


Figure 20. Floor model of the Strand 7.

Model: Verification of bearing reaction forces
Result type: Node reaction
Coordinate system: Global XYZ
Freedom case: 1: Freedom Case 1
Result case: 1: Load Case 1
Group: Model
Properties: All

	FY (kN)
Node 298	-9.931522x 10 ⁰
Node 108	-9.931522x 10 ⁰
Node 26	-8.535634x 10 ⁰
Node 7	-8.535634x 10 ⁰
Node 24	-6.492937x 10 ⁻¹
Node 5	-6.492937x 10 ⁻¹
Node 88	-5.737081x 10 ⁻¹
Node 278	-5.737081x 10 ⁻¹
Node 422	-4.196081x 10 ⁻¹
Node 426	-4.196081x 10 ⁻¹
Node 468	-3.987759x 10 ⁻¹
Node 768	-3.987759x 10 ⁻¹
Node 760	-2.606718x 10 ⁻¹
Node 460	-2.606718x 10 ⁻¹
Node 761	-2.545346x 10 ⁻¹
Node 461	-2.545346x 10 ⁻¹
Node 759	-2.505925x 10 ⁻¹
Node 459	-2.505925x 10 ⁻¹
Node 466	-2.496246x 10 ⁻¹
Node 766	-2.496246x 10 ⁻¹
Node 762	-2.481822x 10 ⁻¹
Node 462	-2.481822x 10 ⁻¹
Node 465	-2.463928x 10 ⁻¹
Node 765	-2.463928x 10 ⁻¹
Node 763	-2.449301x 10 ⁻¹
Node 463	-2.449301x 10 ⁻¹
Node 464	-2.438998x 10 ⁻¹
Node 764	-2.438998x 10 ⁻¹
Node 467	-2.380760x 10 ⁻¹
Node 767	-2.380760x 10 ⁻¹
Node 1779	-4.707807x 10 ⁻²
Node 1019	-4.707807x 10 ⁻²
Node 1058	-3.772272x 10 ⁻²
Node 1818	-3.772272x 10 ⁻²
Node 1098	-8.255814x 10 ⁻³
Node 1858	-8.255814x 10 ⁻³
Node 1819	-4.430312x 10 ⁻³
Node 1059	-4.430312x 10 ⁻³
Node 446	0.000000x 10 ⁰
Node 430	0.000000x 10 ⁰
Node 1018	1.346843x 10 ⁻¹
Node 1778	1.346843x 10 ⁻¹
Node 288	1.407633x 10 ⁻¹
Node 98	1.407633x 10 ⁻¹
Node 979	1.597789x 10 ⁻¹

Node 1739	1.597789x 10 ⁻¹
Node 6	1.611703x 10 ⁻¹
Node 25	1.611703x 10 ⁻¹
Node 22	7.984582x 10 ⁻¹
Node 3	7.984582x 10 ⁻¹
Node 258	1.137775x 10 ⁰
Node 68	1.137775x 10 ⁰
Node 425	1.826168x 10 ⁰
Node 421	1.826168x 10 ⁰
Node 758	1.891977x 10 ⁰
Node 568	1.891977x 10 ⁰
Node 268	2.148105x 10 ⁰
Node 78	2.148105x 10 ⁰
Node 559	2.150283x 10 ⁰
Node 749	2.150283x 10 ⁰
Node 757	2.177407x 10 ⁰
Node 567	2.177407x 10 ⁰
Node 753	2.179989x 10 ⁰
Node 563	2.179989x 10 ⁰
Node 754	2.180040x 10 ⁰
Node 564	2.180040x 10 ⁰
Node 562	2.183583x 10 ⁰
Node 752	2.183583x 10 ⁰
Node 755	2.185964x 10 ⁰
Node 565	2.185964x 10 ⁰
Node 561	2.189040x 10 ⁰
Node 751	2.189040x 10 ⁰
Node 560	2.198895x 10 ⁰
Node 750	2.198895x 10 ⁰
Node 756	2.204832x 10 ⁰
Node 566	2.204832x 10 ⁰
Node 4	2.435147x 10 ⁰
Node 23	2.435147x 10 ⁰
Node 1738	2.857911x 10 ⁰
Node 978	2.857911x 10 ⁰
Node 939	3.094466x 10 ⁰
Node 1699	3.094466x 10 ⁰
Node 1859	1.488316x 10 ¹
Node 1099	1.488316x 10 ¹
Node 1138	1.560354x 10 ¹
Node 1898	1.560354x 10 ¹

Table 2. Node reaction results.

3.4 Finite element modelling of flooring structures

3.4.1 Geometrical modelling

The CFS floor structure consists of three main parts, respectively: back-to-back I-section beams, joist, and floor. The top view of the floor model is shown in Figure 21, with a floor beam span of 4.5m and a joist span of 4.8m spaced at 0.45m. The front view of the floor model is shown in Figures 22, 23, and 24 for no composite action, partial composite action, and full composite action, respectively. These three cases represent the transition from no soldering to complete soldering. These three cases represent the transition from unwelded to fully welded, with the intermediate cases being fastened with bolts at every $4.5/4 = 1.125\text{m}$.

Moreover, it can be seen from the drawing that the joist forms a truss structure with an angle of 45° between the inclined members and the horizontal construction, and the distance between the two horizontal joists is 300mm. In addition, the two members of the back-to-back beam are spaced 2 mm apart, and the joist is also spaced 2 mm apart from the beam. The total length of the floor model is, therefore, 9.798m with a width of 4.5m.

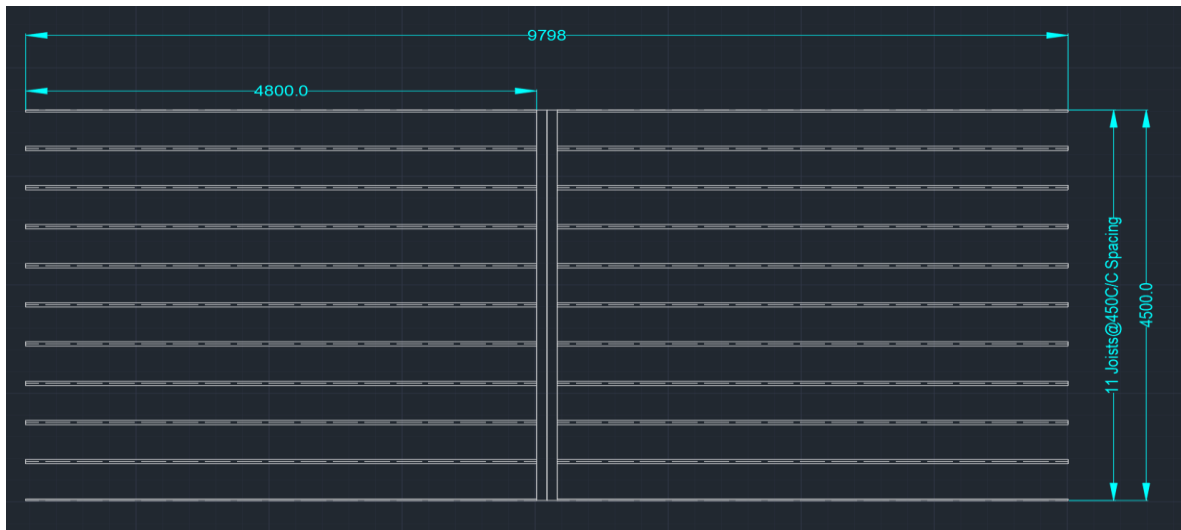


Figure 21. Top view of the floor (in mm).

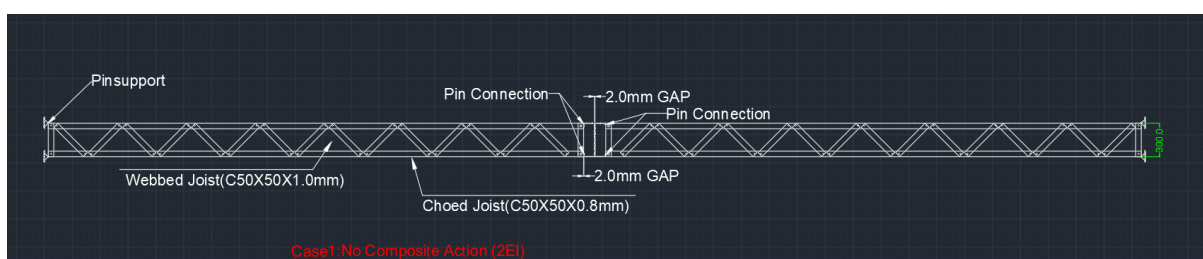


Figure 22. Front view of the floor (Case 1: No Composite Action).

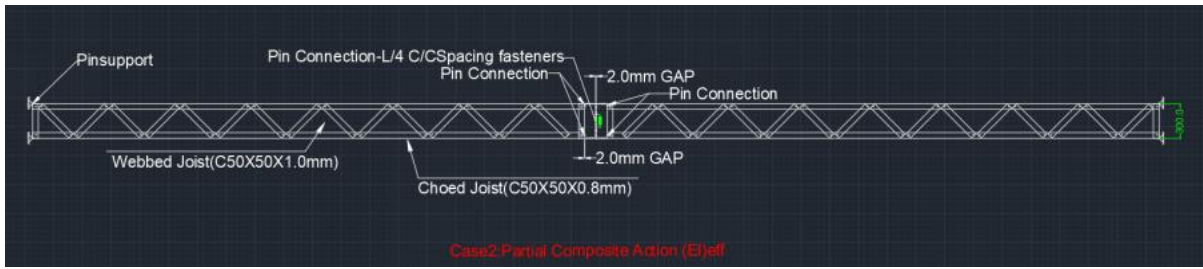


Figure 23. Front view of the floor (Case 2: Partial Composite Action).

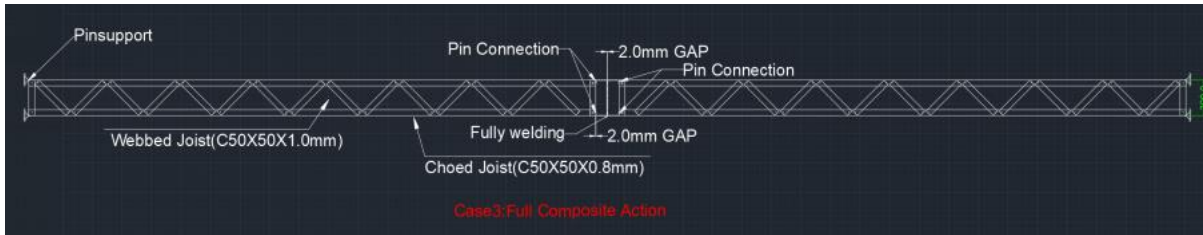
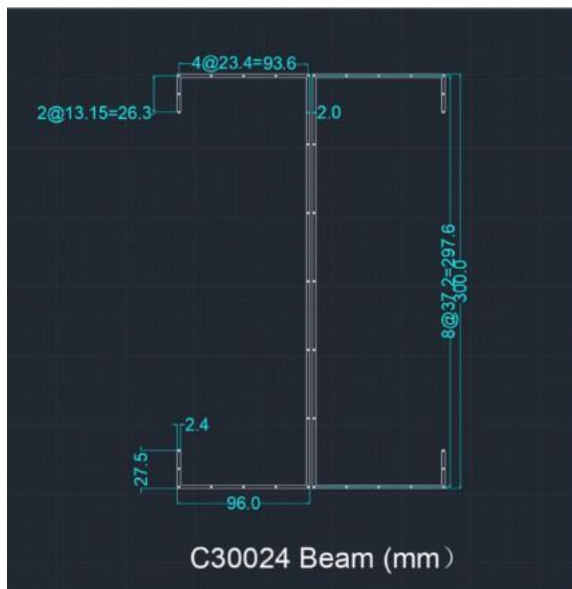


Figure 24. Front view of the floor (Case 3: Full Composite Action).

In addition, as CFS C30024 was chosen as the beam material for this project, Figure 25 shows the cross-section and dimensions of the back-to-back I-shaped CFS beam using CAD according to the standard. The horizontal joist is called "Chord" and is made of CFS C50*50*1, i.e., 50 mm long, 50 mm wide, and 1 mm thick, with the dimensions and properties shown in Figure 26. The inclined joist called "web," as in Figure 27 is made of CFS C50*50*0.5.



(a) Beam section and dimension

Zed and Cee Sections - Dimensions and properties

Dimensions of Zeds & Cees

Catalogue number	t mm	D mm	Mass per unit length kg/m	E mm	F mm	L mm	B mm	Cees L mm
ZAC10010	1.0	102	1.79	53	49	12.5	51	12.5
ZAC10012	1.2	102	2.10	53	49	12.5	51	12.5
ZAC10015	1.5	102	2.62	53	49	13.5	51	13.5
ZAC10019	1.9	102	3.29	53	49	14.5	51	14.5
ZAC15012	1.2	152	2.89	65	61	15.5	64	14.5
ZAC15015	1.5	152	3.59	65	61	16.5	64	15.5
ZAC15019	1.9	152	4.51	65	61	17.5	64	16.5
ZAC15024	2.4	152	5.70	66	60	19.5	64	18.5
ZAC20015	1.5	203	4.49	79	74	15.0	76	15.5
ZAC20019	1.9	203	5.74	79	74	18.5	76	19.0
ZAC20024	2.4	203	7.24	79	73	21.5	76	21.0
ZAC25019	1.9	254	4.50	79	74	18.0	76	18.5
ZAC25024	2.4	254	6.16	79	73	21.0	76	20.5
ZAC30024	2.4	300	10.09	100	93	27.0	96	27.5
ZAC30030	3.0	300	13.76	100	93	31.0	96	31.5
ZAC35030	3.0	350	15.23	120	121	30.0	120	30.0

(b) Zed and Cee Sections–Dimensions and Properties

Figure 25. Beam sections and dimensions.

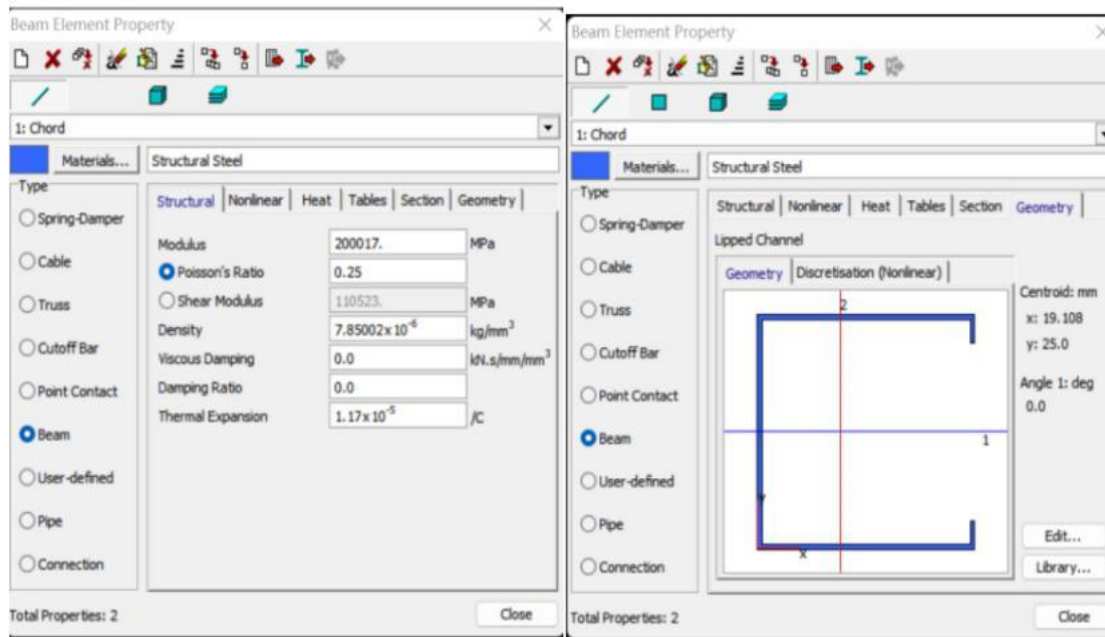


Figure 26. Dimensions and properties of Chord.

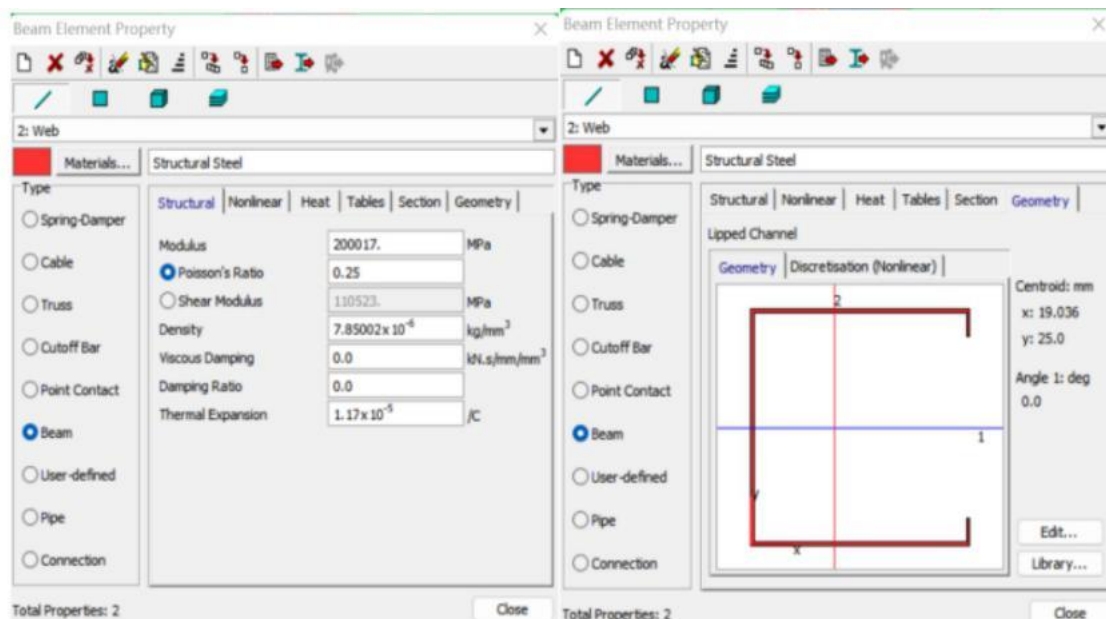


Figure 27. Dimensions and properties of Web.

The following begins modeling the structure in Strand 7 by first creating a two-dimensional floor structure based on the co-ordinate points in Table 3 and connecting the points using line elements. The two-dimensional model is then transformed into a three-dimensional model using Strand 7's Copy and Extrude. The beam is then turned into a plate element using "Subdivide." The properties of the elements are then set according to the nature of the parts. The model of the steel structure without the floor is shown in Figure 28.

	A	B	C	D	E	F	G	H	I	J	K	L	M	N	O	P	Q	R	S	T
1																				
2		1	2	3	4	5	6	7	8	9	10	11	12	13	14	15	16	17	18	19
3	Z	-94.6	-94.6	-94.6	-71.2	-47.8	-24.4	-1	-1	-1	-1	-1	-1	-1	-24.4	-47.8	-71.2	-94.6	-94.6	-94.6
4	Y	-122.5	-135.05	-148.8	-148.8	-148.8	-148.8	-148.8	-99.2	-49.6	0	49.6	99.2	148.8	148.8	148.8	148.8	148.8	135.05	122.5
5	X	0	0	0	0	0	0	0	0	0	0	0	0	0	0	0	0	0	0	0
6																				
7		20	21	22	23	24	25	26	27	28	29	30	31	32	33	34	35	36	37	38
8	Z	94.6	94.6	94.6	71.2	47.8	24.4	1	1	1	1	1	1	1	24.4	47.8	71.2	94.6	94.6	94.6
9	Y	-122.5	-135.05	-148.8	-148.8	-148.8	-148.8	-148.8	-99.2	-49.6	0	49.6	99.2	148.8	148.8	148.8	148.8	148.8	135.05	122.5
10	X	0	0	0	0	0	0	0	0	0	0	0	0	0	0	0	0	0	0	0
11																				
12		419	420	421	422	423	424	425	426											
13	X	0	0	0	0	0	0	0	0											
14	Y	150	-150	-150	150	150	-150	-150	150											
15	Z	97.8	97.8	4897.8	4897.8		-97.8	-97.8	-4897.8											
16		427	428	429	430	431	432	433	434	435	436	437	438	439	440	441	442			
17	X	0	0	0	0	0	0	0	0	0	0	0	0	0	0	0	0			
18	Y	-150	-150	-150	-150	-150	-150	-150	-150	150	150	150	150	150	150	150	150			
19	Z	247.8	847.8	1447.8	2047.8	2647.8	3247.8	3847.8	4447.8	5047.8	5647.8	6247.8	6847.8	7447.8	8047.8	8647.8	9247.8			
20																				
21		443	444	445	446	447	448	449	450	451	452	453	454	455	456	457	458			
22	X	0	0	0	0	0	0	0	0	0	0	0	0	0	0	0	0			
23	Y	-150	-150	-150	-150	-150	-150	-150	-150	150	150	150	150	150	150	150	150			
24	Z	-247.8	-847.8	-1447.8	-2047.8	-2647.8	-3247.8	-3847.8	-4447.8	-5047.8	-5647.8	-6247.8	-6847.8	-7447.8	-8047.8	-8647.8	-9247.8			

Table 3. Coordinates of modelling points.

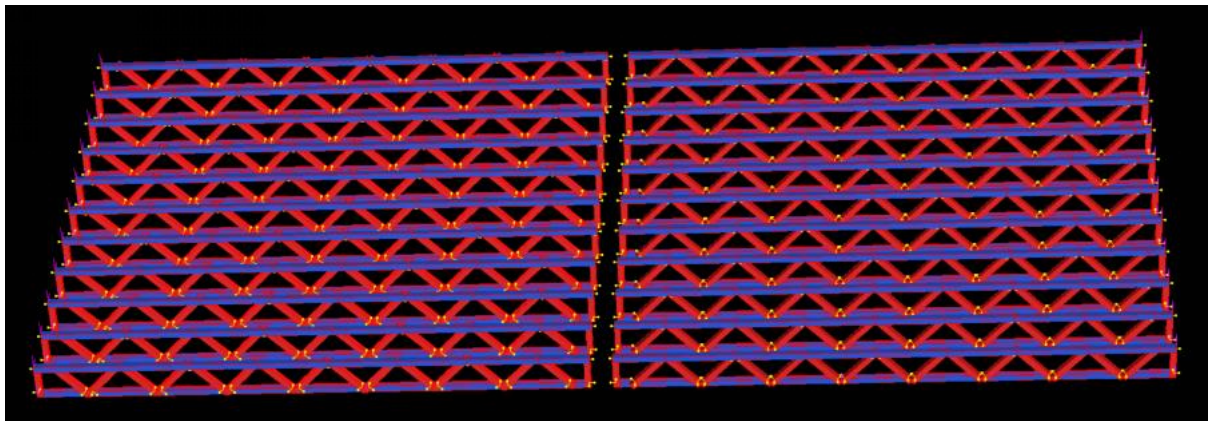


Figure 28. Finite element model of the internal structure of the floor.

Finally, a wooden floor of 15 mm thickness was laid on top of the steel floor structure and adjusted to the proper position using the "Off Set" in Strand 7. Figure 29 depicts the floor's final geometric model.

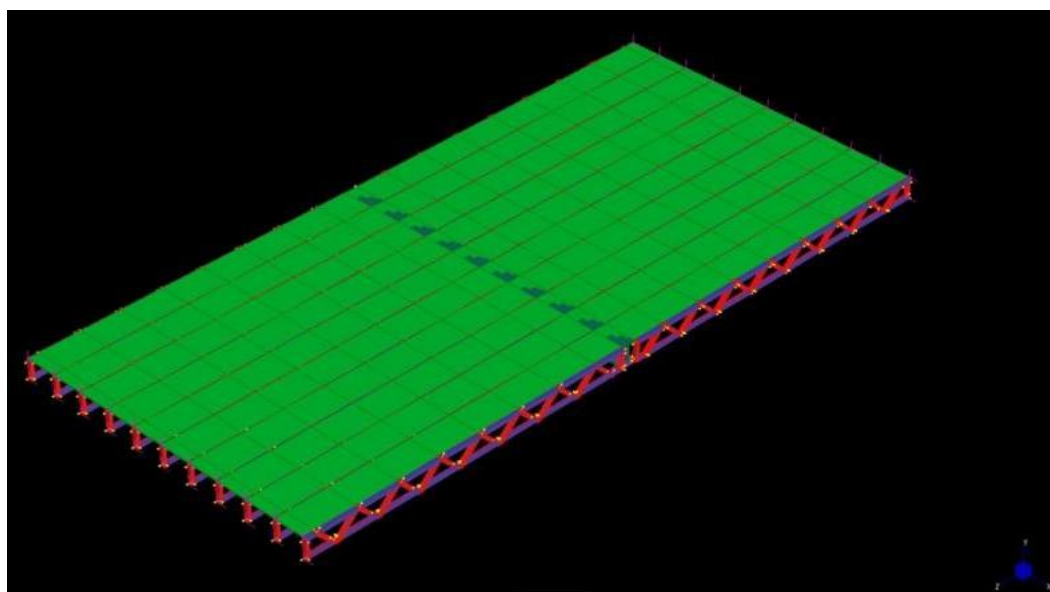


Figure 29. Finite element model of the floor.

3.4.2 Connection point modelling

The steel is usually bolted to each other on a natural CFS floor. In this project, the bolted parts are replaced by rigid links, and the shear forces at the truss are released to simulate a realistic structure. The feasibility of idealizing the bolts and rigid links has been verified in 3.3.1. As the practical effects of welding and bolting are similar, rigid links are also used to simulate the effects of welding for beams of built-up steel. However, because there is no method to mimic the minor wear induced by friction between individual components, this model can only reflect the situation under perfect circumstances.

3.4.3 Element types and meshing

In the modeling process, line elements are used for the joist part and plate elements for the beam part. As the CFS joist elements are thinner and more complex than the beam elements, and as the main focus of this project is on the effect of different beams, the line elements are most suitable.

A minimum number of plate elements is used for the beam section. The time required to solve the model varies due to the accuracy of the different number of elements. In the floor model with different numbers of elements, it was found that the higher the number of elements, the larger the displacements obtained and eventually stabilized, as shown in Figure 31. Table 4 shows that the higher the number of elements, the longer the running time for the calculation. However, the difference in displacement results was slight, so choosing the smallest number of elements saves modeling and calculation time, and the results are equally informative.

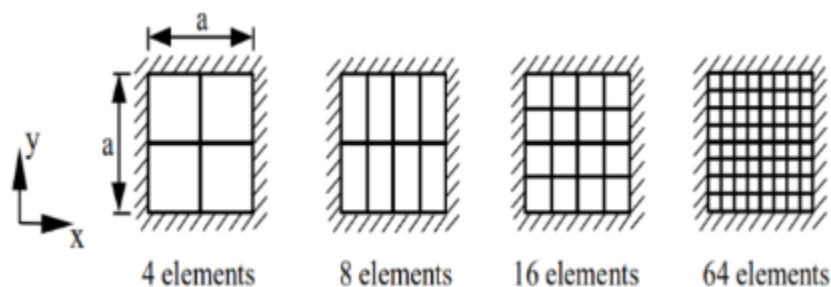


Figure 30. Number of elements.

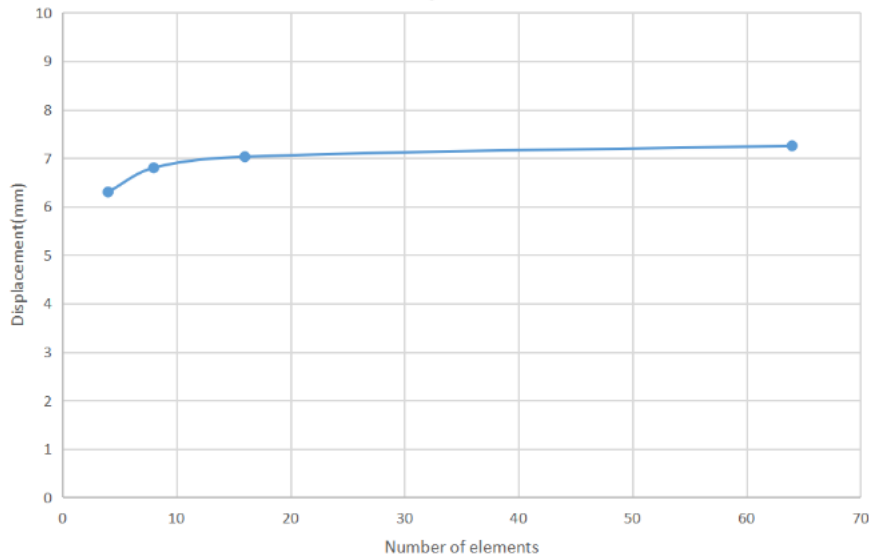


Figure 31. Floor centre displacement for different element models.

Number of elements	4	8	16	64
Displacement (mm)	6.300356	6.799626	7.02824	7.254394
Simulation time(s)	1.781 Seconds (0:00:02)	5.172 Seconds (0:00:05)	8.625 Seconds (0:00:09)	55.078 Seconds (0:00:55)

Table 4. Running times for different numbers of elements.

3.4.4 Boundary conditions

To enhance the effects of floor vibrations by further compounding the problem and reducing the limits on the floor system. The boundary limiting conditions are described primarily based on the axial settings in the lower right-hand corner of Figure 29. Based on the situation, the floor slab is not constrained by deflection in all directions. Restriction in the X and Y-axis directions for joists. Restriction in all directions for beams at one end to simulate essential support and release displacement in one direction at the other end to intensify vibration effects by restricting displacement in the Y and Z-axis directions only.

3.4.5 Application of loading forces

The loading here simulates the footfall of an adult weighing 50 kg on the floor to simulate floor vibrations properly. Assuming that four such adults stand on one square meter, they weigh $50 \times 4 = 200\text{kg}$, which is approximately 2 kN. Therefore a surface force of 2 kPa needs to be applied to the floor surface in the finite element model to obtain Figure 32.

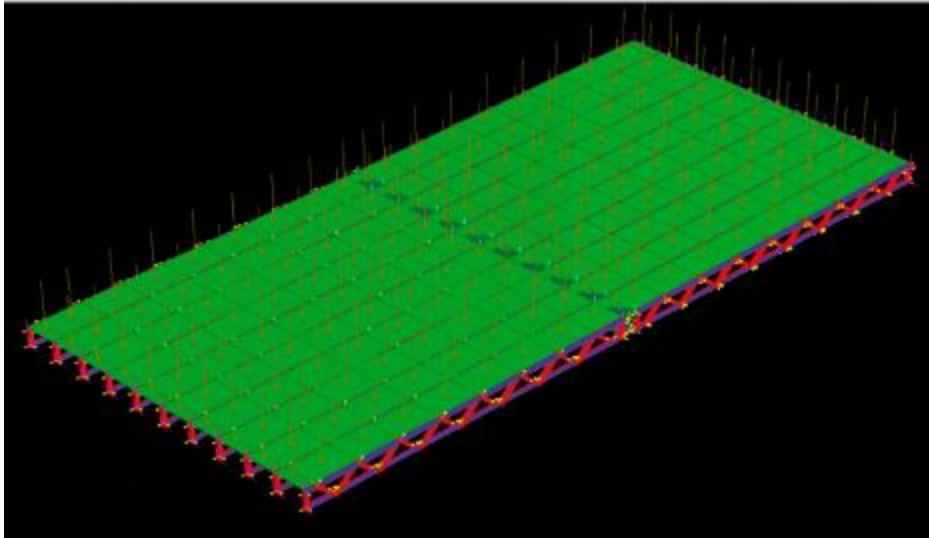


Figure 32. Floor structure after adding load.

4 FOOTFALL ANALYSIS RESULTS

This chapter shows the results obtained from the analysis of the finite element models using the footstep analysis method. The three models are given different names to make the FEA more accessible and comparable. "Case 1" refers to a composite beam that is not welded and has no composite action; "Case 2" refers to a partially bolted beam with partial composite action, whereas "Case 3" refers to a fully welded beam with full composite action. And the beams used for the floor in the three cases are shown in Figure 33. The vibration of the model is described below in three aspects: natural frequency, dynamic response, and static displacement.

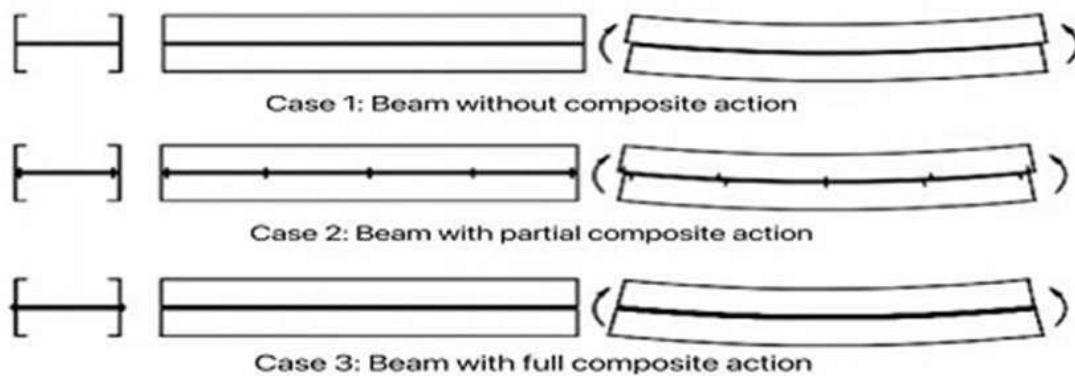


Figure 33. Three cases of beams.

4.1 Natural Frequency

The natural frequency of floor vibrations affects how humans perceive floor vibrations. Human beings feel the vibration most strongly when the natural frequency of the floor is between 4 Hz and 8 Hz (Grether, 1971). For this reason, it is desirable to have a natural frequency of more than 10 Hz for general construction.

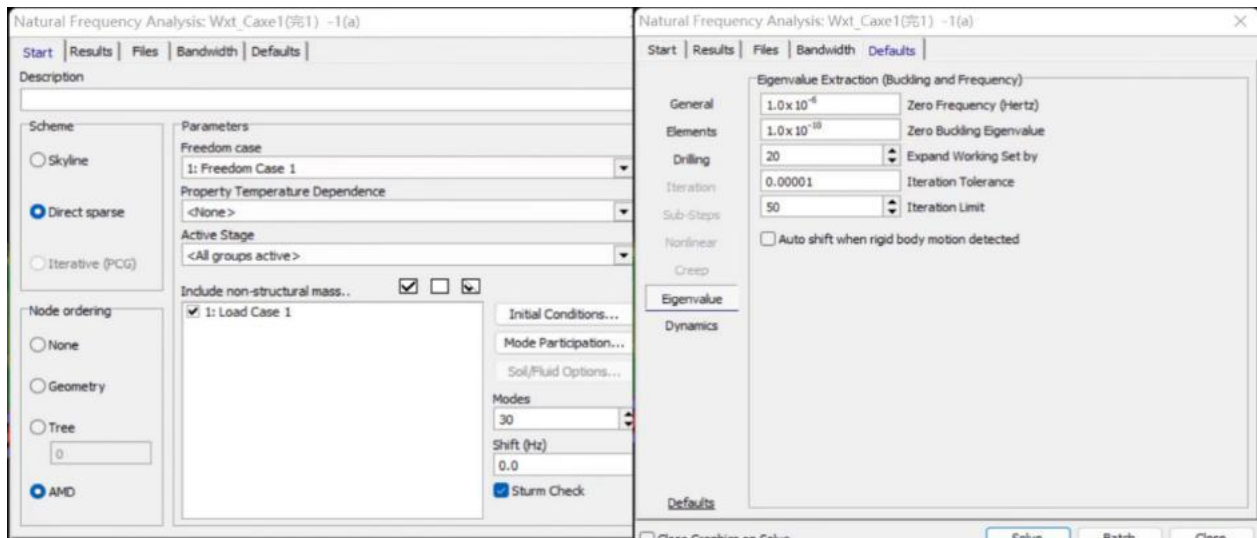


Figure 34. Natural frequency solver and setup details.

For this project, the model was analysed for three cases using the natural frequency analysis solver in Strand 7 (see Figure 34). All solution procedures are shown in Appendix A. The first analysis was a floor model of a CFS beam without composite action, which was found to have a natural frequency range of 7.1784 Hz to 15.26 Hz using the solver. Four natural frequencies within this range were then selected to view the floor model as shown in Figures 35 and 36.

One example was between 4 and 8 Hz, two cases between 8 and 10 Hz, and one case more prominent than 10 Hz were chosen. From Figure 34, it can be seen that when the natural frequency is 7.63039 Hz, the maximum displacement of the floor is approximately 0.468 mm; at a natural frequency of 8.926 Hz, the maximum displacement is approximately 0.229 mm. It can be seen that at this point, the floor displacement decreases as the natural frequency increases. However, as shown in Figure 35, the natural frequencies of 9.11511 Hz and 12.7273 Hz are 0.603 mm and 1.752 mm, respectively, where the displacements increase as the natural frequency increases. Natural frequencies beyond 10 Hz, on the other hand, are less detectable to humans, implying that natural frequency displacements have a more negligible effect on the human body.

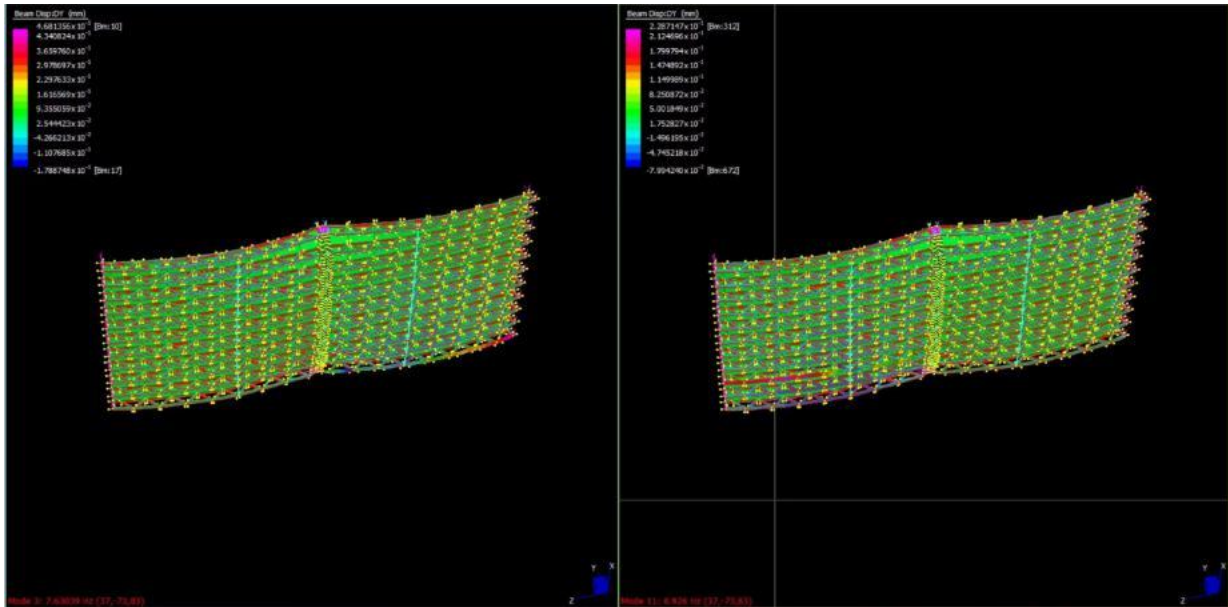


Figure 35. Floor model with natural frequencies at 7.63039 Hz and 8.926 Hz respectively (Case 1).

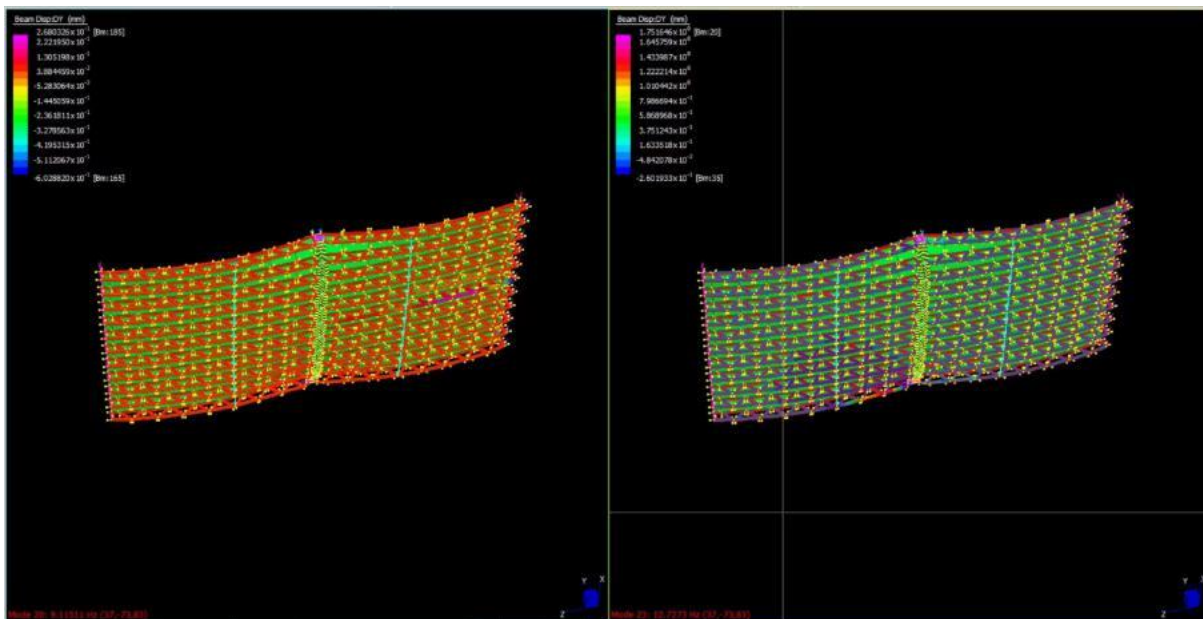


Figure 36. Floor model with natural frequencies at 9.11511 Hz and 12.7273 Hz respectively (Case 1).

The exact solver was used to analyse the floor model with a partially compound-acting beam, and the solution procedure is shown in the appendix A. The solver gives it a natural frequency range of 9.1495 Hz to 11.1267 Hz. As shown in Figure 37 for the floor model at 9.1495 Hz and 11.1261 Hz, the floor displacements are 0.00253 mm and 0.00234 mm, respectively.

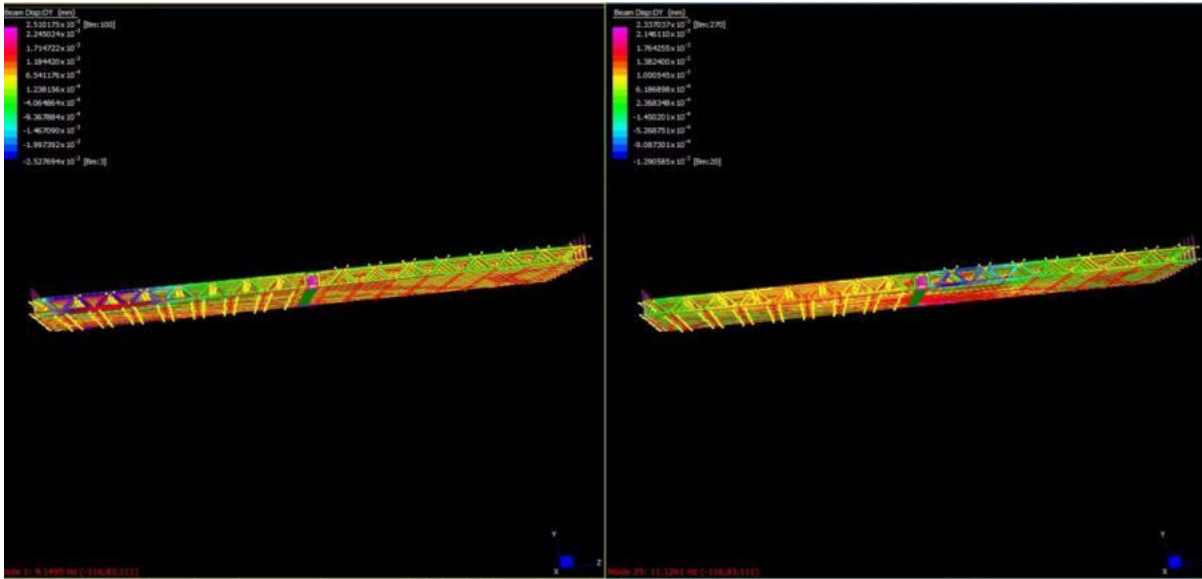


Figure 37. Floor model with natural frequencies at 9.1495 Hz and 11.1261 Hz respectively (Case 2).

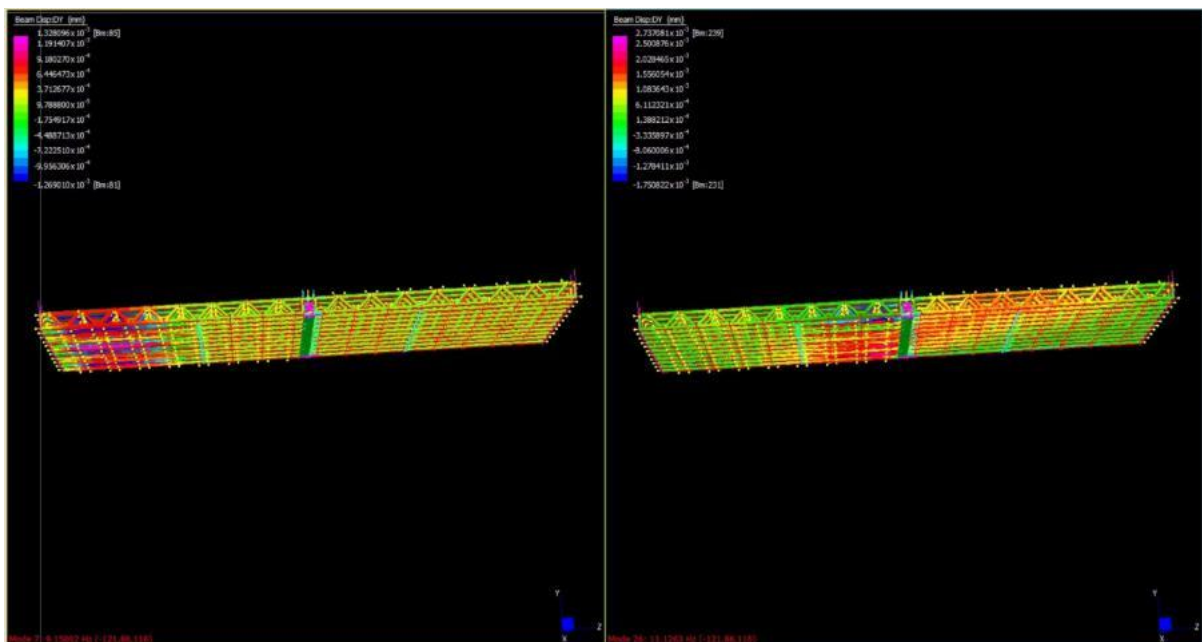


Figure 38. Floor model with natural frequencies at 9.15002 Hz and 11.1263 Hz respectively (Case 3).

For the floor model with a fully composite acting beam, the solution analysis yielded a natural frequency range of 9.1495 Hz to 11.1267 Hz and the solution procedure is shown in the Appendix A. As shown in Figure 38 for the floor models at 9.15002 Hz and 11.1263 Hz respectively, the floor displacements were 0.00133 mm and 0.00274 mm respectively.

The analysis of the natural frequencies shows that the natural frequencies of the floor without composite action beams are lower than in the other two cases and that the natural frequency range is essentially the same in the other two cases. Furthermore, with a non-composite active beam, the minimum natural frequency of the floor is less than 8 Hz, when humans are more sensitive to vibrations that are not suited for practical procedures. In contrast, the minimum natural frequency for both partially and fully composite beams is 9.1495 Hz, greater than 8 Hz, and can be used in practical engineering.

4.2 Harmonic Response

Harmonic response, a constant frequency-based analysis, is often used in Strand 7 to analyse floor vibrations. Here the harmonic response analysis will be carried out using the solver as in Figure 39. The response factor, peak acceleration, and peak displacement will be calculated from the equations and then plotted for comparison.

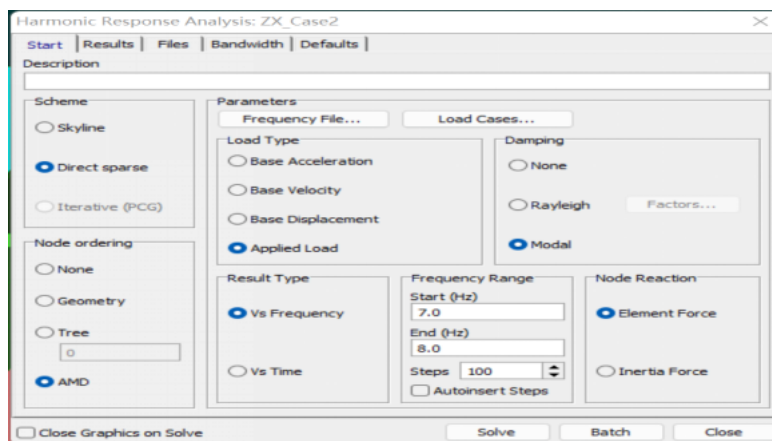


Figure 39. Harmonic response solver.

The floor without composite action beams was first examined for the fourth harmonic response based on the results of the natural frequencies of the floor and the vibrations created by human walking, and the parameter intervals are displayed in Table 5. The data obtained were entered into an Excel sheet, and the linear acceleration and total RMS Acceleration (SRSS) were calculated using the following formulae. The peak acceleration of individual harmonics is known as $A_{h,Peak}$.

$$\text{Linear Acceleration Sum} = \sum_{\text{Harmonics}} A_{h,Peak} \quad (1)$$

$$\text{Total RMS Acceleration} = \sqrt{\sum_{\text{Harmonics}} A_{h,RMS}^2}$$

(2)

$$A_{h,RMS} = \frac{A_{h,Peak}}{\sqrt{2}} \quad (3)$$

Harmonic	Start(Hz)	End(Hz)
First	1	2.8
Second	2	5.6
Third	3	8.4
Fourth	4	11.2

Table 5. Parameters for four executions of the Harmonic Response solver.

The results were calculated and plotted as a graph in Figure 40, and the data in Excel are shown in the Appendix B. The horizontal coordinate of the curve is the natural frequency interval, the first interval is 1.8 Hz the next three are multiples of 1.8, so they are all based on 1.8; the vertical coordinate is the value of the acceleration produced. The results are mainly observed in the fourth harmonic analysis, and the peaks are found. The graph shows two peaks in acceleration, in the third and fourth analysis, respectively, with a maximum acceleration of $1.12 \cdot 10^3 \text{ mm/s}^2$, the third at 2.55, i.e., $2.55 \cdot 3 = 7.64 \text{ Hz}$, and the fourth at 1.91, i.e., $1.91 \cdot 4 = 7.64 \text{ Hz}$.

Since the third analysis was carried out in the interval from 3 Hz to 8.4 Hz and the fourth in the interval from 4 Hz to 11.2 Hz, there was overlap so that both analyses produced a maximum in the same place.

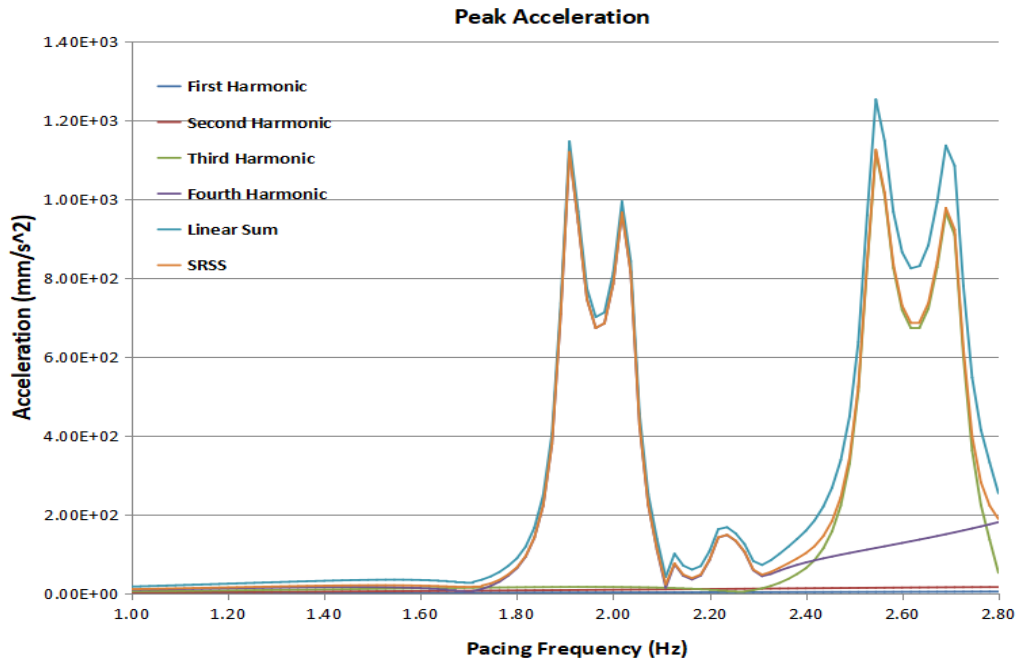


Figure 40. Peak Acceleration (Case 1).

Next, the response factor is solved according to the equation. The ratio of the peak value to the root mean square of the sine curve is used to compute the amplitude baseline response factor.

$$R_{\text{base}} = \begin{cases} \sqrt{2} \frac{1}{100\sqrt{f}}, & f < 4\text{Hz} \\ \sqrt{2} \frac{1}{200}, & 4\text{Hz} \leq f \leq 8\text{Hz} \\ \sqrt{2} \frac{1}{200} \frac{f}{8}, & 8\text{Hz} < f \end{cases} \quad (4)$$

The following is the response factor equation:

$$R = \frac{a_{\text{vertical}}}{a_{R=1}} \quad (5)$$

And $a_{R=1} = R_{\text{base}}$.

Furthermore,, the graph necessitates the use of the following equation to calculate the overall response factor.

$$R_{\text{total}} = \sqrt{R_1^2 + R_2^2 + R_3^2 + R_4^2} \quad (6)$$

The calculated response factor image is plotted in Figure 41, which has the exact horizontal coordinates as Figure 40 for the natural frequency intervals; the vertical coordinates are for the response factor. Using Excel in the same way to find the peak value, it was found that the maximum value occurred at the natural frequency of 7.64 Hz in the third and fourth analyses, with a response factor of 1.58×10^5 .

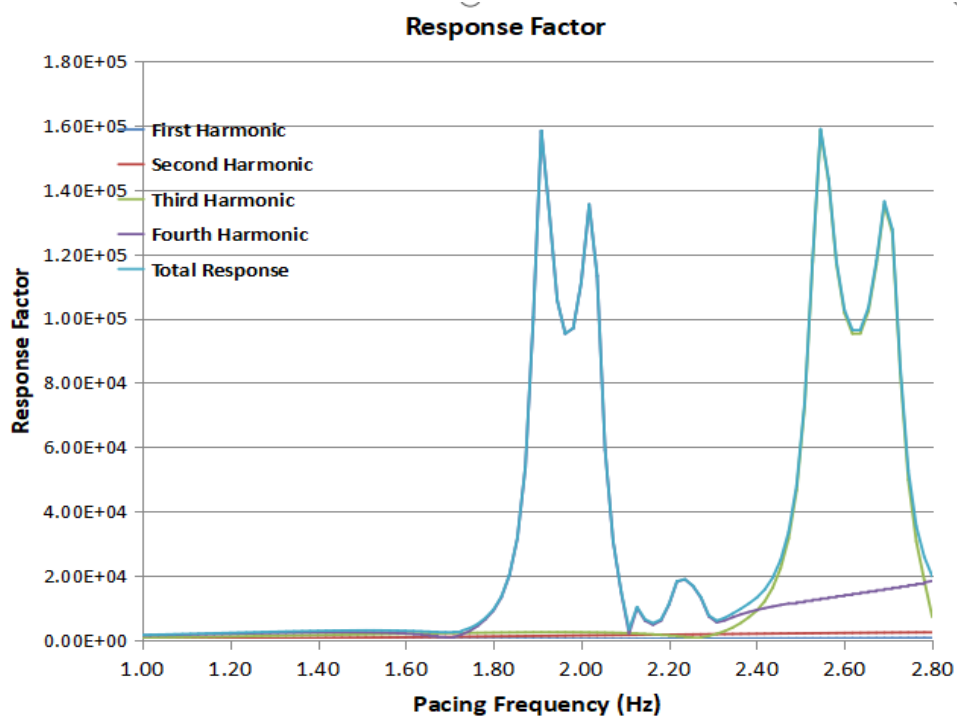


Figure 41. Response Factor (Case 1).

Solving for displacement has the same considerations and uses the same methods as solving for acceleration. Similar to the previous two analyses, the maximum is derived as a displacement of 4.86×10^{-1} mm at 7.64 Hz (see Figure 42). It can be seen that this value is relatively small and is largely ignored in realistic engineering.

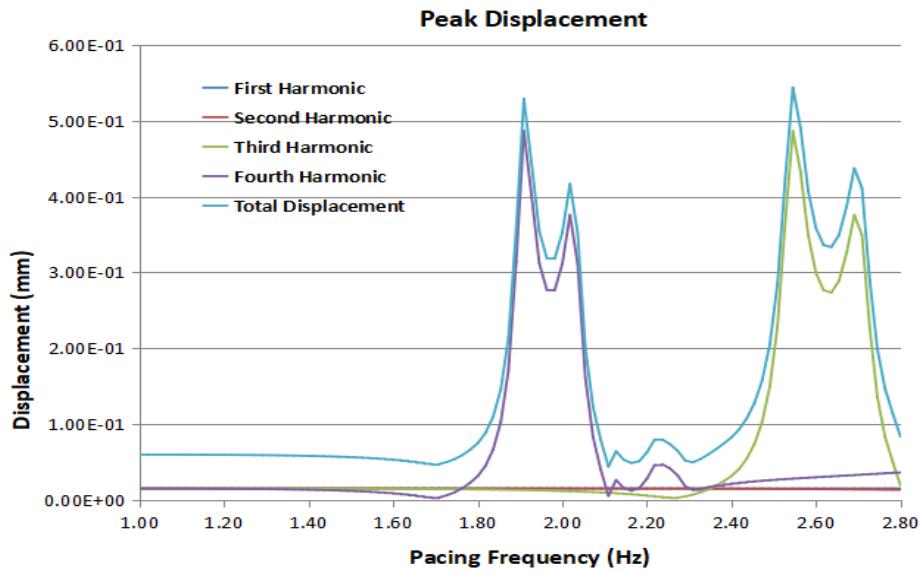


Figure 42. Peak Displacement (Case 1).

Similarly, for floors with partially acting beams, the same analysis as in Case 1 was carried out by first solving with the solver and then plotting the curves after substituting the formulae in an Excel sheet respectively; the resulting curves are shown in Figures 43, 44 and 45. The peaks all occur at the natural frequency of 11.13 Hz, with a maximum acceleration of 5.37 mm/s^2 , a maximum response factor of 5.46×10^2 , and a maximum displacement of $1.1 \times 10^{-3} \text{ mm}$.

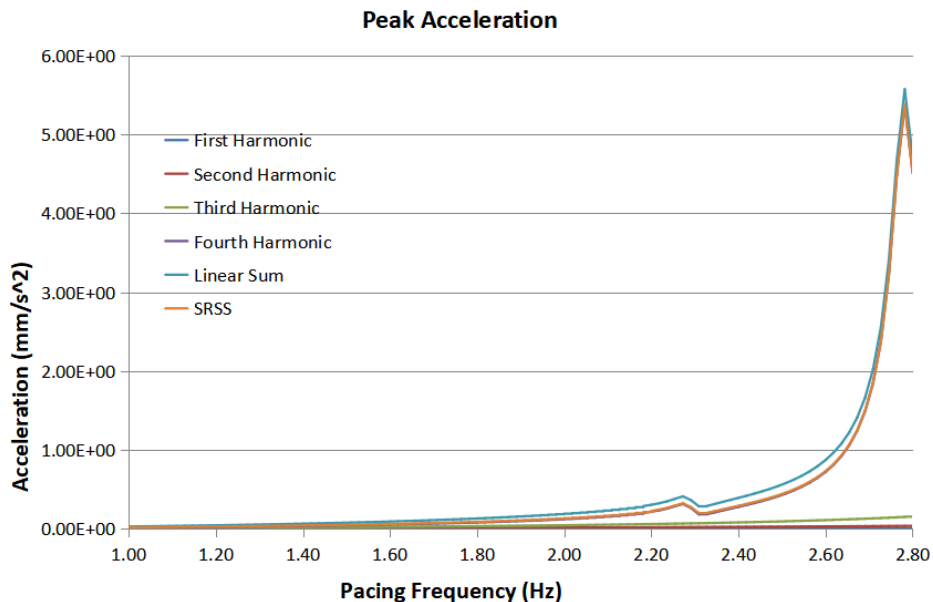


Figure 43. Peak Acceleration (Case 2).

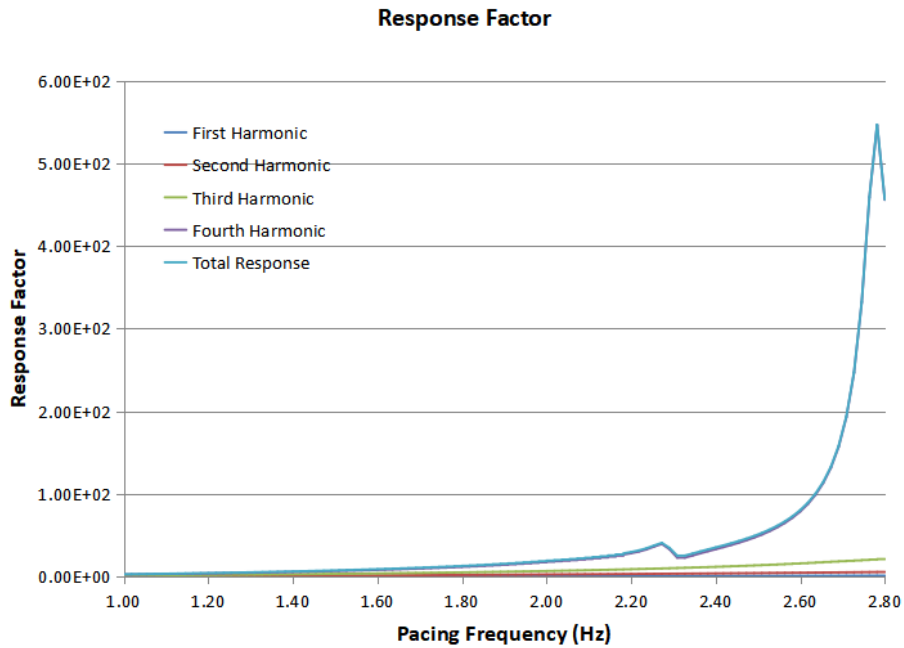


Figure 44. Response Factor (Case 2).

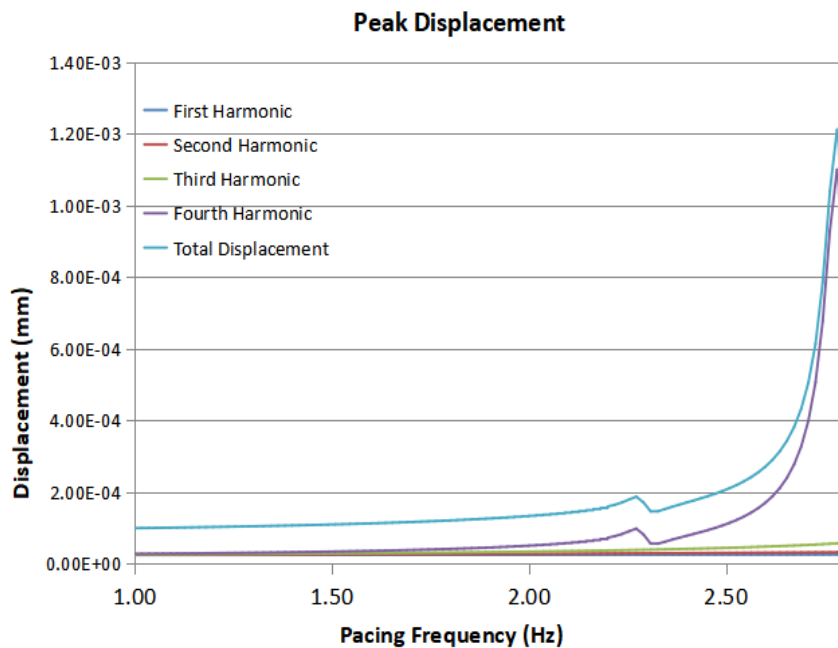


Figure 45. Peak Displacement (Case 2).

For the floor of the fully composite acting beam, the same analysis was used for the two previous cases. The curves obtained are shown in Figures 46, 47, and 48 after first solving with the solver and then plotting the curves after substituting the equations in an Excel sheet. Their peaks occur at the natural frequency of 11.13 Hz with a maximum acceleration of 6.61 mm/s^2 , a maximum response factor of $6.72 \cdot 10^2$, and a maximum displacement of $1.35 \cdot 10^{-3} \text{ mm}$.

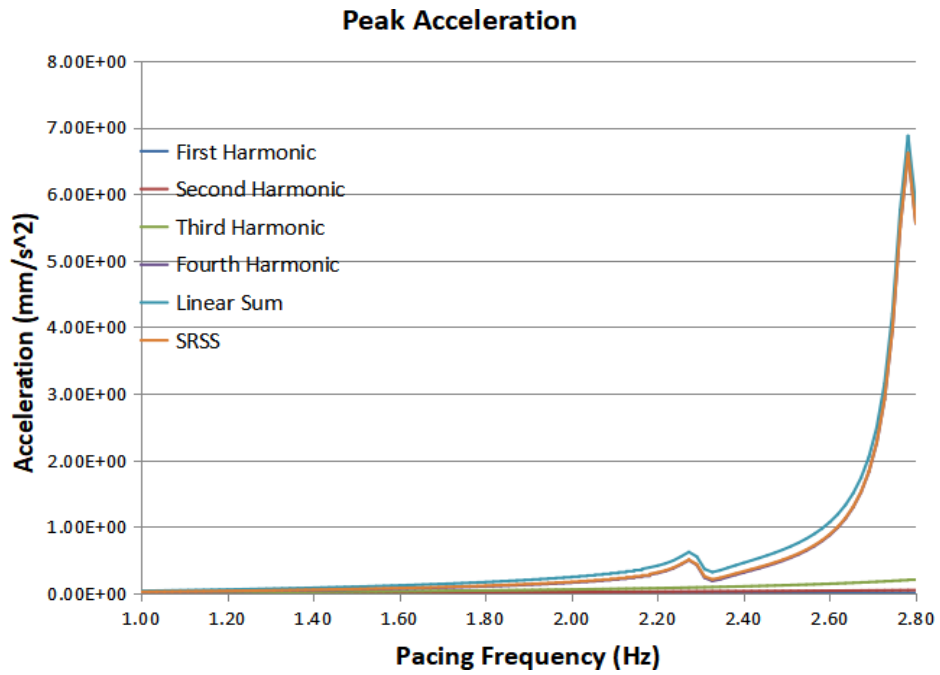


Figure 46. Peak Acceleration (Case 3).

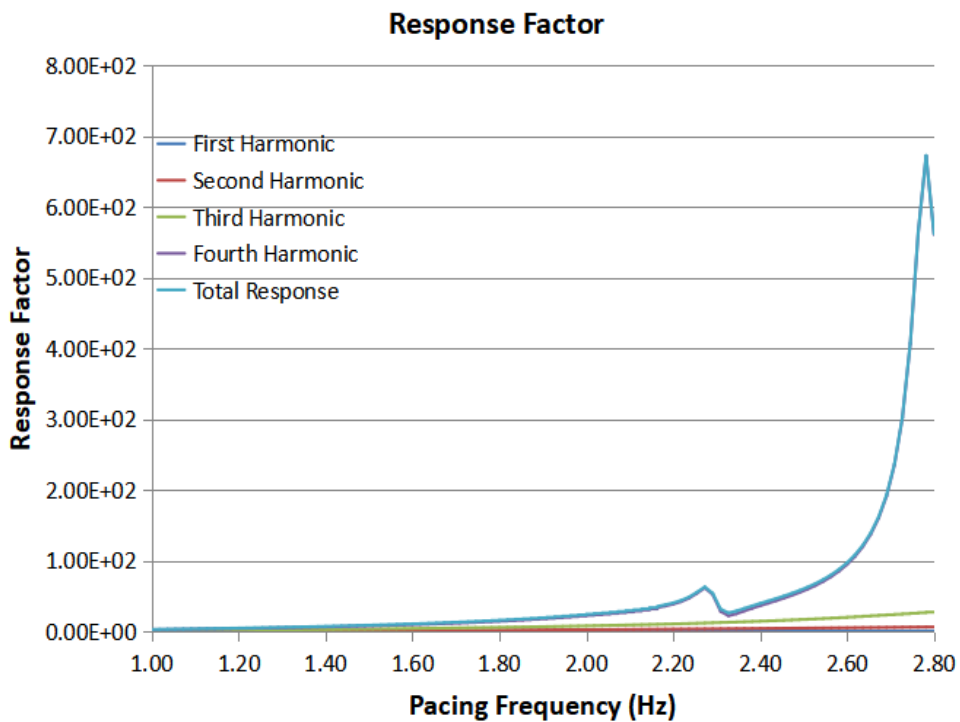


Figure 47. Response Factor (Case 3).

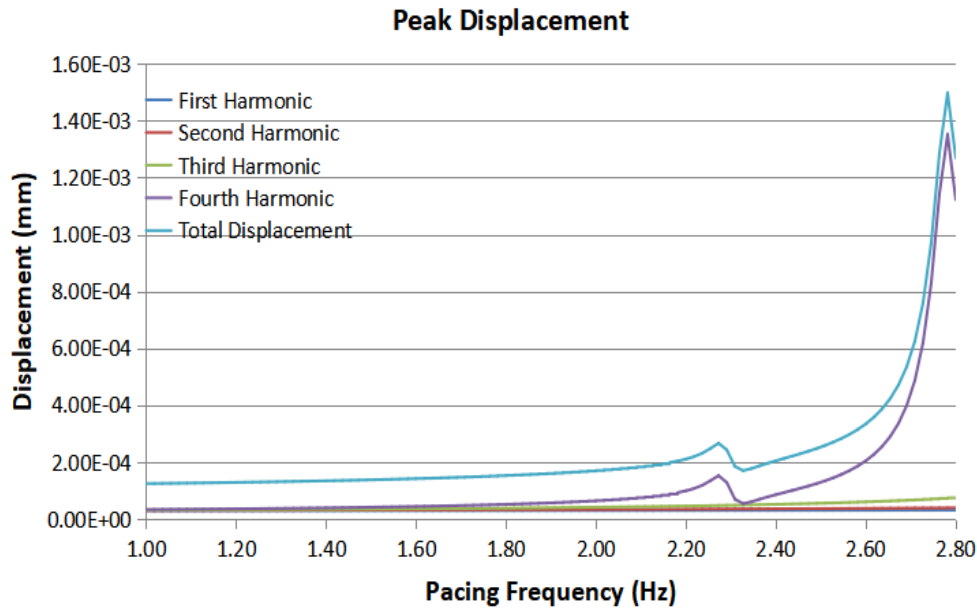


Figure 48. Peak Displacement (Case 3).

	Natural frequency	Peak Acceleration	Response Factor	Peak Displacement
Case 1	7.64 Hz	$1.12 \cdot 10^3 \text{ mm/s}^2$	$1.58 \cdot 10^5$	$4.86 \cdot 10^{-1} \text{ mm}$
Case 2	11.13 Hz	5.37 mm/s^2	$5.46 \cdot 10^2$	$1.1 \cdot 10^{-3} \text{ mm}$
Case 3	11.13 Hz	6.61 mm/s^2	$6.72 \cdot 10^2$	$1.35 \cdot 10^{-3} \text{ mm}$

Table 6. Three parameters in three cases.

Table 6 summarises the maximum values of the three parameters for the three situations, and the larger the three parameters, the more uncomfortable the body perceives the vibration. After comparison, it was found that the floor without the composite action beam produced the highest acceleration, response coefficient, and displacement and was about 1000 times larger than the other two cases, which may be uncomfortable for humans. This is because 7.64 Hz is between 4 and 8 Hz when the floor resonates with humans. In contrast, these three parameters in the second and third cases are not very different and are much smaller than in the first case, indicating that humans do not readily perceive floor vibrations at this time.

4.3 Static Displacement

The analysis of static displacements in Strand 7 uses the linear static solver in Figure 49. As specified, the final maximum displacement obtained needs to be less than $L/480$, which in this project needs to be less than $4800/480 = 10 \text{ mm}$.

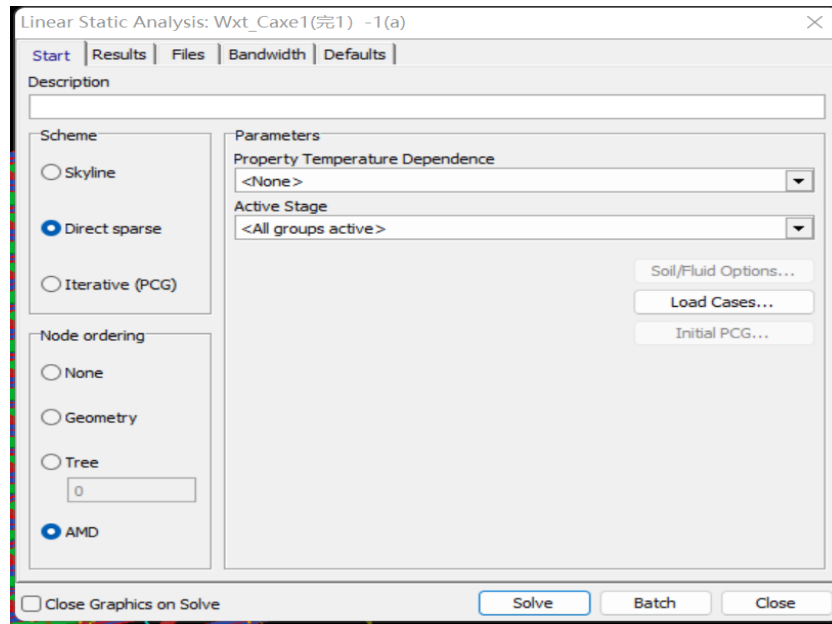


Figure 49. Linear Static Analysis Solver.

The results obtained from the static analysis of the floor without the composite action beam are shown in Figures 50 and 51, and the analysis process is shown in the Appendix C. It can be seen that the absolute value of the maximum displacement of the first case is 5.193687 mm direction downwards, less than 10 mm, so composite requirements.

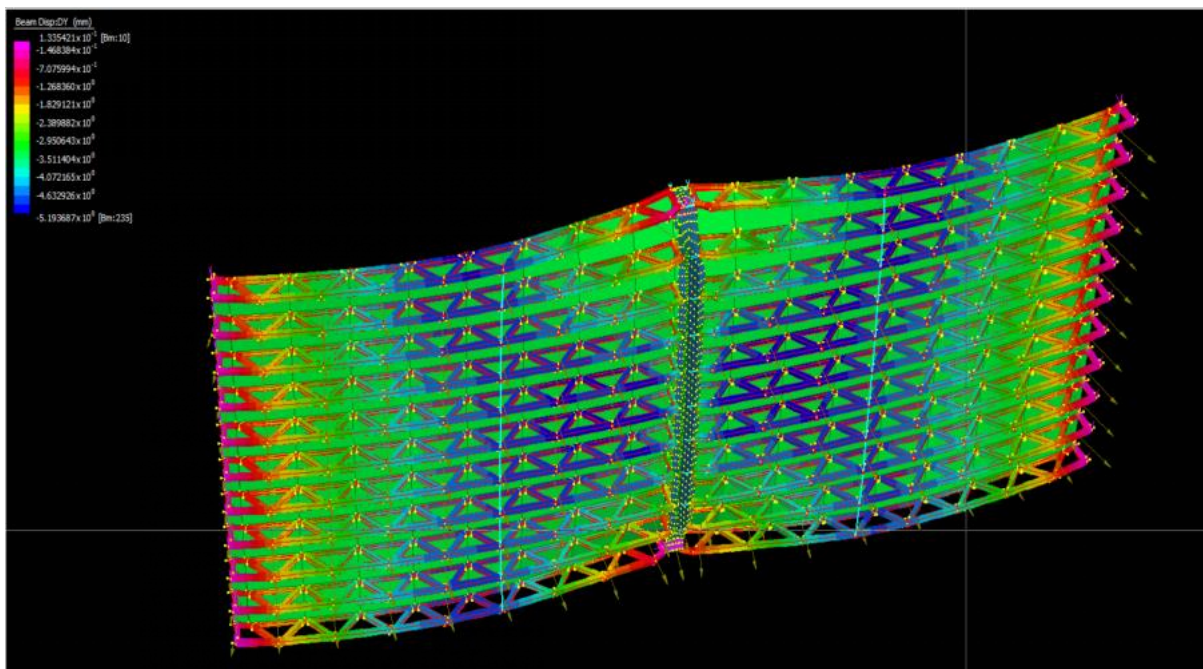


Figure 50. Colour chart for Beams Static displacement (Case 1).

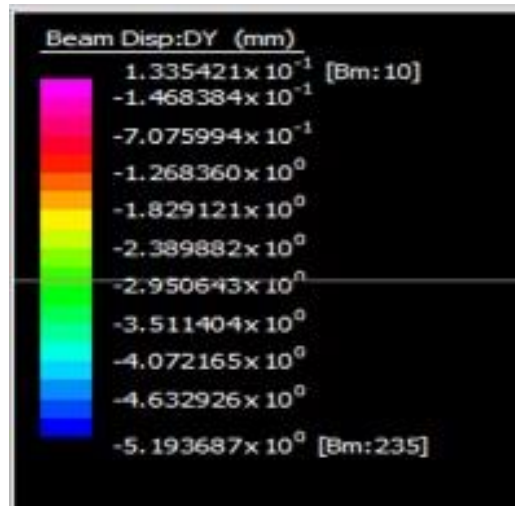


Figure 51. Values of static displacement (Case 1).

Static analysis was used for the floor of the partially composite action beam (see appendix for procedure). As in Figures 52 and 53, the absolute value of the maximum displacement for the second case is 6.300356 mm in the downward direction, less than 10 mm, so composite requirements.

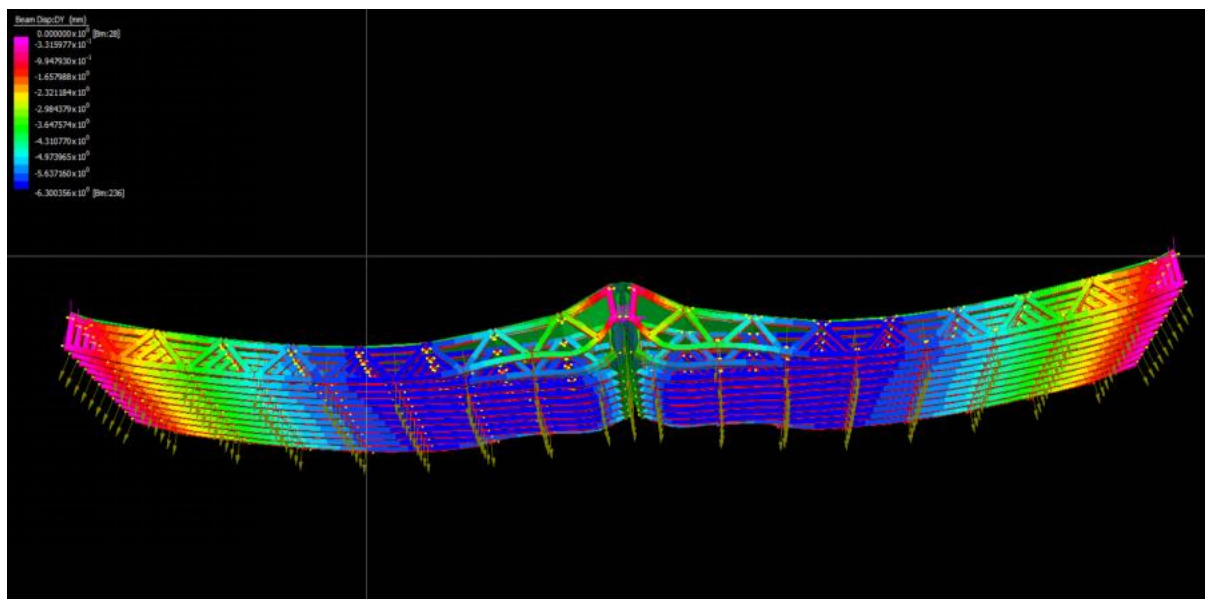


Figure 52. Colour chart for beams static displacement (Case 2).

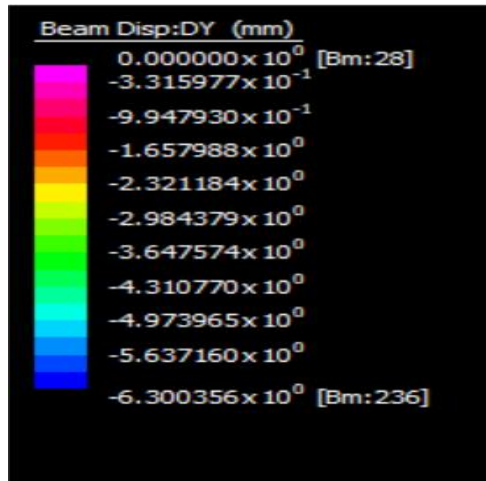


Figure 53. Values of static displacement (Case 2).

Figures 54 and 55 show the static analysis results for the floor of the composite active beam (see Appendix for the analysis procedure). The absolute value of the maximum displacement for the third case is 5.158536 mm in the downward direction, which is less than 10 mm following the requirements.

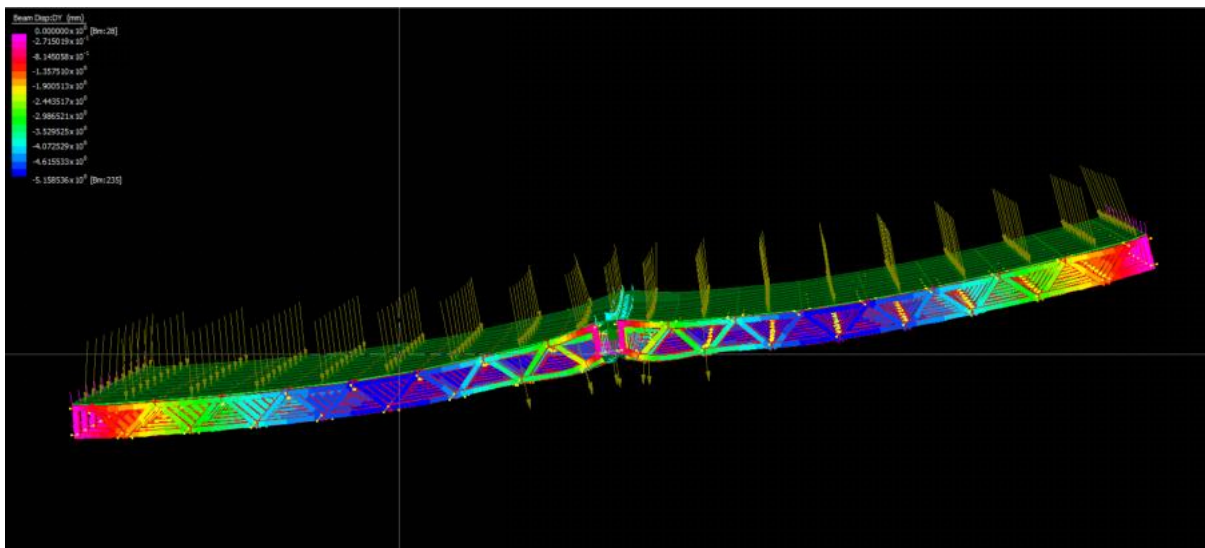


Figure 54. Colour chart for beams static displacement (Case 3).

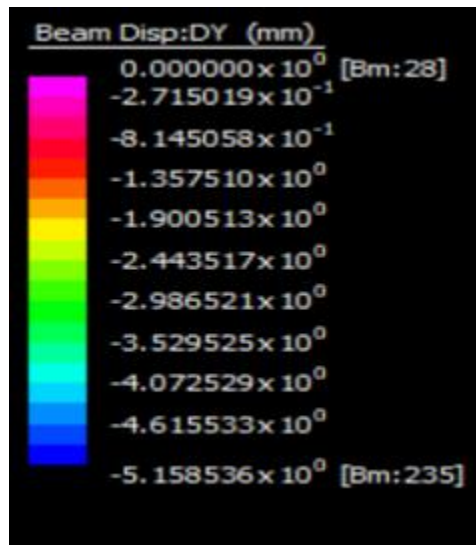


Figure 55. Values of static displacement (Case 3).

The analysis revealed that the maximum displacement for all three cases was less than $L/480 = 10$ mm, with the smallest static displacement for the floor without composite action beams, followed by the floor with full-composite action beams, and the largest static displacement for the floor with partially tightly confined beams via bolts.

5 DISCUSSION

Three indicators compared floor vibrations and human perception for the three cases. This project found that the static displacements produced by the floor from a floor without composite acting beams to a floor with fully composite acting beams were less than $L/480$, indicating that all three cases can be used in practical engineering.

However, human perception of vibration can vary in these three situations. The natural frequency range of a floor without composite action beams is 7.1784 Hz - 15.26 Hz, with a minimum value between 4 Hz and 8 Hz. It is effortlessly resonating with humans when they are most sensitive to vibration perception. The natural frequencies of a floor with partially composite acting beams and a floor with fully composite beams are 9.1495 Hz - 11.1267 Hz and 9.1495 Hz to 11.1268 Hz, respectively when resonance is not readily generated. This also indicates that the flexural stiffness of the beams in Case2 and Case3, as in Figure 55, is more significant and has approximately the same effect. Similarly, in the harmonic response analysis, the difference between the results for Case 2 and Case 3 is minimal, and the results for each data are much smaller than for Case 1, which is a further indication that the I-shaped beams with composite and complete composite action are much more stable than the regular I-shaped beams without composite action.

The static displacement of Case2 is 0.9 mm more than that of Case1 in the static analysis, which does not match the actual scenario. The possible reason for this is that there is a difference between the way the bolts are confined between the beams in the finite element model and the actual construction. Because the position of the bolts in the vertical direction also affects the stability of the beam in the actual project, the slight difference between the model and the actual one creates an error. The good news is that the 0.9 mm is negligible and will not affect the rest of the analysis.

In summary, although I-section beams without composite action, such as Case 1, are now used in many projects, floors with partially and fully composite action beams give better serviceability. The Case 2 beam is the better choice in floor construction as it takes more time, effort, and money to fully weld, and the results do not differ much from those of a beam confined with bolts.

6 CONCLUSIONS

The purpose of this article was to investigate the vibration of a floor consisting of a C-shaped CFS joist and an I-shaped built-up CFS beam and to compare the stability of the floor with the beam in the three composite states. By building a finite element model using Strand 7 and performing FEA, the following conclusions were obtained:

- This light floor with C-shaped CFS and its composite parts vibrates to produce static displacements of less than $L/480$ composite construction requirements.
- A comparison of the natural frequencies of the three cases reveals that the floor without the composite action beam is susceptible to resonance with humans. The other two cases have a similar range of natural frequencies and are not in the sensitive range for human resonance.
- The harmonic response shows that the impact of the floor's acceleration, response factor, and displacement without the composite action beam are the greatest in all three cases. The results for the other two cases are similar, almost 1000 times smaller than case 1.

Due to the tendency of mild steel flooring to cause irritating vibrations, serviceability is reduced. By using built-up CFS beams that are either fastened or welded, vibrations in light steel floors are effectively controlled, but considering economic costs and time, a partially composite beam floor with bolted confinement is more advantageous and more suitable for the actual project. Vibration problems in light steel floor constructions can therefore be solved and serviceability improved by using composite CFS beams with bolt fastening.

7 REFERENCE

Davies, J. M. (2000). Recent research advances in CFS structures. *Journal of Constructional Steel Research*, 55(1), 267-288. [https://doi.org/10.1016/S0143-974X\(99\)00089-9](https://doi.org/10.1016/S0143-974X(99)00089-9)

Debney, P., & Willford, M. (2009). Footfall vibration and finite element analysis. *Sound & Vibration*, 43(11), 11-14.

Grether, W. F. (1971). Vibration and Human Performance. *Human Factors*, 13(3), 203 – 216. <https://doi.org/10.1177/001872087101300301>

Hancock, G. J. (2003). *CFS structures*. Elsevier Ltd. [https://doi.org/10.1016/S0143-974X\(02\)00103-7](https://doi.org/10.1016/S0143-974X(02)00103-7)

ISO. (1997). *Mechanical Vibration and Shock - Evaluation of Human Exposure to Whole-Body Vibration*(ISO 2631-1).

ISO.(1989). *Evaluation of human exposure to whole-body vibration – Part 2: Human Exposure to continuous and shock-induced vibrations in buildings (1 to 80 Hz)*(ISO 2631 – 2).

Kyvelou, P., Gardner, L., & Nethercot, D. A. (2017). Design of composite CFS flooring systems. *Structures (Oxford)*, 12, 242-252. <https://doi.org/10.1016/j.istruc.2017.09.006>

Lenzen, K.H. (1966). Vibration of steel joist-concrete slab floors. *Engineering Journal, American Institute of Steel Construction(AISC)*, 3(1966), 133–136.

Nguyen, H. A. U. (2013). *Walking induced floor vibration design and control* (Doctoral dissertation, Swinburne University of Technology).

Negreira, J., Trollé, A., Jarnerö, K., Sjökvist, L. -, & Bard, D. (2015). Psycho-vibratory evaluation of timber floors – towards the determination of design indicators of vibration acceptability and vibration annoyance. *Journal of Sound and Vibration*, 340, 383-408. <https://doi.org/10.1016/j.jsv.2014.12.001>

Phan, D. K., & Rasmussen, K. J. R. (2019). Flexural rigidity of CFS built-up members. *Thin-Walled Structures*, 140, 438-449. <https://doi.org/10.1016/j.tws.2019.03.051>

Racic, V., Pavic, A., & Brownjohn, J. M. W. (2009). Experimental identification and analytical modelling of human walking forces: Literature review. *Journal of Sound and Vibration*, 326(1), 1-49. <https://doi.org/10.1016/j.jsv.2009.04.020>

Roy, K., Ho Lau, H., Ting, T. C. H., Chen, B., & Lim, J. B. P. (2021). Flexural behaviour of back-to-back built-up CFS channel beams: Experiments and finite element modelling. *Structures (Oxford)*, 29, 235-253. <https://doi.org/10.1016/j.istruc.2020.10.052>

Rinchen, & Rasmussen, K. J. R. (2019). Numerical modelling of CFS single C-section portal frames. *Journal of Constructional Steel Research*, 158, 143-155. <https://doi.org/10.1016/j.jcsr.2019.03.024>

Rasmussen, K. J. R., Khezri, M., Schafer, B. W., & Zhang, H. (2020). The mechanics of built-up CFS members. *Thin-Walled Structures*, 154, 106756. <https://doi.org/10.1016/j.tws.2020.106756>

Roy, K., Ting, T. C. H., Lau, H. H., & Lim, J. B. P. (2018). Effect of thickness on the behaviour of axially loaded back-to-back CFS built-up channel sections - experimental and numerical investigation. *Structures (Oxford)*, 16, 327-346. <https://doi.org/10.1016/j.istruc.2018.09.009>

Shaikh, F. U. A. (2012). Role of commercial software in teaching finite element analysis at undergraduate level: A case study. *Engineering Education (Loughborough)*, 7(2), 2-6. <https://doi.org/10.11120/ened.2012.07020002>

Saidi, I., Gad, E. F., Wilson, J. L., & Haritos, N. (2011). Development of passive viscoelastic damper to attenuate excessive floor vibrations. *Engineering Structures*, 33(12), 3317-3328. <https://doi.org/10.1016/j.engstruct.2011.05.017>

Saidi, I. (2012). *Development of a viscoelastic tuned mass damper to reduce walking induced vibrations in building floors* (Doctoral dissertation, Thesis of Doctor of Philosophy, Swinburne University of Technology, Melbourne).

Shi, Y, Zhou, XH, Gao, TT, et al. (2015) Research on flexural capacity of CFS double limbs built-up box beams. *Journal of Building Structures* 36(11): 20–28

Wang, S. (2009). *Collapse site of steel frame of factory building under construction* [Image]. <http://news.sohu.com/20090414/n263383372.shtml>

Wanniarachchi, S. (2005). *Flexural behaviour and design of CFS beams with rectangular hollow flanges* (Doctoral dissertation, Queensland University of Technology).

Xu, L. (2011). Floor vibration in lightweight CFS framing. *Advances in Structural Engineering*, 14(4), 659-672. <https://doi.org/10.1260/1369-4332.14.4.659>

Yu, W., 1924, LaBoube, R. A., Chen, H. (., & Knovel. (2019). *CFS design* (Fifth ed.). Wiley.

Yao, X., Zhou, X., Shi, Y., Guan, Y., & Zou, Y. (2020). Simplified calculation method for flexural moment capacity of CFS built-up section beams. *Advances in Structural Engineering*, 23(14), 3153-3167. <https://doi.org/10.1177/1369433220931208>

Zhou, X., Guan, Y., Gao, T., & Shi, Y. (2016). Study on flexural capacity of CFS double-limb built-up I-shape beams.

Zhang, S., Xu, L., & Qin, J. (2017). Vibration of lightweight steel floor systems with occupants: Modelling, formulation and dynamic properties. *Engineering Structures*, 147, 652-665. <https://doi.org/10.1016/j.engstruct.2017.06.008>

Zhang, S., & Xu, L. (2022). Vibration serviceability evaluation of lightweight CFS floor systems. *Structures (Oxford)*, 38, 1368-1379. <https://doi.org/10.1016/j.istruc.2022.02.009>

8 APPENDICES

8.1 APPENDIX A—Natural frequency solving process

Case1

```

THE FIRST 30 EIGENVALUES HAVE CONVERGED
FINAL FREQUENCY RESULTS
Mode      Eigenvalue      Frequency (rad/s)      Frequency (Hz)
1          2.03429823E+03      4.51031953E+01        7.17839649E+00
2          2.25304234E+03      4.74662232E+01        7.55448405E+00
3          2.29854668E+03      4.79431610E+01        7.63039105E+00
4          2.58931525E+03      5.08853147E+01        8.09864936E+00
5          2.60018917E+03      5.09920500E+01        8.11563682E+00
6          2.77946339E+03      5.27206164E+01        8.39074670E+00
7          2.80204928E+03      5.29343866E+01        8.42476928E+00
8          2.84552225E+03      5.33434368E+01        8.48987164E+00
9          3.07181615E+03      5.54239673E+01        8.82099836E+00
10         3.07837364E+03      5.54830933E+01        8.83040855E+00
11         3.14538217E+03      5.60837668E+01        8.92599917E+00
12         3.18097049E+03      5.64000930E+01        8.97635360E+00
13         3.19102788E+03      5.64891838E+01        8.99053283E+00
14         3.22170489E+03      5.67600642E+01        9.03364479E+00
15         3.2217058E+03       5.67641664E+01        9.03429767E+00
16         3.23011063E+03      5.68340627E+01        9.04542194E+00
17         3.23175831E+03      5.68485559E+01        9.04772868E+00
18         3.23472518E+03      5.68746444E+01        9.05188080E+00
19         3.24409088E+03      5.69569213E+01        9.06497556E+00
20         3.28007326E+03      5.77719238E+01        9.12510978E+00
21         3.31083908E+03      5.75398912E+01        9.15775812E+00
22         3.32098184E+03      5.76279606E+01        9.17177479E+00
23         6.39492192E+03      7.99682557E+01        1.27273432E+01
24         8.81967805E+03      9.39131410E+01        1.49467406E+01
25         8.86656751E+03      9.41624528E+01        1.49864198E+01
26         9.04670756E+03      9.51141817E+01        1.51378922E+01
27         9.08512883E+03      9.53159422E+01        1.51700034E+01
28         9.11876429E+03      9.54922211E+01        1.51980590E+01
29         9.13114980E+03      9.55570500E+01        1.52083769E+01
30         9.19326241E+03      9.58815019E+01        1.52600150E+01

COUNTING MODES IN RANGE      : 7.17031487E+00 to 1.52680966E+01
Reducing 13751 Equations (Using 12.1 MB RAM)...
Reducing 13751 Equations (Using 12.1 MB RAM)...
STURM CHECK RESULTS
There is no natural frequency below 7.170E+00 Hz.
There are 30 frequencies below 1.527E+01 Hz.
All eigenvalues are found.

TOTAL CPU TIME                : 8,859 Seconds ( 0:00:09)
*Solution completed on 13/06/2022 at 00:19:46
*Solution time: 9 Seconds

*SUMMARY OF MESSAGES
*Number of Notes      : 0
*Number of Warnings   : 0
*Number of Errors     : 0

```

Case2

```

THE FIRST 30 EIGENVALUES HAVE CONVERGED
FINAL FREQUENCY RESULTS
Mode      Eigenvalue      Frequency (rad/s)      Frequency (Hz)
1          3.30487001E+03      7.48799898E+01        9.14949919E+00
2          3.30487129E+03      7.48803908E+01        9.14950096E+00
3          3.30487882E+03      7.4880555E+01         9.14951138E+00
4          3.30488018E+03      7.4880873E+01         9.14951326E+00
5          3.30519245E+03      7.49008032E+01        9.14994551E+00
6          3.30519342E+03      7.49008116E+01        9.14994685E+00
7          3.30524564E+03      7.4912658E+01         9.15001913E+00
8          3.30524653E+03      7.4912715E+01         9.15002036E+00
9          3.30531307E+03      7.4918527E+01         9.15011247E+00
10         3.30531995E+03      7.49185998E+01        9.15011369E+00
11         3.30538772E+03      7.4924971E+01         9.15021510E+00
12         3.30538772E+03      7.4925014E+01         9.15021579E+00
13         3.30544434E+03      7.4929938E+01         9.15029416E+00
14         3.30544507E+03      7.4930007E+01         9.15029518E+00
15         3.30550384E+03      7.4935113E+01         9.15037657E+00
16         3.30550691E+03      7.4935307E+01         9.15037953E+00
17         3.30550657E+03      7.4935357E+01         9.15038038E+00
18         3.30550659E+03      7.4935357E+01         9.15038033E+00
19         3.30555597E+03      7.4939647E+01         9.15044868E+00
20         3.30555701E+03      7.4939736E+01         9.15045010E+00
21         3.30557365E+03      7.4941358E+01         9.15047591E+00
22         3.30557647E+03      7.4941429E+01         9.15047705E+00
23         4.88645400E+03      6.99031759E+01        1.11254360E+01
24         4.88657371E+03      6.99040321E+01        1.1125523E+01
25         4.88702928E+03      6.99072908E+01        1.11266908E+01
26         4.88725750E+03      6.99089229E+01        1.11263506E+01
27         4.88729689E+03      6.99092046E+01        1.11263955E+01
28         4.88734964E+03      6.99095819E+01        1.11264555E+01
29         4.88743855E+03      6.99102178E+01        1.11265567E+01
30         4.88753875E+03      6.99109344E+01        1.11266708E+01

COUNTING MODES IN RANGE      : 9.14752202E+00 to 1.11266734E+01
Reducing 13676 Equations (Using 12.1 MB RAM)...
Reducing 13676 Equations (Using 12.1 MB RAM)...
STURM CHECK RESULTS
There is no natural frequency below 9.148E+00 Hz.
There are 36 frequencies below 1.113E+01 Hz.
There are 6 missing eigenvalues.

TOTAL CPU TIME                : 4.484 Seconds ( 0:00:04)
*Solution completed on 13/06/2022 at 00:22:07
*Solution time: 5 Seconds

*SUMMARY OF MESSAGES
*Number of Notes      : 0
*Number of Warnings   : 0
*Number of Errors     : 0

```

Case3

```

THE FIRST 30 EIGENVALUES HAVE CONVERGED

FINAL FREQUENCY RESULTS
Mode      Eigenvalue      Frequency (rad/s)  Frequency (Hz)
1         3.30486981E+03   5.74879971E+01    9.14949891E+00
2         3.30487049E+03   5.74880030E+01    9.14949984E+00
3         3.30487846E+03   5.74880723E+01    9.14951087E+00
4         3.30487846E+03   5.74880723E+01    9.14951088E+00
5         3.30519110E+03   5.74907914E+01    9.14994364E+00
6         3.30519111E+03   5.74907915E+01    9.14994365E+00
7         3.30524425E+03   5.74912536E+01    9.15001720E+00
8         3.30524425E+03   5.74912537E+01    9.15001720E+00
9         3.30531177E+03   5.74918409E+01    9.15011067E+00
10        3.30531195E+03   5.74918425E+01    9.15011092E+00
11        3.30538549E+03   5.74924820E+01    9.15021270E+00
12        3.30538549E+03   5.74924820E+01    9.15021271E+00
13        3.30544310E+03   5.74929830E+01    9.15029244E+00
14        3.30544402E+03   5.74929910E+01    9.15029372E+00
15        3.30550432E+03   5.74935154E+01    9.15037718E+00
16        3.30550432E+03   5.74935155E+01    9.15037718E+00
17        3.30550461E+03   5.74935180E+01    9.15037759E+00
18        3.30550754E+03   5.74935434E+01    9.15038163E+00
19        3.30555487E+03   5.74939551E+01    9.15044715E+00
20        3.30555489E+03   5.74939552E+01    9.15044717E+00
21        3.30557414E+03   5.74941227E+01    9.15047382E+00
22        3.30557416E+03   5.74941228E+01    9.15047384E+00
23        4.88647454E+03   6.99033228E+01    1.11254594E+01
24        4.88714715E+03   6.99061336E+01    1.11262250E+01
25        4.88724012E+03   6.99087986E+01    1.11263309E+01
26        4.88730285E+03   6.99092473E+01    1.11264023E+01
27        4.88740807E+03   6.99099855E+01    1.11265198E+01
28        4.88745754E+03   6.99103536E+01    1.11265784E+01
29        4.88753481E+03   6.99109062E+01    1.11266663E+01
30        4.88758004E+03   6.99112297E+01    1.11267178E+01

COUNTING MODES IN RANGE      :  9.14752169E+00 to 1.11267399E+01
Reducing 13086 Equations (Using 11.9 MB RAM)...
Reducing 13086 Equations (Using 11.9 MB RAM)...

STURM CHECK RESULTS
There is no natural frequency below 9.148E+00 Hz.
There are 40 frequencies below 1.113E+01 Hz.
There are 10 missing eigenvalues.

TOTAL CPU TIME                : 5.766 Seconds ( 0:00:06)

*Solution completed on 13/06/2022 at 00:23:16
*Solution time: 6 Seconds

*SUMMARY OF MESSAGES
*Number of Notes      : 0
*Number of Warnings   : 0
*Number of Errors     : 0

```

8.2 APPENDIX B—Harmonic response solving process

Case1

First Harmonic				Second Harmonic				Third Harmonic				Fourth Harmonic				Total Response	Linear
Frequency	Accelerati	Frequency	Accelerati	Frequency	Accelerati	Frequency	Accelerati	Baseline	Response	Baseline	Response	Baseline	Response	Factor	SRSS	SRSS	
1.00	5.985E-01	2.00	2.365E-00	3.00	5.325E-00	4.00	9.405E-00	1.41E-02	4.13E-01	1.00E-02	2.36E-02	8.16E-03	6.51E-02	1.07E-03	1.30E-03	1.77E-01	
1.02	6.08E-01	2.04	2.44E-00	3.05	5.51E-00	4.07	9.74E-00	1.40E-02	4.34E-01	9.91E-03	2.46E-02	8.09E-03	6.51E-02	1.07E-03	1.38E-03	1.83E-01	
1.04	6.20E-01	2.07	2.52E-00	3.11	5.71E-00	4.15	1.01E-01	1.39E-02	4.52E-01	9.82E-03	2.58E-02	8.02E-03	6.51E-02	1.07E-03	1.42E-03	1.89E-01	
1.05	6.32E-01	2.11	2.62E-00	3.18	5.91E-00	4.22	1.04E-01	1.38E-02	4.74E-01	9.74E-03	2.69E-02	7.95E-03	6.46E-02	1.07E-03	1.47E-03	1.96E-01	
1.07	6.55E-01	2.15	2.71E-00	3.22	6.12E-00	4.29	1.08E-01	1.37E-02	4.94E-01	9.66E-03	2.81E-02	7.88E-03	6.46E-02	1.07E-03	1.52E-03	2.03E-01	
1.09	6.69E-01	2.18	2.81E-00	3.27	6.33E-00	4.36	1.11E-01	1.35E-02	5.16E-01	9.57E-03	2.93E-02	7.82E-03	6.40E-02	1.07E-03	1.57E-03	2.09E-01	
1.11	7.02E-01	2.23	2.90E-00	3.33	6.54E-00	4.44	1.14E-01	1.34E-02	5.37E-01	9.50E-03	3.05E-02	7.75E-03	6.40E-02	1.07E-03	1.62E-03	2.16E-01	
1.13	7.46E-01	2.25	3.00E-00	3.38	6.76E-00	4.51	1.18E-01	1.32E-02	5.60E-01	9.42E-03	3.18E-02	7.69E-03	6.39E-02	1.07E-03	1.67E-03	2.23E-01	
1.15	7.70E-01	2.29	3.09E-00	3.44	6.97E-00	4.59	1.21E-01	1.30E-02	5.83E-01	9.34E-03	3.31E-02	7.63E-03	6.34E-02	1.07E-03	1.72E-03	2.30E-01	
1.16	7.94E-01	2.33	3.19E-00	3.49	7.20E-00	4.65	1.25E-01	1.28E-02	6.06E-01	9.27E-03	3.44E-02	7.57E-03	6.31E-02	1.07E-03	1.77E-03	2.37E-01	
1.18	8.20E-01	2.36	3.29E-00	3.55	7.43E-00	4.73	1.28E-01	1.26E-02	6.30E-01	9.20E-03	3.58E-02	7.51E-03	6.29E-02	1.07E-03	1.82E-03	2.44E-01	
1.20	8.45E-01	2.40	3.40E-00	3.60	7.65E-00	4.80	1.32E-01	1.24E-02	6.53E-01	9.13E-03	3.72E-02	7.45E-03	6.23E-02	1.07E-03	1.88E-03	2.51E-01	
1.22	8.71E-01	2.44	3.50E-00	3.65	7.88E-00	4.87	1.35E-01	1.22E-02	6.80E-01	9.06E-03	3.86E-02	7.40E-03	6.17E-02	1.07E-03	1.91E-03	2.58E-01	
1.24	8.97E-01	2.47	3.61E-00	3.71	8.11E-00	4.95	1.39E-01	1.20E-02	7.05E-01	8.99E-03	4.01E-02	7.34E-03	6.15E-02	1.07E-03	1.96E-03	2.65E-01	
1.25	9.24E-01	2.51	3.71E-00	3.76	8.35E-00	5.02	1.42E-01	1.18E-02	7.32E-01	8.92E-03	4.16E-02	7.29E-03	6.15E-02	1.07E-03	2.01E-03	2.72E-01	
1.27	9.51E-01	2.55	3.82E-00	3.82	8.59E-00	5.09	1.45E-01	1.15E-02	7.58E-01	8.85E-03	4.31E-02	7.24E-03	6.10E-02	1.07E-03	2.05E-03	2.79E-01	
1.29	9.78E-01	2.58	3.93E-00	3.87	8.83E-00	5.16	1.48E-01	1.14E-02	7.86E-01	8.78E-03	4.47E-02	7.19E-03	6.05E-02	1.07E-03	2.09E-03	2.85E-01	
1.31	1.01E-01	2.62	4.05E-00	3.93	9.07E-00	5.24	1.51E-01	1.12E-02	8.14E-01	8.74E-03	4.63E-02	7.14E-03	6.02E-02	1.07E-03	2.14E-03	2.92E-01	
1.33	1.03E-01	2.65	4.16E-00	3.99	9.32E-00	5.31	1.54E-01	1.10E-02	8.42E-01	8.68E-03	4.79E-02	7.09E-03	6.02E-02	1.07E-03	2.17E-03	2.99E-01	
1.35	1.06E-01	2.69	4.28E-00	4.04	9.57E-00	5.38	1.56E-01	1.08E-02	8.72E-01	8.62E-03	4.96E-02	7.07E-03	6.02E-02	1.07E-03	2.21E-03	3.06E-01	
1.36	1.09E-01	2.73	4.39E-00	4.09	9.82E-00	5.45	1.59E-01	1.06E-02	9.02E-01	8.56E-03	5.13E-02	7.07E-03	6.02E-02	1.07E-03	2.24E-03	3.12E-01	
1.38	1.12E-01	2.76	4.51E-00	4.15	1.01E-01	5.53	1.61E-01	1.04E-02	9.32E-01	8.51E-03	5.30E-02	7.07E-03	6.02E-02	1.07E-03	2.27E-03	3.19E-01	
1.40	1.15E-01	2.80	4.63E-00	4.20	1.03E-01	5.60	1.63E-01	1.02E-02	9.63E-01	8.45E-03	5.48E-02	7.07E-03	6.02E-02	1.07E-03	2.30E-03	3.24E-01	
1.42	1.18E-01	2.84	4.75E-00	4.25	1.05E-01	5.67	1.64E-01	1.00E-02	9.95E-01	8.40E-03	5.66E-02	7.07E-03	6.02E-02	1.07E-03	2.33E-03	3.29E-01	
1.44	1.21E-01	2.87	4.87E-00	4.31	1.08E-01	5.75	1.65E-01	9.80E-03	1.02E-01	8.34E-03	5.84E-02	7.07E-03	6.02E-02	1.07E-03	2.36E-03	3.34E-01	
1.45	1.24E-01	2.91	5.00E-00	4.36	1.11E-01	5.82	1.65E-01	9.75E-03	1.04E-01	8.29E-03	6.03E-02	7.07E-03	6.02E-02	1.07E-03	2.39E-03	3.39E-01	
1.47	1.27E-01	2.95	5.13E-00	4.42	1.14E-01	5.89	1.65E-01	9.70E-03	1.06E-01	8.24E-03	6.23E-02	7.07E-03	6.02E-02	1.07E-03	2.43E-03	3.42E-01	
1.49	1.31E-01	2.98	5.25E-00	4.47	1.16E-01	5.96	1.64E-01	9.65E-03	1.08E-01	8.19E-03	6.41E-02	7.07E-03	6.02E-02	1.07E-03	2.47E-03	3.45E-01	
1.51	1.34E-01	3.00	5.38E-00	4.53	1.19E-01	6.04	1.63E-01	9.60E-03	1.10E-01	8.14E-03	6.61E-02	7.07E-03	6.02E-02	1.07E-03	2.49E-03	3.48E-01	
1.53	1.37E-01	3.05	5.51E-00	4.58	1.21E-01	6.11	1.59E-01	9.55E-03	1.12E-01	8.09E-03	6.81E-02	7.07E-03	6.02E-02	1.07E-03	2.54E-03	3.49E-01	
1.55	1.40E-01	3.09	5.65E-00	4.64	1.24E-01	6.18	1.54E-01	9.50E-03	1.14E-01	8.04E-03	7.02E-02	7.07E-03	6.02E-02	1.07E-03	2.58E-03	3.49E-01	
1.58	1.44E-01	3.13	5.78E-00	4.69	1.27E-01	6.25	1.48E-01	9.45E-03	1.16E-01	8.00E-03	7.23E-02	7.07E-03	6.02E-02	1.07E-03	2.60E-03	3.47E-01	
1.59	1.47E-01	3.16	5.91E-00	4.75	1.29E-01	6.33	1.40E-01	9.40E-03	1.18E-01	7.95E-03	7.44E-02	7.07E-03	6.02E-02	1.07E-03	2.65E-03	3.42E-01	
1.60	1.50E-01	3.20	6.05E-00	4.80	1.32E-01	6.40	1.30E-01	9.35E-03	1.20E-01	7.91E-03	7.65E-02	7.07E-03	6.02E-02	1.07E-03	2.73E-03	3.37E-01	
1.62	1.54E-01	3.24	6.19E-00	4.85	1.34E-01	6.47	1.17E-01	9.30E-03	1.22E-01	7.86E-03	7.87E-02	7.07E-03	6.02E-02	1.07E-03	2.64E-03	3.29E-01	
1.64	1.57E-01	3.27	6.33E-00	4.91	1.37E-01	6.55	1.01E-01	9.25E-03	1.24E-01	7.82E-03	8.10E-02	7.07E-03	6.02E-02	1.07E-03	2.54E-03	3.17E-01	
1.65	1.61E-01	3.31	6.47E-00	4.96	1.39E-01	6.62	8.10E-02	9.20E-03	1.26E-01	7.77E-03	8.32E-02	7.07E-03	6.02E-02	1.07E-03	2.43E-03	3.01E-01	
1.67	1.65E-01	3.35	6.61E-00	5.02	1.42E-01	6.69	5.94E-02	9.15E-03	1.28E-01	7.73E-03	8.55E-02	7.07E-03	6.02E-02	1.07E-03	2.34E-03	2.87E-01	
1.69	1.69E-01	3.38	6.76E-00	5.07	1.44E-01	6.76	4.19E-02	9.10E-03	1.30E-01	7.69E-03	8.79E-02	7.07E-03	6.02E-02	1.07E-03	2.25E-03	2.70E-01	
1.71	1.73E-01	3.42	6.90E-00	5.13	1.47E-01	6.84	2.59E-02	9.05E-03	1.32E-01	7.65E-03	9.02E-02	7.07E-03	6.02E-02	1.07E-03	2.15E-03	2.42E-01	
1.73	1.75E-01	3.45	7.05E-00	5.18	1.49E-01	6.91	1.17E-01	9.00E-03	1.34E-01	7.61E-03	9.26E-02	7.07E-03	6.02E-02	1.07E-03	2.06E-03	2.24E-01	
1.75	1.79E-01	3.49	7.20E-00	5.24	1.51E-01	6.98	1.90E-01	8.95E-03	1.36E-01	7.57E-03	9.51E-02	7.07E-03	6.02E-02	1.07E-03	2.06E-03	2.17E-01	
1.76	1.83E-01	3.53	7.35E-00	5.29	1.53E-01	7.05	2.99E-01	8.90E-03	1.38E-01	7.53E-03	9.76E-02	7.07E-03	6.02E-02	1.07E-03	2.06E-03	2.10E-01	
1.78	1.87E-01	3.56	7.50E-00	5.35	1.55E-01	7.13	4.49E-01	8.85E-03	1.40E-01	7.49E-03	1.00E-01	7.07E-03	6.02E-02	1.07E-03	2.06E-03	2.03E-01	
1.80	1.91E-01	3.60	7.65E-00	5.40	1.57E-01	7.20	6.39E-01	8.80E-03	1.42E-01	7.45E-03	1.03E-01	7.07E-03	6.02E-02	1.07E-03	2.06E-03	1.96E-01	
1.82	1.94E-01	3.64	7.80E-00	5.45	1.59E-01	7.27	9.23E-01	8.75E-03	1.44E-01	7.41E-03	1.06E-01	7.07E-03	6.02E-02	1.07E-03	2.06E-03	1.89E-01	
1.84	1.98E-01	3.67	7.96E-00	5.51	1.60E-01	7.35	1.41E-01	8.70E-03	1.46E-01	7.38E-03	1.09E-01	7.07E-03	6.02E-02	1.07E-03	2.06E-03	1.82E-01	
1.85	2.02E-01	3.71	8.11E-00	5.56	1.62E-01	7.42	2.23E-01	8.65E-03	1.48E-01	7.34E-03	1.12E-01	7.07E-03	6.02E-02	1.07E-03	2.06E-03	1.75E-01	
1.87	2.06E-01	3.75	8.27E-00	5.62	1.63E-01	7.49	3.19E-01	8.60E-03	1.50E-01	7.31E-03	1.15E-01	7.07E-03	6.02E-02	1.07E-03	2.06E-03	1.68E-01	
1.89	2.10E-01	3.78	8.43E-00	5.67	1.64E-01	7.56	4.39E-01	8.55E-03	1.52E-01	7.27E-03	1.18E-01	7.07E-03	6.02E-02	1.07E-03	2.06E-03	1.61E-01	
1.91	2.14E-01	3.82	8.59E-00	5.73	1.65E-01	7.64	5.93E-01	8.50E-03	1.54E-01	7.24E-03	1.21E-01	7.07E-03	6.02E-02	1.07E-03	2.06E-03	1.54E-01	
1.93	2.19E-01	3.85	8.75E-00	5.78	1.65E-01	7.71	7.92E-01	8.45E-03	1.56E-01	7.20E-03	1.24E-01	7.07E-03	6.02E-02	1.07E-03	2.06E-03	1.47E-01	
1.95	2.23E-01	3.89	8.91E-00	5.84	1.65E-01	7.78	1.07E-01	8.40E-03	1.58E-01	7.17E-03	1.27E-01	7.07E-03	6.02E-02	1.07E-03	2.06E-03	1.40E-01	
1.96	2.27E-01	3.93	9.07E-00	5.89	1.65E-01	7.85	1.44E-01	8.35E-03	1.60E-01	7.14E-03	1.30E-01	7.07E-03	6.02E-02	1.07E-03	2.06E-03	1.33E-01	
1.98	2.31E-01	3.96	9.24E-00	5.95	1.64E-01	7.93	1.93E-01	8.30E-03	1.62E-01	7.11E-03	1.33E-01	7.07E-03	6.02E-02	1.07E-03	2.06E-03	1.26E-01	
2.00	2.36E-01	4.00	9.40E-00	6.00	1.63E-01	8.00	2.66E-01	8.25E-03	1.64E-01	7.07E-03	1.36E-01	7.07E-03	6.02E-02	1.07E-03	2.06E-03	1.19E-01	
2.02	2.40E-01	4.04	9.57E-00	6.05	1.61E-01	8.07	3.68E-01	8.20E-03	1.66E-01	7.04E-03	1.39E-01	7.07E-03	6.02E-02	1.07E-03	2.06E-03	1.12E-01	
2.																	

Case2

First Harmonic	Second Harmonic	Third Harmonic	Fourth Harmonic	Baseline	Response Factor	Total Response	Total Acceleration								
Frequency	Acceleration	Frequency	Acceleration	Frequency	Acceleration	Frequency	Acceleration	Frequency	Acceleration	Frequency	Acceleration	g	Linear Sum g		
1.00	9.15E-04	2.00	3.75E-03	3.00	8.02E-03	4.00	1.67E-02	1.41E-02	6.47E-03	1.00E-02	3.75E-03	8.18E-03	1.00E-02	2.01290870	
1.02	9.45E-04	2.04	3.90E-03	3.05	9.17E-03	4.07	1.74E-02	1.40E-02	6.77E-03	9.91E-03	3.95E-03	8.69E-03	1.13E-02	2.14E-02	0.00104069
1.04	9.80E-04	2.07	4.04E-03	3.11	9.51E-03	4.15	1.80E-02	1.39E-02	7.08E-03	9.50E-03	4.11E-03	8.82E-03	1.19E-02	2.27E-02	0.00109355
1.05	1.00E-03	2.11	4.19E-03	3.16	9.90E-03	4.22	1.86E-02	1.38E-02	7.39E-03	9.74E-03	4.20E-03	8.95E-03	1.24E-02	2.40E-02	0.00114641
1.07	1.05E-03	2.15	4.34E-03	3.22	1.03E-02	4.29	1.92E-02	1.37E-02	7.70E-03	9.98E-03	4.30E-03	9.08E-03	1.29E-02	2.53E-02	0.00119927
1.09	1.09E-03	2.18	4.50E-03	3.27	1.07E-02	4.36	2.00E-02	1.36E-02	8.02E-03	1.02E-02	4.40E-03	9.21E-03	1.34E-02	2.66E-02	0.00125213
1.11	1.13E-03	2.22	4.65E-03	3.33	1.11E-02	4.44	2.08E-02	1.35E-02	8.34E-03	1.04E-02	4.50E-03	9.34E-03	1.39E-02	2.79E-02	0.00130500
1.13	1.17E-03	2.25	4.81E-03	3.38	1.15E-02	4.51	2.16E-02	1.34E-02	8.66E-03	1.07E-02	4.60E-03	9.47E-03	1.44E-02	2.92E-02	0.00135786
1.15	1.20E-03	2.29	4.97E-03	3.44	1.19E-02	4.59	2.24E-02	1.33E-02	8.98E-03	1.10E-02	4.70E-03	9.60E-03	1.49E-02	3.05E-02	0.00141072
1.16	1.24E-03	2.33	5.14E-03	3.49	1.23E-02	4.65	2.32E-02	1.32E-02	9.30E-03	1.12E-02	4.80E-03	9.73E-03	1.54E-02	3.18E-02	0.00146358
1.18	1.28E-03	2.36	5.31E-03	3.55	1.27E-02	4.72	2.40E-02	1.31E-02	9.62E-03	1.15E-02	4.90E-03	9.86E-03	1.59E-02	3.31E-02	0.00151644
1.20	1.32E-03	2.40	5.49E-03	3.60	1.31E-02	4.80	2.48E-02	1.30E-02	9.94E-03	1.18E-02	5.00E-03	1.00E-02	1.64E-02	3.44E-02	0.00156930
1.22	1.36E-03	2.44	5.67E-03	3.65	1.35E-02	4.87	2.56E-02	1.29E-02	1.02E-02	1.20E-02	5.10E-03	1.01E-02	1.69E-02	3.57E-02	0.00162216
1.24	1.40E-03	2.47	5.85E-03	3.71	1.41E-02	4.95	2.70E-02	1.28E-02	1.05E-02	1.22E-02	5.20E-03	1.02E-02	1.74E-02	3.70E-02	0.00167502
1.25	1.45E-03	2.51	6.03E-03	3.76	1.45E-02	5.02	2.80E-02	1.27E-02	1.08E-02	1.24E-02	5.30E-03	1.03E-02	1.79E-02	3.83E-02	0.00172788
1.27	1.49E-03	2.55	6.21E-03	3.82	1.50E-02	5.09	2.90E-02	1.26E-02	1.10E-02	1.26E-02	5.40E-03	1.04E-02	1.84E-02	3.96E-02	0.00178074
1.29	1.53E-03	2.58	6.40E-03	3.87	1.55E-02	5.16	3.00E-02	1.25E-02	1.13E-02	1.28E-02	5.50E-03	1.05E-02	1.89E-02	4.09E-02	0.00183360
1.31	1.58E-03	2.62	6.59E-03	3.93	1.60E-02	5.24	3.10E-02	1.24E-02	1.15E-02	1.30E-02	5.60E-03	1.06E-02	1.94E-02	4.22E-02	0.00188646
1.33	1.63E-03	2.66	6.79E-03	3.99	1.65E-02	5.31	3.20E-02	1.23E-02	1.18E-02	1.32E-02	5.70E-03	1.07E-02	1.99E-02	4.35E-02	0.00193932
1.35	1.67E-03	2.69	6.99E-03	4.04	1.71E-02	5.38	3.30E-02	1.22E-02	1.20E-02	1.34E-02	5.80E-03	1.08E-02	2.04E-02	4.48E-02	0.00200000
1.36	1.71E-03	2.73	7.19E-03	4.09	1.76E-02	5.45	3.38E-02	1.21E-02	1.23E-02	1.36E-02	5.90E-03	1.09E-02	2.09E-02	4.61E-02	0.00206068
1.38	1.76E-03	2.76	7.39E-03	4.15	1.82E-02	5.53	3.47E-02	1.20E-02	1.25E-02	1.38E-02	6.00E-03	1.10E-02	2.14E-02	4.74E-02	0.00212136
1.40	1.81E-03	2.80	7.60E-03	4.20	1.87E-02	5.60	3.54E-02	1.19E-02	1.28E-02	1.40E-02	6.10E-03	1.11E-02	2.19E-02	4.87E-02	0.00218204
1.42	1.86E-03	2.84	7.82E-03	4.25	1.93E-02	5.67	3.62E-02	1.18E-02	1.30E-02	1.42E-02	6.20E-03	1.12E-02	2.24E-02	4.99E-02	0.00224272
1.44	1.90E-03	2.87	8.05E-03	4.31	1.99E-02	5.75	3.70E-02	1.17E-02	1.33E-02	1.44E-02	6.30E-03	1.13E-02	2.29E-02	5.12E-02	0.00230340
1.45	1.95E-03	2.91	8.29E-03	4.36	2.05E-02	5.82	3.78E-02	1.16E-02	1.35E-02	1.46E-02	6.40E-03	1.14E-02	2.34E-02	5.25E-02	0.00236408
1.47	2.00E-03	2.95	8.54E-03	4.42	2.11E-02	5.89	3.86E-02	1.15E-02	1.38E-02	1.48E-02	6.50E-03	1.15E-02	2.39E-02	5.38E-02	0.00242476
1.48	2.05E-03	2.98	8.79E-03	4.47	2.17E-02	5.96	3.94E-02	1.14E-02	1.40E-02	1.50E-02	6.60E-03	1.16E-02	2.44E-02	5.51E-02	0.00248544
1.51	2.11E-03	3.02	9.04E-03	4.53	2.24E-02	6.04	4.02E-02	1.13E-02	1.43E-02	1.52E-02	6.70E-03	1.17E-02	2.49E-02	5.64E-02	0.00254612
1.53	2.16E-03	3.05	9.29E-03	4.58	2.30E-02	6.11	4.10E-02	1.12E-02	1.45E-02	1.54E-02	6.80E-03	1.18E-02	2.54E-02	5.77E-02	0.00260680
1.55	2.21E-03	3.09	9.54E-03	4.64	2.37E-02	6.18	4.18E-02	1.11E-02	1.48E-02	1.56E-02	6.90E-03	1.19E-02	2.59E-02	5.90E-02	0.00266748
1.56	2.26E-03	3.13	9.79E-03	4.69	2.44E-02	6.25	4.26E-02	1.10E-02	1.50E-02	1.58E-02	7.00E-03	1.20E-02	2.64E-02	6.03E-02	0.00272816
1.58	2.32E-03	3.16	1.01E-02	4.75	2.51E-02	6.32	4.34E-02	1.09E-02	1.53E-02	1.60E-02	7.10E-03	1.21E-02	2.69E-02	6.16E-02	0.00278884
1.60	2.37E-03	3.20	1.03E-02	4.80	2.58E-02	6.40	4.42E-02	1.08E-02	1.55E-02	1.62E-02	7.20E-03	1.22E-02	2.74E-02	6.29E-02	0.00284952
1.62	2.43E-03	3.24	1.06E-02	4.85	2.66E-02	6.47	4.50E-02	1.07E-02	1.58E-02	1.64E-02	7.30E-03	1.23E-02	2.79E-02	6.42E-02	0.00291020
1.64	2.49E-03	3.27	1.09E-02	4.91	2.73E-02	6.55	4.58E-02	1.06E-02	1.60E-02	1.66E-02	7.40E-03	1.24E-02	2.84E-02	6.55E-02	0.00297088
1.65	2.54E-03	3.31	1.12E-02	4.96	2.81E-02	6.62	4.66E-02	1.05E-02	1.63E-02	1.68E-02	7.50E-03	1.25E-02	2.89E-02	6.68E-02	0.00303156
1.67	2.60E-03	3.35	1.15E-02	5.02	2.89E-02	6.69	4.74E-02	1.04E-02	1.65E-02	1.70E-02	7.60E-03	1.26E-02	2.94E-02	6.81E-02	0.00309224
1.69	2.66E-03	3.38	1.18E-02	5.07	2.97E-02	6.76	4.82E-02	1.03E-02	1.68E-02	1.72E-02	7.70E-03	1.27E-02	2.99E-02	6.94E-02	0.00315292
1.71	2.72E-03	3.42	1.21E-02	5.13	3.05E-02	6.84	4.90E-02	1.02E-02	1.70E-02	1.74E-02	7.80E-03	1.28E-02	3.04E-02	7.07E-02	0.00321360
1.73	2.77E-03	3.45	1.24E-02	5.18	3.13E-02	6.91	4.98E-02	1.01E-02	1.73E-02	1.76E-02	7.90E-03	1.29E-02	3.09E-02	7.20E-02	0.00327428
1.75	2.84E-03	3.49	1.27E-02	5.24	3.21E-02	6.98	5.06E-02	1.00E-02	1.75E-02	1.78E-02	8.00E-03	1.30E-02	3.14E-02	7.33E-02	0.00333496
1.76	2.90E-03	3.53	1.30E-02	5.29	3.29E-02	7.05	5.14E-02	9.9E-03	1.78E-02	1.80E-02	8.10E-03	1.31E-02	3.19E-02	7.46E-02	0.00339564
1.78	2.96E-03	3.56	1.33E-02	5.35	3.37E-02	7.13	5.22E-02	9.8E-03	1.80E-02	1.82E-02	8.20E-03	1.32E-02	3.24E-02	7.59E-02	0.00345632
1.80	3.02E-03	3.60	1.36E-02	5.40	3.45E-02	7.20	5.30E-02	9.7E-03	1.83E-02	1.84E-02	8.30E-03	1.33E-02	3.29E-02	7.72E-02	0.00351700
1.82	3.08E-03	3.64	1.39E-02	5.45	3.53E-02	7.27	5.38E-02	9.6E-03	1.85E-02	1.86E-02	8.40E-03	1.34E-02	3.34E-02	7.85E-02	0.00357768
1.84	3.15E-03	3.67	1.42E-02	5.51	3.61E-02	7.35	5.46E-02	9.5E-03	1.88E-02	1.88E-02	8.50E-03	1.35E-02	3.39E-02	7.98E-02	0.00363836
1.85	3.21E-03	3.71	1.45E-02	5.56	3.69E-02	7.42	5.54E-02	9.4E-03	1.90E-02	1.90E-02	8.60E-03	1.36E-02	3.44E-02	8.11E-02	0.00369904
1.87	3.28E-03	3.75	1.48E-02	5.62	3.77E-02	7.49	5.62E-02	9.3E-03	1.93E-02	1.92E-02	8.70E-03	1.37E-02	3.49E-02	8.24E-02	0.00375972
1.89	3.34E-03	3.78	1.51E-02	5.67	3.85E-02	7.56	5.70E-02	9.2E-03	1.95E-02	1.94E-02	8.80E-03	1.38E-02	3.54E-02	8.37E-02	0.00382040
1.91	3.41E-03	3.82	1.54E-02	5.73	3.93E-02	7.64	5.78E-02	9.1E-03	1.98E-02	1.96E-02	8.90E-03	1.39E-02	3.59E-02	8.50E-02	0.00388108
1.93	3.48E-03	3.85	1.57E-02	5.78	4.01E-02	7.71	5.86E-02	9.0E-03	2.00E-02	1.98E-02	9.00E-03	1.40E-02	3.64E-02	8.63E-02	0.00394176
1.95	3.54E-03	3.89	1.59E-02	5.84	4.09E-02	7.78	5.94E-02	8.9E-03	2.02E-02	2.00E-02	9.10E-03	1.41E-02	3.69E-02	8.76E-02	0.00400244
1.96	3.61E-03	3.93	1.62E-02	5.89	4.17E-02	7.85	6.02E-02	8.8E-03	2.04E-02	2.02E-02	9.20E-03	1.42E-02	3.74E-02	8.89E-02	0.00406312
1.98	3.68E-03	3.96	1.65E-02	5.95	4.25E-02	7.92	6.10E-02	8.7E-03	2.06E-02	2.04E-02	9.30E-03	1.43E-02	3.79E-02	9.02E-02	0.00412380
2.00	3.75E-03	4.00	1.68E-02	6.00	4.33E-02	8.00	6.18E-02	8.6E-03	2.08E-02	2.06E-02	9.40E-03	1.44E-02	3.84E-02	9.15E-02	0.00418448
2.02	3.82E-03	4.04	1.71E-02	6.05	4.41E-02	8.07	6.26E-02	8.5E-03	2.10E-02	2.08E-02	9.50E-03	1.45E-02	3.89E-02	9.28E-02	0.00424516
2.04	3.89E-03	4.07	1.74E-02	6.11	4.49E-02	8.15	6.34E-02	8.4E-03	2.12E-02	2.10E-02	9.60E-03	1.46E-02	3.94E-02	9.41E-02	0.00430584
2.05	3.95E-03	4.11	1.77E-02	6.16	4.57E-02	8.22	6.42E-02	8.3E-03	2.14E-02	2.12E-02	9.70E-03	1.47E-02	3.99E-02	9.54E-02	0.00436652
2.07	4.04E-03	4.15	1.80E-02	6.22	4.65E-02	8.29	6.50E-02	8.2E-03	2.16E-02	2.14E-02	9.80E-03	1.48E-02	4.04E-02	9.67E-02	0.00442720
2.09	4.11E-03	4.19	1.83E-02	6.27	4.73E-02	8.36	6.58E-02	8.1E-03							

Case3

First Harmonic	Second Harmonic	Third Harmonic	Fourth Harmonic	First Harmonic	Second Harmonic	Third Harmonic	Fourth Harmonic	Total Response	Linear Accelerati
Frequency/Amplitude	Frequency/Amplitude	Frequency/Amplitude	Frequency/Amplitude	Baseline Response	Response	Response	Response	RMS	Linear RMS
1.00 1.16E-03	2.00 4.77E-03	3.00 1.12E-02	4.00 2.12E-02	1.41E-02	8.21E-02	1.00E-02	4.77E-01	3.16E-00	3.84E-02 0.02453
1.02 1.20E-03	2.04 4.93E-03	3.05 1.17E-02	4.07 2.22E-02	1.40E-02	8.40E-02	9.91E-03	4.89E-01	3.09E-00	4.05E-02 0.02538
1.04 1.23E-03	2.07 5.10E-03	3.11 1.21E-02	4.15 2.31E-02	1.39E-02	8.59E-02	9.82E-03	5.02E-01	3.02E-00	4.16E-02 0.02604
1.05 1.25E-03	2.11 5.22E-03	3.16 1.26E-02	4.22 2.41E-02	1.38E-02	8.79E-02	9.74E-03	5.17E-01	2.93E-00	4.32E-02 0.02773
1.07 1.34E-03	2.15 5.32E-03	3.22 1.31E-02	4.29 2.51E-02	1.37E-02	9.00E-02	9.66E-03	5.31E-01	2.83E-00	4.50E-02 0.02934
1.09 1.38E-03	2.18 5.43E-03	3.27 1.36E-02	4.36 2.61E-02	1.36E-02	9.22E-02	9.57E-03	5.47E-01	2.72E-00	4.68E-02 0.03099
1.11 1.42E-03	2.22 5.51E-03	3.33 1.41E-02	4.44 2.72E-02	1.34E-02	9.45E-02	9.48E-03	5.63E-01	2.61E-00	4.86E-02 0.03218
1.13 1.46E-03	2.25 5.62E-03	3.38 1.46E-02	4.51 2.82E-02	1.33E-02	9.70E-02	9.41E-03	5.79E-01	2.50E-00	5.04E-02 0.03339
1.15 1.53E-03	2.29 5.72E-03	3.44 1.51E-02	4.58 2.94E-02	1.32E-02	9.96E-02	9.34E-03	5.97E-01	2.38E-00	5.23E-02 0.03464
1.16 1.56E-03	2.32 5.84E-03	3.49 1.56E-02	4.65 3.05E-02	1.31E-02	1.02E-01	9.27E-03	6.15E-01	2.27E-00	5.43E-02 0.03593
1.18 1.62E-03	2.36 5.93E-03	3.55 1.62E-02	4.73 3.17E-02	1.30E-02	1.05E-01	9.20E-03	6.34E-01	2.15E-00	5.63E-02 0.03725
1.20 1.68E-03	2.40 6.03E-03	3.60 1.67E-02	4.80 3.29E-02	1.29E-02	1.08E-01	9.13E-03	6.54E-01	2.03E-00	5.83E-02 0.03860
1.22 1.73E-03	2.44 6.14E-03	3.65 1.73E-02	4.87 3.42E-02	1.28E-02	1.11E-01	9.06E-03	6.74E-01	1.91E-00	6.03E-02 0.04000
1.24 1.78E-03	2.47 6.26E-03	3.71 1.79E-02	4.95 3.55E-02	1.27E-02	1.14E-01	8.99E-03	6.95E-01	1.79E-00	6.24E-02 0.04145
1.25 1.84E-03	2.51 6.38E-03	3.76 1.85E-02	5.02 3.68E-02	1.26E-02	1.18E-01	8.92E-03	7.16E-01	1.67E-00	6.45E-02 0.04295
1.27 1.89E-03	2.55 6.50E-03	3.82 1.91E-02	5.09 3.82E-02	1.25E-02	1.21E-01	8.86E-03	7.37E-01	1.55E-00	6.67E-02 0.04450
1.29 1.93E-03	2.58 6.63E-03	3.87 1.98E-02	5.16 3.96E-02	1.24E-02	1.25E-01	8.80E-03	7.59E-01	1.43E-00	6.89E-02 0.04610
1.31 2.00E-03	2.62 6.78E-03	3.93 2.04E-02	5.24 4.10E-02	1.24E-02	1.29E-01	8.74E-03	7.81E-01	1.31E-00	7.13E-02 0.04775
1.33 2.06E-03	2.65 6.93E-03	3.98 2.11E-02	5.31 4.25E-02	1.23E-02	1.33E-01	8.68E-03	8.04E-01	1.19E-00	7.38E-02 0.04945
1.35 2.12E-03	2.69 7.09E-03	4.04 2.17E-02	5.38 4.41E-02	1.22E-02	1.37E-01	8.62E-03	8.27E-01	1.07E-00	7.63E-02 0.05120
1.36 2.18E-03	2.72 7.24E-03	4.09 2.24E-02	5.45 4.57E-02	1.21E-02	1.41E-01	8.56E-03	8.51E-01	9.5E-00	7.88E-02 0.05300
1.38 2.24E-03	2.76 7.40E-03	4.15 2.31E-02	5.53 4.74E-02	1.20E-02	1.45E-01	8.51E-03	8.75E-01	8.3E-00	8.14E-02 0.05485
1.40 2.30E-03	2.80 7.57E-03	4.20 2.38E-02	5.60 4.91E-02	1.20E-02	1.49E-01	8.45E-03	9.00E-01	7.1E-00	8.40E-02 0.05675
1.42 2.36E-03	2.84 7.74E-03	4.25 2.46E-02	5.67 5.08E-02	1.19E-02	1.53E-01	8.40E-03	9.25E-01	6.0E-00	8.67E-02 0.05870
1.44 2.42E-03	2.87 7.92E-03	4.31 2.53E-02	5.75 5.27E-02	1.18E-02	1.57E-01	8.34E-03	9.50E-01	5.0E-00	8.94E-02 0.06070
1.45 2.48E-03	2.91 8.10E-03	4.36 2.61E-02	5.82 5.45E-02	1.17E-02	1.61E-01	8.29E-03	9.75E-01	4.1E-00	9.21E-02 0.06275
1.47 2.54E-03	2.95 8.28E-03	4.42 2.69E-02	5.89 5.63E-02	1.17E-02	1.65E-01	8.24E-03	1.00E-01	3.3E-00	9.49E-02 0.06485
1.49 2.61E-03	2.99 8.47E-03	4.47 2.77E-02	5.96 5.82E-02	1.16E-02	1.69E-01	8.19E-03	1.02E-01	2.6E-00	9.77E-02 0.06695
1.51 2.67E-03	3.02 8.66E-03	4.53 2.85E-02	6.04 6.01E-02	1.15E-02	1.73E-01	8.14E-03	1.05E-01	1.9E-00	1.00E-01 0.06910
1.53 2.74E-03	3.05 8.85E-03	4.58 2.94E-02	6.11 6.21E-02	1.14E-02	1.77E-01	8.09E-03	1.08E-01	1.3E-00	1.03E-01 0.07125
1.55 2.81E-03	3.09 9.04E-03	4.64 3.02E-02	6.18 6.41E-02	1.14E-02	1.81E-01	8.04E-03	1.11E-01	7.8E-00	1.06E-01 0.07345
1.56 2.88E-03	3.13 9.23E-03	4.69 3.11E-02	6.25 6.62E-02	1.13E-02	1.85E-01	8.00E-03	1.14E-01	5.5E-00	1.09E-01 0.07565
1.58 2.94E-03	3.16 9.43E-03	4.75 3.20E-02	6.32 6.83E-02	1.12E-02	1.89E-01	7.95E-03	1.17E-01	3.4E-00	1.12E-01 0.07785
1.60 3.01E-03	3.20 9.63E-03	4.80 3.29E-02	6.40 7.04E-02	1.12E-02	1.93E-01	7.91E-03	1.20E-01	2.4E-00	1.15E-01 0.08005
1.62 3.08E-03	3.24 9.83E-03	4.85 3.38E-02	6.47 7.25E-02	1.11E-02	1.97E-01	7.86E-03	1.23E-01	1.6E-00	1.18E-01 0.08225
1.64 3.15E-03	3.27 1.00E-02	4.91 3.47E-02	6.55 7.47E-02	1.10E-02	2.01E-01	7.82E-03	1.26E-01	1.0E-00	1.21E-01 0.08445
1.65 3.23E-03	3.31 1.03E-02	4.96 3.56E-02	6.62 7.69E-02	1.10E-02	2.05E-01	7.77E-03	1.29E-01	6.8E-00	1.24E-01 0.08665
1.67 3.30E-03	3.35 1.07E-02	5.02 3.65E-02	6.69 7.92E-02	1.09E-02	2.09E-01	7.73E-03	1.32E-01	4.7E-00	1.27E-01 0.08885
1.69 3.37E-03	3.38 1.10E-02	5.07 3.75E-02	6.76 8.15E-02	1.09E-02	2.13E-01	7.69E-03	1.35E-01	3.1E-00	1.30E-01 0.09105
1.71 3.45E-03	3.42 1.14E-02	5.13 3.84E-02	6.84 8.38E-02	1.08E-02	2.17E-01	7.65E-03	1.38E-01	2.1E-00	1.33E-01 0.09325
1.73 3.53E-03	3.45 1.18E-02	5.18 3.93E-02	6.91 8.61E-02	1.08E-02	2.21E-01	7.61E-03	1.41E-01	1.4E-00	1.36E-01 0.09545
1.75 3.60E-03	3.49 1.22E-02	5.24 4.02E-02	6.98 8.85E-02	1.07E-02	2.25E-01	7.57E-03	1.44E-01	9.5E-00	1.39E-01 0.09765
1.76 3.68E-03	3.53 1.26E-02	5.29 4.12E-02	7.05 9.09E-02	1.06E-02	2.29E-01	7.53E-03	1.47E-01	6.5E-00	1.42E-01 0.09985
1.78 3.76E-03	3.56 1.30E-02	5.35 4.23E-02	7.13 9.33E-02	1.06E-02	2.33E-01	7.49E-03	1.50E-01	4.4E-00	1.45E-01 0.10205
1.80 3.84E-03	3.60 1.34E-02	5.40 4.33E-02	7.20 9.57E-02	1.05E-02	2.37E-01	7.45E-03	1.53E-01	2.9E-00	1.48E-01 0.10425
1.82 3.92E-03	3.64 1.38E-02	5.45 4.43E-02	7.27 9.81E-02	1.05E-02	2.41E-01	7.41E-03	1.56E-01	1.9E-00	1.51E-01 0.10645
1.84 4.00E-03	3.67 1.43E-02	5.51 4.53E-02	7.35 1.01E-01	1.04E-02	2.45E-01	7.37E-03	1.59E-01	1.3E-00	1.54E-01 0.10865
1.85 4.08E-03	3.71 1.47E-02	5.56 4.63E-02	7.42 1.03E-01	1.04E-02	2.49E-01	7.33E-03	1.62E-01	8.8E-00	1.57E-01 0.11085
1.87 4.16E-03	3.75 1.51E-02	5.62 4.73E-02	7.49 1.05E-01	1.03E-02	2.53E-01	7.29E-03	1.65E-01	5.9E-00	1.60E-01 0.11305
1.89 4.25E-03	3.78 1.55E-02	5.67 4.83E-02	7.56 1.07E-01	1.03E-02	2.57E-01	7.25E-03	1.68E-01	3.9E-00	1.63E-01 0.11525
1.91 4.33E-03	3.82 1.59E-02	5.73 4.93E-02	7.64 1.10E-01	1.02E-02	2.61E-01	7.21E-03	1.71E-01	2.6E-00	1.66E-01 0.11745
1.93 4.42E-03	3.85 1.63E-02	5.78 5.03E-02	7.71 1.13E-01	1.02E-02	2.65E-01	7.17E-03	1.74E-01	1.7E-00	1.69E-01 0.11965
1.95 4.50E-03	3.89 1.67E-02	5.84 5.13E-02	7.78 1.15E-01	1.01E-02	2.69E-01	7.13E-03	1.77E-01	1.1E-00	1.72E-01 0.12185
1.96 4.59E-03	3.92 1.71E-02	5.89 5.23E-02	7.85 1.18E-01	1.01E-02	2.73E-01	7.09E-03	1.80E-01	7.4E-00	1.75E-01 0.12405
1.98 4.68E-03	3.95 1.75E-02	5.95 5.33E-02	7.93 1.21E-01	1.00E-02	2.77E-01	7.05E-03	1.83E-01	5.0E-00	1.78E-01 0.12625
2.00 4.77E-03	4.00 1.79E-02	6.00 5.43E-02	8.00 1.24E-01	1.00E-02	2.81E-01	7.01E-03	1.86E-01	3.3E-00	1.81E-01 0.12845
2.02 4.86E-03	4.04 1.83E-02	6.05 5.53E-02	8.07 1.27E-01	9.95E-03	2.85E-01	6.97E-03	1.89E-01	2.2E-00	1.84E-01 0.13065
2.04 4.95E-03	4.07 1.87E-02	6.11 5.63E-02	8.15 1.29E-01	9.91E-03	2.89E-01	6.93E-03	1.92E-01	1.5E-00	1.87E-01 0.13285
2.05 5.04E-03	4.11 1.91E-02	6.16 5.73E-02	8.22 1.32E-01	9.87E-03	2.93E-01	6.89E-03	1.95E-01	9.8E-00	1.90E-01 0.13505
2.07 5.13E-03	4.15 1.95E-02	6.22 5.83E-02	8.29 1.35E-01	9.82E-03	2.97E-01	6.85E-03	1.98E-01	6.6E-00	1.93E-01 0.13725
2.09 5.22E-03	4.18 1.99E-02	6.27 5.93E-02	8.36 1.37E-01	9.78E-03	3.01E-01	6.81E-03	2.01E-01	4.4E-00	1.96E-01 0.13945
2.11 5.32E-03	4.22 2.03E-02	6.33 6.03E-02	8.44 1.39E-01	9.74E-03	3.05E-01	6.77E-03	2.04E-01	2.9E-00	1.99E-01 0.14165
2.13 5.42E-03	4.25 2.07E-02	6.38 6.13E-02	8.51 1.41E-01	9.70E-03	3.09E-01	6.73E-03	2.07E-01	1.9E-00	2.02E-01 0.14385
2.15 5.52E-03	4.29 2.11E-02	6.44 6.23E-02	8.58 1.43E-01	9.66E-03	3.13E-01	6.69E-03	2.10E-01	1.3E-00	2.05E-01 0.14605
2.16 5.61E-03	4.32 2.15E-02	6.49 6.33E-02	8.65 1.45E-01	9.61E-03	3.17E-01	6.65E-03	2.13E-01	8.8E-00	2.08E-01 0.14825
2.18 5.71E-03	4.36 2.19E-02	6.55 6.43E-02	8.73 1.47E-01	9.57E-03	3.21E-01	6.61E-03	2.16E-01	5.9E-00	2.11E-01 0.15045
2.20 5.81E-03	4.40 2.23E-02	6.60 6.53E-02	8.80 1.49E-01	9.53E-03	3.25E-01	6.57E-03	2.19E-01	3.9E-00	2.14E-01 0.15265
2.22 5.91E-03	4.44 2.27E-02	6.65 6.63E-02	8.87 1.51E-01	9.49E-03	3.29E-01	6.53E-03	2.22E-01	2.6E-00	2.17E-01 0.15485
2.24 6.01E-03	4.47 2.31E-02	6.71 6.73E-02	8.95 1.53E-01	9.45E-03	3.33E-01	6.49E-03	2.25E-01	1.7E-00	2.20E-01 0.15705
2.25 6.12E-03	4.51 2.35E-02	6.76 6.83E-02	9.02 1.55E-01	9.40E-03	3.37E-01	6.45E-03	2.28E-01	1.1E-00	2.23E-01 0.15925
2.27 6.22E-03	4.55 2.39E-02	6.82 6.93E-02	9.09 1.57E-01	9.36E-03	3.41E-01	6.41E-03	2.31E-01	7.4E-00	2.26E-01 0.16145
2.29 6.32E-03	4.59 2.43E-02	6.87 7.03E-02	9.16 1.59E-01	9.32E-03	3.45E-01	6.37E-03	2.34E-01	5.0E-00	2.29E-01 0.16365
2.31 6.42E-03	4.62 2.47E-02	6.93 7.13E-02	9.24 1.61E-01	9.28E-03	3.49E-01	6.33E-03	2.37E-01	3.3E-00	2.32E-01 0.16585
2.33 6.54E-03	4.65 2.51E-02	6.98 7.23E-02	9.31 1.63E-01	9.24E-03	3.53E-01	6.29E-03	2.40E-01	2.2E-00	2.35E-01 0.16805
2.35 6.64E-03	4.69 2.55E-02	7.0							

8.3 APPENDIX C—Static displacement solving process

Case1

```

TOTALS
Nodes          : 2378
Beams          : 770
Plates        : 1990
Bricks        : 0
Links         : 64

SOLVER UNITS
Length        : mm
Mass         : t
Force        : N
Stress       : MPa

FREEDOM CASE   : "Freedom Case 1"
LOAD CASES    : "Load Case 1"
STORAGE SCHEME : Sparse
SORTING METHOD : AMD
SOLUTION TYPE : Direct

NUMBER OF EQUATIONS : 13751
MATRIX FILL-IN     : 77.4%
[K] MATRIX SIZE    : 12.0 MB
OPTIMUM RAM NEEDED : 2.6 MB
FREE SCRATCH SPACE : 63.5 GB

SUMMATION OF APPLIED LOADS (Name: "Load Case 1")
      FX      FY      FZ      MX      MY      MZ
Beams -1.45709E-15 -4.09291E+03  4.12821E-15  2.31811E+00 -9.48098E-14 -6.53381E+02
Plates -1.11130E+02 -9.28232E+04 -6.67580E-01 -1.28445E-01  5.38605E-02 -9.70318E+01
Total  -3.11130E+02 -9.69101E+04 -6.67580E-01  2.18907E+00  5.38605E-02 -7.10583E+02
Vector -3.09562E+02 -9.53450E+04 -6.67580E-01  8.90138E+01  5.38605E-02  5.69891E+05

SUMMATION OF MOMENTS OF APPLIED LOADS ABOUT THE ORIGIN [Load Vector]
      Mx0      My0      Mz0
      1.06004E+06 -7.05138E+05 -2.15295E+08

Reducing 13751 Equations (Using 12.1 MB RAM)...
MAXIMUM PIVOT : 5.705340E+10 (Node 618 RZ)
MINIMUM PIVOT : 2.064255E+01 (Node 588 DX)

Results for 1 Load Case...

MAXIMUM DISPLACEMENT MAGNITUDES
Case 1
      DX      DY      DZ      RX      RY      RZ      Name
      1  6.67699E+00  5.14764E+00  1.66824E+00  4.47157E-02  3.40980E-02  1.91204E-01  "Load Case 1"

TOTAL CPU TIME: 0.656 Seconds
*Solution completed on 13/06/2022 at 00:18:27
*Solution time: 1 Second

SUMMARY OF MESSAGES
*Number of Notes : 0
*Number of Warnings : 0
*Number of Errors : 0

```

Case2

```

TOTALS
Nodes          : 2386
Beams          : 770
Plates        : 1990
Bricks        : 0
Links         : 74

SOLVER UNITS
Length        : mm
Mass         : t
Force        : N
Stress       : MPa

FREEDOM CASE   : "Freedom Case 1"
LOAD CASES    : "Load Case 1"
STORAGE SCHEME : Sparse
SORTING METHOD : AMD
SOLUTION TYPE : Direct

NUMBER OF EQUATIONS : 13676
MATRIX FILL-IN     : 77.5%
[K] MATRIX SIZE    : 12.1 MB
OPTIMUM RAM NEEDED : 2.7 MB
FREE SCRATCH SPACE : 63.5 GB

SUMMATION OF APPLIED LOADS (Name: "Load Case 1")
      FX      FY      FZ      MX      MY      MZ
Beams -1.30980E-29 -4.06068E+03  0.00000E+00  6.82121E-13  4.90872E-29  9.44765E-12
Plates 0.00000E+00 -9.26173E+04  0.00000E+00  0.00000E+00  0.00000E+00  0.00000E+00
Total -1.30980E-29 -9.66780E+04  0.00000E+00  6.82121E-13  4.90872E-29  9.44765E-12
Vector -1.95998E-29 -9.53164E+04  0.00000E+00  9.82719E+03  1.09912E-11  -5.65734E+05

SUMMATION OF MOMENTS OF APPLIED LOADS ABOUT THE ORIGIN [Load Vector]
      Mx0      My0      Mz0
      6.59138E+00  2.43816E-26  -2.14012E+08

Reducing 13676 Equations (Using 12.1 MB RAM)...
MAXIMUM PIVOT : 1.011937E+12 (Node 446 RY)
MINIMUM PIVOT : 3.823116E+01 (Node 588 DX)

Results for 1 Load Case...

MAXIMUM DISPLACEMENT MAGNITUDES
Case 1
      DX      DY      DZ      RX      RY      RZ      Name
      1  5.54341E-01  6.28142E+00  9.81964E-01  4.45548E-02  5.66145E-03  1.18425E-02  "Load Case 1"

DIRECT SUMMATION OF NODE REACTION FORCES
Case 1
      FX      FY      FZ      MX      MY      MZ      Name
      1 -2.60540E-08  9.66780E+04  -5.81945E-10  -4.57621E-08  -9.22984E-07  1.57208E-06  "Load Case 1"

TOTAL CPU TIME : 0.703 Seconds
*Solution completed on 13/06/2022 at 00:20:53
*Solution time: 1 Second

SUMMARY OF MESSAGES
*Number of Notes : 0
*Number of Warnings : 0
*Number of Errors : 0

```

Case3

```

TOTALS
Nodes          : 2378
Beams          : 770
Plates        : 1990
Bricks        : 0
Links         : 222

SOLVER UNITS
Length        : mm
Mass          : t
Force        : N
Stress       : MPa

FREEDOM CASE  : "Freedom Case 1"

LOAD CASES    : "Load Case 1"

STORAGE SCHEME : Sparse
SORTING METHOD  : ARD
SOLUTION TYPE  : Direct

NUMBER OF EQUATIONS : 13086
MATRIX FILL-IN    : 77.5%
[K] MATRIX SIZE   : 11.9 MB
OPTIMUM RAM NEEDED : 3.2 MB
FREE SCRATCH SPACE : 63.5 GB

SUMMATION OF APPLIED LOADS (Name: "Load Case 1")
Beams  -1.30980E-29 -4.06068E+03 0.00000E+00 6.82121E-13 4.90872E-29 9.44765E-12
Plates 0.00000E+00 -9.26173E+04 0.00000E+00 0.00000E+00 0.00000E+00 0.00000E+00
TOTAL  -1.30980E-29 -9.66780E+04 0.00000E+00 6.82121E-13 4.90872E-29 9.44765E-12
Vector -1.96044E-29 -9.51164E+04 0.00000E+00 9.82355E+03 1.09912E-11 -5.65734E+05

SUMMATION OF MOMENTS OF APPLIED LOADS ABOUT THE ORIGIN [Load Vector]
Mx0  My0  Mz0
2.22973E-07 5.81011E-26 -2.14012E+08

Reducing 13086 Equations (Using 11.9 MB RAM)...

MAXIMUM PIVOT : 9.904257E+11 (Node 430 RY)
MINIMUM PIVOT : 3.823116E+01 (Node 588 DX)

Results for 1 Load Case...

MAXIMUM DISPLACEMENT MAGNITUDES
Case 1 6.85060E-01 5.02643E+00 8.27958E-01 3.28873E-02 5.74506E-03 9.13198E-03 Name "Load Case 1"

DIRECT SUMMATION OF NODE REACTION FORCES
Case 1 -1.96801E-08 9.66780E+04 6.50708E-11 -3.57963E+04 8.82119E+01 2.38821E-08 Name "Load Case 1"

TOTAL CPU TIME : 0.781 Seconds
*Solution completed on 13/06/2022 at 00:23:52
*Solution time: 1 Second

*SUMMARY OF MESSAGES
*Number of Notes : 0
*Number of Warnings : 0
*Number of Errors : 0

```